UNIVERSIDADE FEDERAL DE MINAS GERAIS
Programa de Pós-Graduação em Engenharia Metalúrgica, Materiais e de Minas

Dissertação de Mestrado

Metallurgical characteristics of Samarco Mineração's product portfolio and their influences on Western European blast furnace operations

Autor: Plínio Gomes Bueno
Orientador: Professor Luiz Fernando Andrade de Castro

Dezembro/2015

Plinio Gomes Bueno

Plinio Gomes Bueno

Metallurgical characteristics of Samarco Mineração's product portfolio and their influences on Western European blast furnace operations

Dissertação de mestrado apresentada ao Programa de Pós-Graduação em Engenharia Metalúrgica, Materiais e de Minas da Escola de Engenharia da Universidade Federal de Minas Gerais, como requisito parcial para obtenção do Grau de Mestre em Engenharia Metalúrgica, Materiais e de Minas.

Área de Concentração: Metalurgia Extrativa

Orientador: Professor Luiz Fernando Andrade de Castro

Belo Horizonte
Universidade Federal de Minas Gerais
Escola de Engenharia
2015

Bueno, Plínio Gomes.
B928m Metallurgical characteristics of Samarco Mineração's product portfolio and their influences on Western European blast furnace operations [manuscrito] / Plínio Gomes Bueno. - 2015.
xvi, 122 f., enc.: il.

Orientador: Luiz Fernando Andrade de Castro.

Dissertação (mestrado) - Universidade Federal de Minas Gerais, Escola de Engenharia.

Bibliografia: f.118-122.

1. Engenharia metalúrgica - Teses. 2. Metalurgia extrativa - Teses. 3. Altos-fornos - Teses. I. Castro, Luiz Fernando Andrade de. II. Universidade Federal de Minas Gerais. Escola de Engenharia. III. Título.

CDU: 669(043)

To my father José Antônio Bueno,
the responsible for my first steps in
the world of metallurgy

The author would like to thank the various stakeholders who contributed to this dissertation:

Helio Cardoso and Mauricio Otaviano for their coaching lessons on technical, professional and personal levels.

My senior managers Roberto Carvalho, Leonardo Sarlo and Erik Scholten who believed and supported my plan of achieving a master degree next to the challenging work agenda at Samarco Netherlands.

The technical support team of Samarco comprised of Flavio Lopes, Vicente Campanharo, Francisco Pinheiro, Philippe Rocha, Maciel Bianchi, Ana Maria Guilherme, Rafael Camelo and Welter Santos.

Samarco's Process Engineering staff for the test work and analyses, especially Heidy Simões, Thiago Marchezi, Vinicius Perin and Alaecio Meschiatti.

My colleagues at Samarco Iron Ore B.V. Wellington Ceciliano, Douwe Bergsma, Samantha Maldonado and Shirley Elwards for their patience and support.

Dr. Volker Ritz from Studiengesellschaft fuer Eisenerzaufbereitung (SGA), for the metallurgy lessons and great collaborative work.

The technical stakeholders at the various integrated steel works in Europe, whom I learned a lot from in my career path, especially Elisabeth Marliere, Philippe Lacroix, Laurence Petit Nicolas (ArcelorMittal Sourcing), Frederik van de Velde, Alain Daelman (ArcelorMittal Gent), Walter Hartig (Rogesa mBH), Antoine Steeghs, Susanne Doepp, Ronald Jonckbloedt, Jolanda Lambroek (Tata Steel Europe – Ijmuiden Works), Richard Brown, Jeff Ingham, Dean Cartwright, Richie Hart, Mike Paskins, Jonathan Evans (Tata Steel Europe – Port Talbot Works).

Summary

LIST OF FIGURES

LIST OF TABLES:

LIST OF ANNOTATIONS:

ΔP	Pressure differential between the inlet and outlet of a solid burden being percolated by a gas flow, Pa;
H	Extension of the solid burden, m;
μ	Viscosity of gas, poise;
ε	Void fractions in a burden, adimensional;
v_0	Velocity of gas inlet, m/s;
ρ	Specific mass of gas kg/m3;
ψ	Sphericity of the solid particles, adimensional;
d_p	Diameter of the particles in the burden, m.
PBFMB45	Blast furnace pellet – Binary basicity 0.45
PBFSTD	Blast furnace pellet – Binary basicity 0.8
PBFHB	Blast furnace pellet – Binary basicity 1.0
SGA	Studiengesellschaft Für Eisenerzaufbereitung
REAS	Softening and melting test – SGA standard

Abstract

Western European Blast Furnaces have been increasing the participation of pellets in their burden in substitution of sinter and lump ores through time. The hot metal production process as a whole is therefore becoming more subject to the quality characteristics of this ferrous agglomerate. This study provides a comprehensive evaluation of the metallurgical characteristics of three low-slag pellets from Samarco Mineração's blast furnace portfolio which differ significantly in binary basicity (CaO/SiO_2). As to assess the influence of these pellets in the behavior of a blast furnace's granular zone, low temperature disintegration, reducibility and swelling tests were carried out. As to understand the behavior of the subject pellets in the cohesive zone of a blast furnace, reduction under load tests and rounds of softening and melting tests with individual pellet types and their combination with a typical Western European sinter were made in partnership with Studiengesellschaft Für Eisenerzaufbereitung (SGA).

Pellets and sinter samples have been produced in pilot plants of Samarco Mineração and SGA, respectively. Metallurgical results point at low degradation during reduction for all pellet types and relative higher reducibility of pellets, especially the fluxed types when compared to sinter. Different swelling, softening, melting and dripping temperatures of pellets are closely associated to their reduction degree, slag content, basicity and microstructural characteristics. The microstructures of oxide pellets with different basicities significantly change in relation to grain sizes, coalescence and recrystallization levels.

When mixtures of pellets and typical Western European Sinter are subject to the REAS methodology, a strong interaction between the agglomerate types is noticed, promoting changes in the overall softening, melting and dripping behavior of the bulk.

Key Words

Blast furnace, pellets, sinter, swelling, reduction index, delta P, hot metal, softening and melting.

Resumo

Altos-Fornos do oeste europeu tem aumentado a participação de pelotas em seus leitos em substituição ao sinter e granulado através dos tempos. A produção de gusa está, desta maneira, se tornando mais dependente das características de qualidade deste aglomerado de ferro. Este estudo fornece uma avaliação completa das características metalúrgicas de três pelotas de baixa escória do portfólio de produtos da Samarco Mineração, que diferem significativamente em basicidade binária (CaO/SiO_2). Para medir a influencia destas pelotas no comportamento da zona granular de um Alto-Forno, testes de degradação à baixa temperatura, redutibilidade e inchamento foram realizados. Para entendimento do comportamento destas pelotas na zona coesiva de um Alto-Forno, testes de redução sob-pressão e amolecimento fusão em pelotas e misturas de pelotas com um sínter típico do oeste europeu foram feitos em parceria com o laboratório alemão Studiengesellschaft Für Eisenerzaufbereitung (SGA).

As amostras de pelotas e sínter foram produzidas nas plantas piloto da Samarco Mineração e SGA, respectivamente. Resultados metalúrgicos apontam baixa degradação sob-redução em todas as pelotas e relativamente maior redutibilidade de pelotas, especialmente as fluxantes, quando comparadas ao sínter. Diferentes níveis de inchamento, temperaturas de amolecimento, fusão e gotejamento de pelotas estão bastante associados aos seus graus de redução, níveis de escória, basicidade e suas características microestruturais. As microestruturas de pelotas com diferentes basicidades variam significativamente em termos de tamanho de grão e níveis de coalescimento e recristalização.

Quando misturas de pelotas e sínter típico do oeste europeu são submetidas à metodologia REAS, uma forte interação do leito é notada, promovendo mudanças em seu comportamento geral de amolecimento, fusão e gotejamento.

Palavras-chave

Alto-Forno, pelotas, sínter, inchamento, grau de redução, delta P, gusa, amolecimento e fusão.

1. Introduction

Iron ores and their different forms have been changing in quality characteristics and availability throughout time. This fact has caused integrated steel mills to adapt themselves on the way they process this raw material. European plants significantly changed their operating standards when migrating from mostly domestic iron ore sources to the seaborne market in the second half of the 20th century. Throughout this period blast furnaces grew in size and efficiency and had their number significantly decreased. Many steel works sought access to the Atlantic Ocean where availability of high grade iron ore production had been on the rise, especially in Brazil. With the advancements of sintering technology, most plants were in this period of time running mainly on sinter and lump ore for the production of hot metal. Later in time, factors like environmental constraints, the decrease of quality of natural sinter feed and lump ore and the increase of iron ore concentrates for pelletizing, led to the partial replacement of other ferrous sources by pellets as direct charge in Western European Blast Furnaces.

Hot metal production in the EU 15 member countries (blast furnace operating countries in Europe which are organized in the European Blast Furnace Committee) had fluctuated from 89 to 96 million tons per year between 1990 and 2007, while the number of active blast furnaces decreased from 92 to 57. After the slump in production caused by the economic crisis of 2008 and 2009, the industry in this region has partially recovered to a hot metal production of 75.9 million tons in 2013 with 45 active blast furnaces[(1)]. In 1990 European Blast furnaces were operated at sinter rates of 80% whereas nowadays pellet rates of 30 to 45% are common, especially because cost reduction strategies have caused major players to concentrate production in best performing reactors. As the most extreme scenario, Swedish and Finnish blast furnaces run at around 90% pellet, 10% briquette rates, having completely eliminated sinter plant operations. High grade iron ore pellets therefore contribute to process stability and productivity by influencing important blast furnace process KPIs such as slag, coke and PCI rates.

The reasons mentioned above have made Europe the biggest pellet importer of the seaborne market, relying on materials which mostly derive from Brazil, Sweden and Canada. Within this context, Samarco Mineração figures among the largest pellet exporters to Western European steel works. It is therefore of importance for Samarco

to understand the technical aspects of its products and how they fit the process conditions of West European blast furnaces, not only in relation to physical and chemical qualities but also metallurgical consistency, especially when combined with typical sinters from the region.

Samarco's blast furnace portfolio has been extensively utilized in many integrated steel works of this refereed region; however, opinions can significantly diverge on the most suitable pellet type for an optimum operation. The criteria for burden selection are complex and involve many variables, but metallurgical consistency is always one of the highly praised items. The relevance of this study is in the fact that it encompasses an in-depth evaluation of the most important metallurgical characteristics of Samarco pellets. This information will be used as tool for understanding the industrial performance of Samarco pellets.

2. Objectives

This work aims at determining the most relevant metallurgical characteristics of Samarco Mineração's pellet portfolio and their influences on the operational behavior of the granular and cohesive zones of Western European blast furnaces. Especially in relation to the behavior of the cohesive zone, a series of softening & melting tests encompassing agglomerates individually and sinter/pellet mixtures is made for evaluation of burden interaction.

3. Literature review

3.1. The importance of steel to society, contextualization of traded volumes and deployment to the seaborne pellets requirement.

Steel is an extremely versatile metal in terms of ranging properties, applications and recycling capacity. It can be considered the most important existing metal and is almost omnipresent in one's daily life[1,2,3]. Steel represents roughly 90% of the total amount of metals utilized globally. There are altogether about 2,400 grades of steel, 1,500 of which are classified as special steels in the Register of European Steels[3]. Figure 1 depicts the difference in production scale of steel compared to other metals and alternative materials in 1970 and 2013.

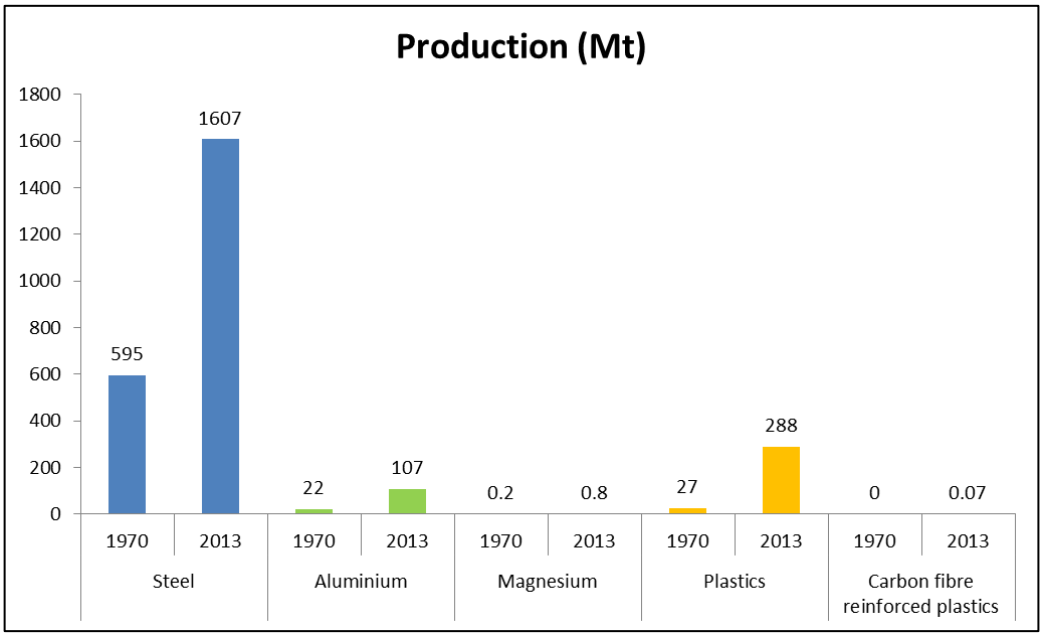

Figure 1: Production of steel versus other metals and competitor materials in 1970 and 2013[3].

Various techniques have been applied industrially across the time for the production of steel, however nowadays it is reasonable to state that practically two major processes coexist in the world: Basic Oxygen Furnaces (BOFs) and Electric Arc Furnaces (EAFs). Steel production through BOFs is present at integrated steel complexes and has hot metal as its main intake (roughly 75 to 90%) whereas EAFs are present at semi-integrated steel complexes which can run with 100% scrap, DRI/HBI, pig iron or with a

mix of these ferrous sources. BOF and EAF production accounted for about 83% and 27% of the world's steel output in 2014, respectively.

China has its steel production based on integrated mills, being the biggest BOF producer globally, with over 730 million tons as output in 2014. A distinct example comes from North America, where EAF production corresponds to the largest output of the country's crude steel, due to reasons like shorter recycling cycle of steel triggered by consumption patterns and, more recently, due to the revitalization of natural gas availability for DRI production. EAF production in North America corresponded to over 71 million tons of output in 2014. Figures 2, 3 and 4 illustrate the breakdown of BOF/EAF contribution to crude steel production globally and the volumes produced by these routes in each geographical location.

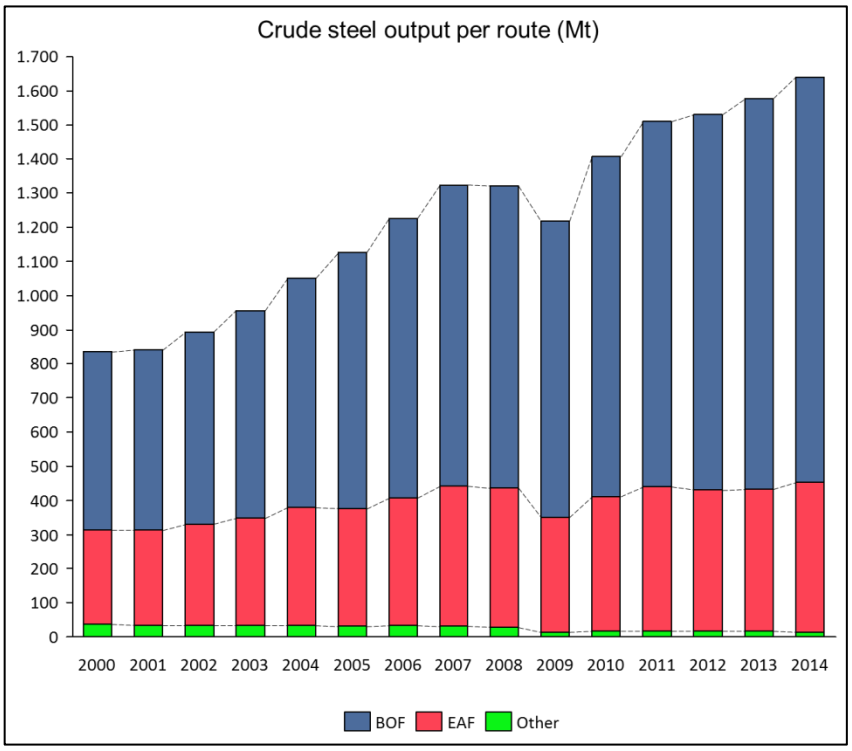

Figure 2: Crude steel production through BOF and EAF routes[4].

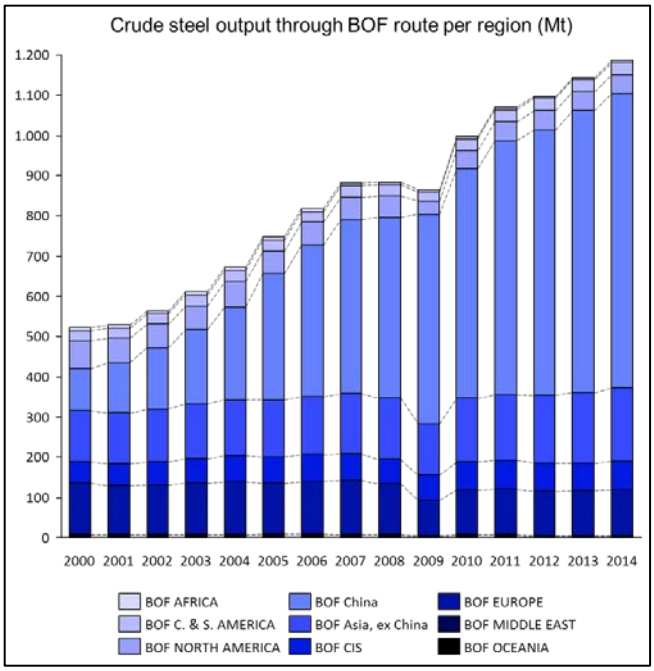

Figure 3: Crude steel production through BOF route per region[(4)].

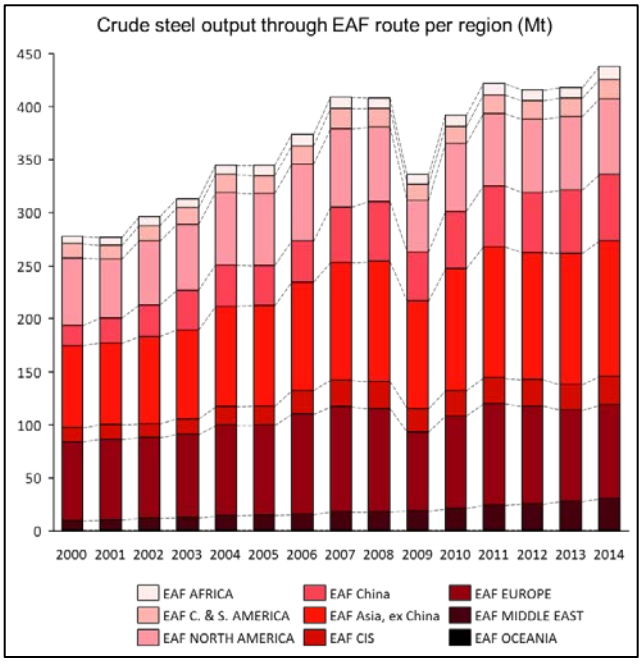

Figure 4: Crude steel production through EAF route per region[(4)].

Hot metal accounted for roughly 75% of the world's ferrous sources utilized in crude steel production in 2014, having reached over 1.2 billion tons of production. It can be

virtually all associated to integrated BOF based steel mills. For the production of hot metal mostly three ferrous burden components are utilized: pellets, sinter and lump ores. Pellets and the European consumption of this raw material are the subject matter of this dissertation; therefore it is of interest to categorize the size of this market for understanding the relevance of the present study. Figures 5 and 6 depict the global hot metal output per year, and the pellet rates of blast furnaces per region.

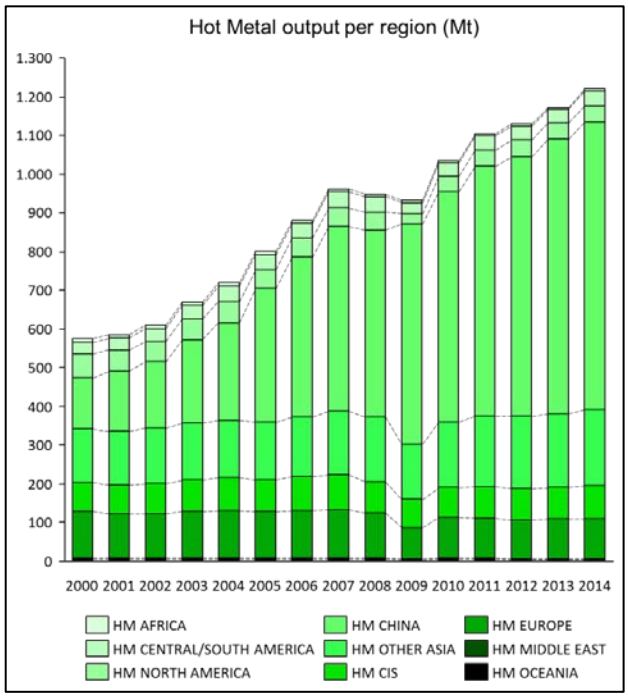

Figure 5: Hot metal production per region[(4)].

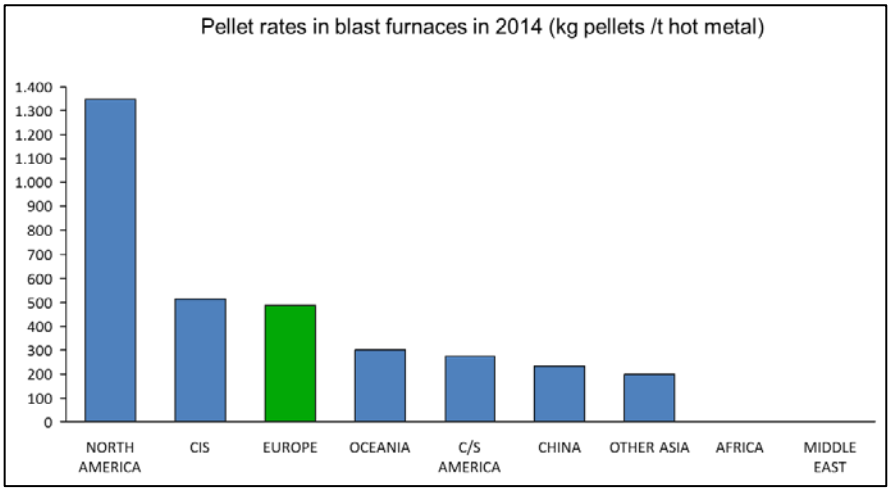

Figure 6: Pellet rates in blast furnaces in 2014(4).

Although North America and CIS have on average more pellet participation in blast furnace burdens, they typically do not rely on the seaborne pellet trade whereas Europe is very dependent on the ore shipments through the Atlantic Ocean route. The European continent is the largest destination of pellet shipments on the globe, as depicted in figure 7.

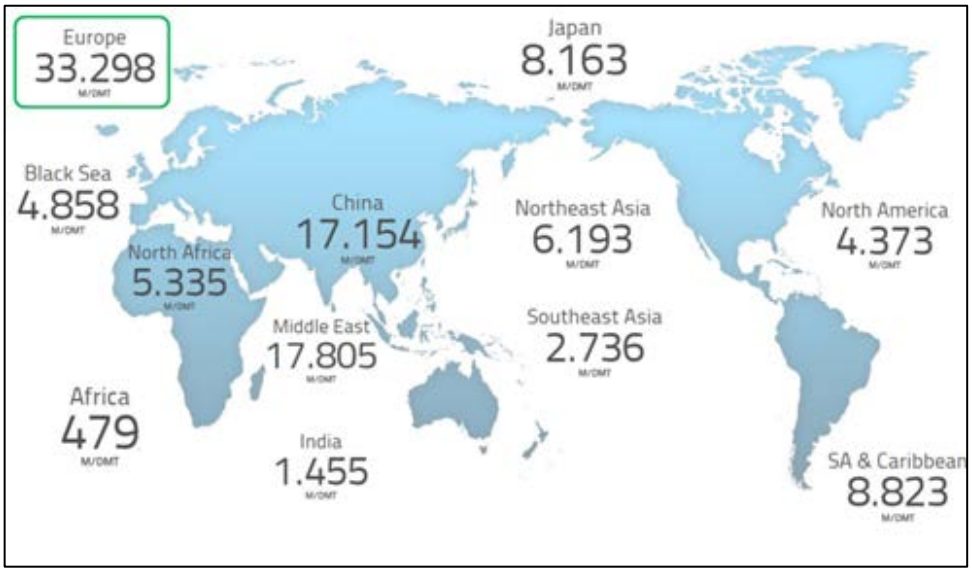

Figure 7: Global consumption of seaborne pellets in 2014[4].

Samarco Mineração operates entirely on the seaborne market with an export capacity of 30.5 million tons per year of pellets to all regions. Therefore, understanding the quality requirements of clients situated in the largest consuming market for pellets is a company's necessity which justifies the present academic study.

3.2. A brief history of ironmaking

As early as 3000 years ago, iron was already serving as basis for human culture and civilization[3]. The first important iron smelting method was the bloomery hearth furnace, comprised of a low underground – or shaft – furnace in which iron ore was slowly melted down to a lump of up to 300kg of weight by the use of charcoal. This lump contained slag that was later removed by repeated heating and forging[2,5]. In the Middle Age the search for more productivity led to the evolution of bloomery hearth furnaces into the bloomery furnaces, which had increased height and improvements in

the air blast (through man power or water wheels). Finally, the continuous improvement led to further increase in heights and continuous flow of hot metal gave start to the blast furnace era. The first blast furnace is believed to have been developed in the banks of Rhine River in Marches Les Dames, Belgium, around 1340.

Due to environmental pressures in the United Kingdom over deforestation for the production of charcoal, mineral coals started being used for ironmaking in 1700. However, the use of mineral coals largely grew in importance only in 1707 with the development of the coking process. The first hot metal purely based on coke was produced in 1709[5]. Coke is able to support much higher static pressure in a blast furnace stack when compared to charcoal and it enabled further increases in heights for more production capacity.

Refining technologies also progressed through time, always with the objective of more capacity and lower cost in steel production. The most relevant evolution steps in hot metal, steel, refining, casting and rolling technologies, are all depicted in figure 8. It is important to mention that the major drivers for a steeper steel production curve in the XX and XXI centuries are the industrial revolution and the rise of China as major global steel manufacturer, respectively.

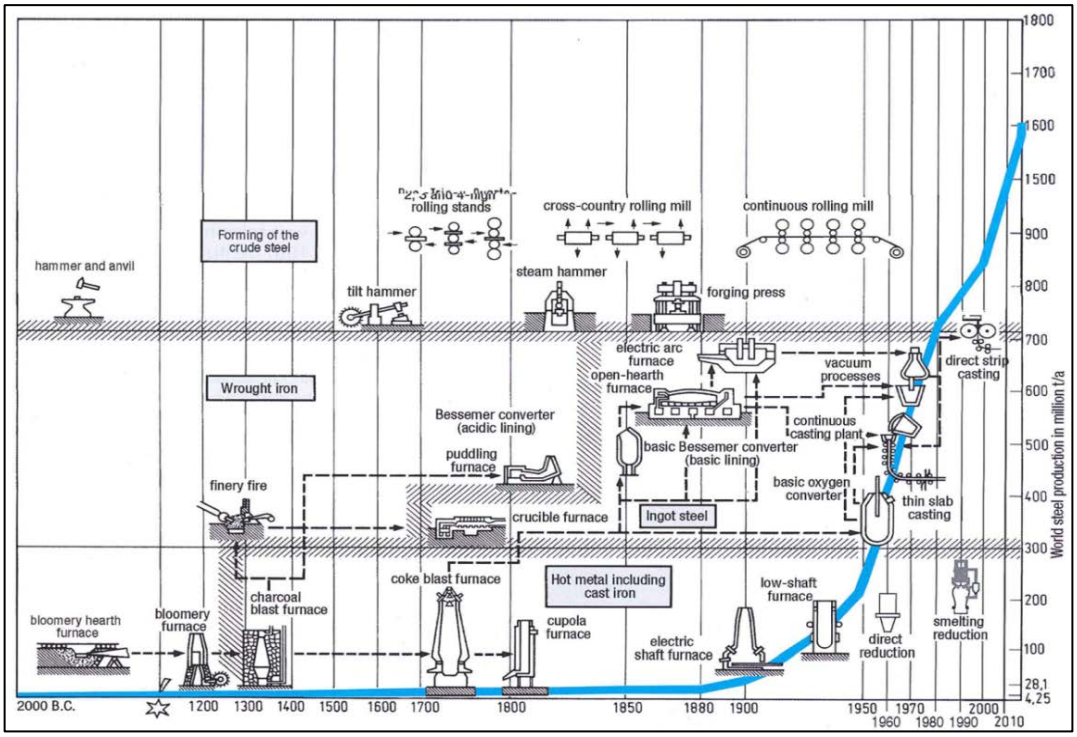

Figure 8: Steelmaking historical evolution[3].

More recently in time, new technologies have been arising for the production of primary iron either in the form of hot metal, iron nuggets, DRI or HBI. As a matter of fact, although other processes are technically and commercially viable, the blast furnaces have been modernized and adapted to today's requirements of extremely high productivity at large scale and low production costs. Figure 9 depicts an assessment of the maturity state of technologies available for the production of primary iron[6]. The blast furnace, although once considered to be under threat by other technologies, is today and for the foreseeable future the most important technology for the production of primary iron.

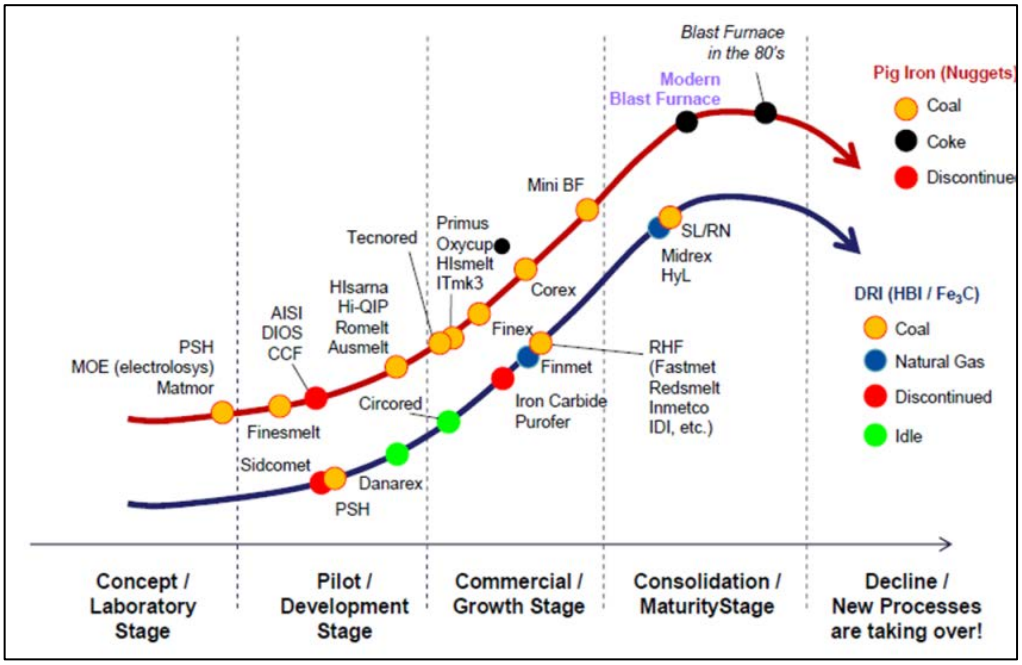

Figure 9: Maturity curve of available technologies for the production of primary iron[6].

3.3. Contextualization of modern blast furnace operations

The blast furnace has been described as a countercurrent packet-bed reactor in which reducing gases ascend and reduce descending iron ore particles[7]. It is a continuously operating shaft furnace which chemically reduces and physically converts iron oxides into liquid iron called "hot metal"[2,8].

Blast furnaces can be studied and discussed from many different perspectives. This dissertation gives emphasis to ferrous burden characteristics and its influence in a blast furnace behavior, however a small contextualization of the status quo of the

technology, basic concepts of thermodynamics and kinetics are required before the core of the study is unfolded.

3.3.1. Thermodynamics

Considering the whole blast furnace as a system, reduction of iron ore takes place through the use of reductants (C, CO and H_2). The reducing agents tie oxygen by own oxidation therefore extracting it from the ores. Reduction however is only possible when oxygen potential of the admitted material is smaller than that of the iron oxide. This is determined by the partial pressure of oxygen and by the temperature. The reduction takes place in stages towards oxides with lower oxygen content and finally to metallic Fe.

Traditionally, reduction reactions in a blast furnace are divided into two parts:

- Indirect reduction: takes place through CO and H_2 gases at thermodynamic conditions that allow the presence of CO_2 and H_2O as final products.
- Direct reduction: takes place mostly through reduction by CO and H_2 gases in direct presence of carbon at thermodynamic conditions which favor the regeneration of H_2O and CO_2 into CO as final product[2,7,8,9].

3.3.1.1. Indirect reduction of iron ores

The indirect reduction takes place as the ferrous burden descends in the shaft. Temperature ranges of the reduction steps are roughly 500^oC for the conversion of hematite (Fe_2O_3) to magnetite (Fe_3O_4), 600 to 900^oC for the conversion of magnetite to wüstite (FeO) and further reduction to metallic Fe takes place above 900^oC.

As oxygen potentials of the new oxides generated are always lower than their successor, the ratio CO/CO_2 has to exceed stoichiometric value, otherwise equilibrium will be shifted towards reversed reactions (right to left)[2].

$3Fe_2O_{3(s)} + CO_{(g)} \rightleftarrows 2Fe_3O_{4(s)} + CO_{2(g)}$ + 52.85 kJ (3.1)

$3Fe_2O_{3(s)} + H_{2(g)} \rightleftarrows 2Fe_3O_{4(s)} + H_2O_{(g)}$ + 4.86 kJ (3.2)

$Fe_3O_{4(s)} + m\ CO_{(g)} \rightleftarrows 3FeO_{(s)} + CO_{2(g)} + (m-1)\ CO_{(g)}$ - 36.46 kJ (3.3)

$Fe_3O_{4(s)} + n\ H_{2(g)} \rightleftarrows 3FeO_{(s)} + H_2O_{(g)} + (n-1)\ H_{2(g)}$ - 84.45 kJ (3.4)

$FeO_{(s)} + p\ CO_{(g)} \rightleftarrows Fe_{(s)} + CO_{2(g)} + (p-1)\ CO_{(g)}$ + 17.13 kJ (3.5)

$FeO_{(s)} + q\ H_{2(g)} \rightleftarrows Fe_{(s)} + H_2O_{(g)} + (q-1)\ H_{2(g)}$ -30.86kJ (3.6)

It has to be mentioned that p > m and q > n, due to the higher CO/CO_2 ratio requirement for the reduction of wustite. On an industrial operation, the blast furnace tall design copes with this concept: the lower in the stack, the higher is the CO partial pressure to help with shifting the equilibrium towards the right. A resumed version of the indirect reduction equations is presented below:

$Fe_2O_{3(s)} + 3CO_{(g)} \rightleftarrows 2Fe_{(s)} + 3CO_{2(g)}$ +27.52 kJ (3.7)

$Fe_2O_{3(s)} + 3\ H_{2(g)} \rightleftarrows 2Fe_{(s)} + 3H_2O_{(g)}$ -88.44 kJ (3.8)

The first versions of iron – oxygen – carbon and iron – oxygen – hydrogen diagrams are depicted in figures 10 and 11. The corresponding equilibrium conditions to the reactions presented above are represented by lines as follows: (3.1) and (3.2) closely follow the x axis, (3.3) and (3.4) equals to (A) and (A'), (3.5) and (3.6) equals to (B) and (B').

Figure 10 also encompasses line (D) which represents the Boudouard curve. This curve divides the equilibrium of the diagram into two areas: the gas composition in the left side hinders the reduction process and the one on the right side favors it. Boudouard reaction is very pressure sensitive and line (D) represents it at 1atm.

$$CO_{2(g)} + C_{(s)} \rightleftarrows 2CO_{(g)} \qquad -172.47\ kJ \qquad (3.9)$$

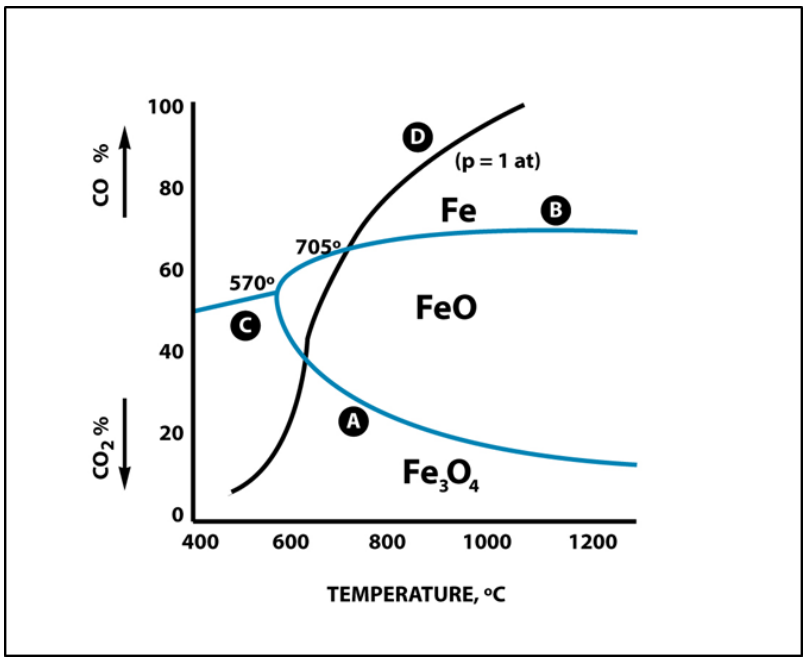

Figure 10: Iron – oxygen – carbon diagram.

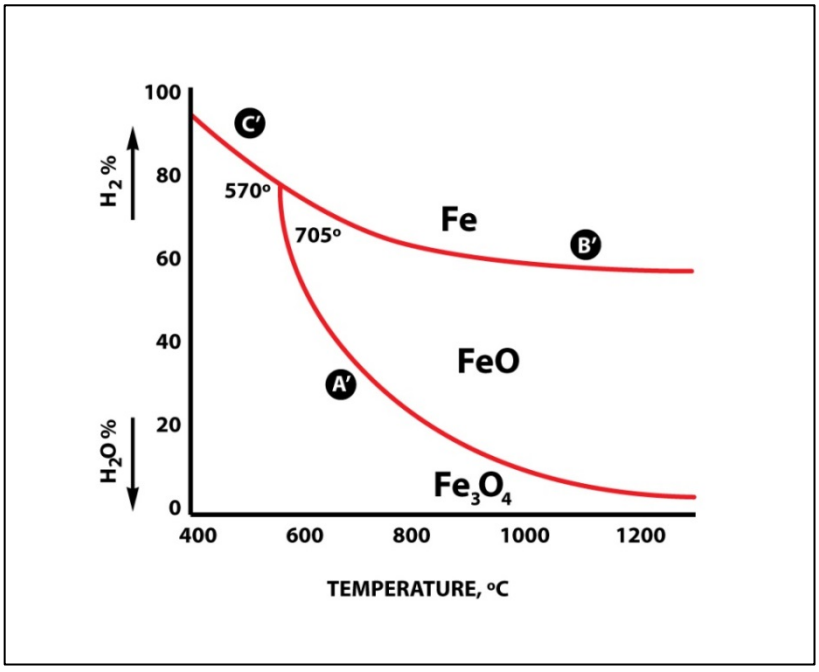

Figure 11: Iron – oxygen – hydrogen diagram.

As a gaseous mixture of H, H_2, CO and CO_2 is present in the indirect reduction, the "ηH/C" aims at expressing the relationship between partial pressures by the following equation:

$$\eta H/C = \frac{\%H_2 + \%H_2O}{\%CO + \%CO_2} \qquad (3.9)$$

The curve in the new diagram Fe-C-H-O is changed when ηH/C is altered. Overall it can be noticed that H_2 is a stronger reductant than CO, however its higher participation (ηH/C towards zero) would lead to higher energy requirements for the reduction process, as depicted in figure 12.

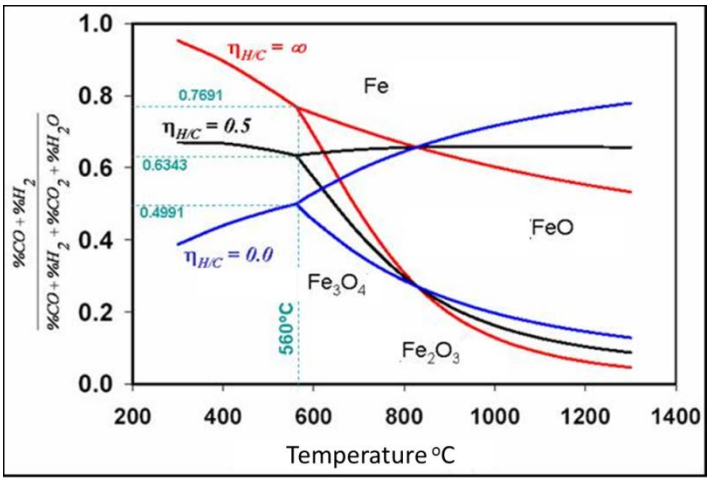

Figure 12: Iron – oxygen – carbon – hydrogen diagram.

3.3.1.2. Direct reduction of iron ores

The below reactions describe the final state of reduction process:

$$3Fe_2O_{3(s)} + C_{(s)} \rightleftarrows 2Fe_3O_{4(s)} + CO_{(g)} \quad - 119.62\ kJ \qquad (3.10)$$

$$Fe_3O_{4(s)} + C_{(s)} \rightleftarrows 3FeO_{(s)} + CO_{(g)} \quad - 208.93\ kJ \qquad (3.11)$$

$$FeO_{(s)} + C_{(s)} \rightleftarrows 3FeO_{(s)} + CO_{(g)} \quad - 155.34\ kJ \qquad (3.12)$$

In blast furnaces direct reduction of solid iron oxides by coke and coal char is negligible. Direct reduction of oxides in primary slag by coke is limited but present. Iron oxides react with carbon monoxide as detailed in reactions 3.1, 3.3 and 3.5, however at temperatures higher than the 950^{o}C to 1000^{o}C range, the carbon dioxide will react with carbon through the Boudouard reaction. Direct reduction can therefore be explained by the total reactions below for both carbon and hydrogen as reductants:

$FeO_{(s)} + CO_{(g)} \rightleftarrows Fe_{(s)} + CO_{2(g)}$ + 17.3 kJ (3.13)

$\underline{CO_{2(g)} + C_{(s)} \rightleftarrows 2CO_{(g)}}$ - 172.47 kJ (3.14)

$FeO_{(s)} + C_{(s)} \rightleftarrows Fe_{(s)} + CO_{(g)}$ - 155.34 kJ (3.15)

$FeO_{(s)} + H_{2(g)} \rightleftarrows Fe_{(s)} + H_2O_{(g)}$ - 30.86 kJ (3.16)

$\underline{H_2O_{(g)} + C_{(s)} \rightleftarrows H_{2(g)} + CO_{(g)}}$ - 124.48 kJ (3.17)

$FeO_{(s)} + C_{(s)} \rightleftarrows FeO_{(s)} + CO_{(g)}$ - 155.34 kJ (3.18)

Due to the higher energy requirements of the direct reduction against the indirect reduction, blast furnace operators must enhance the indirect reduction in the granular zone as to achieve lower coke + PCI rates[2,8].

Figure 13 depicts the location of reduction reactions as well as direct and indirect reduction regions of a typical blast furnace operation.

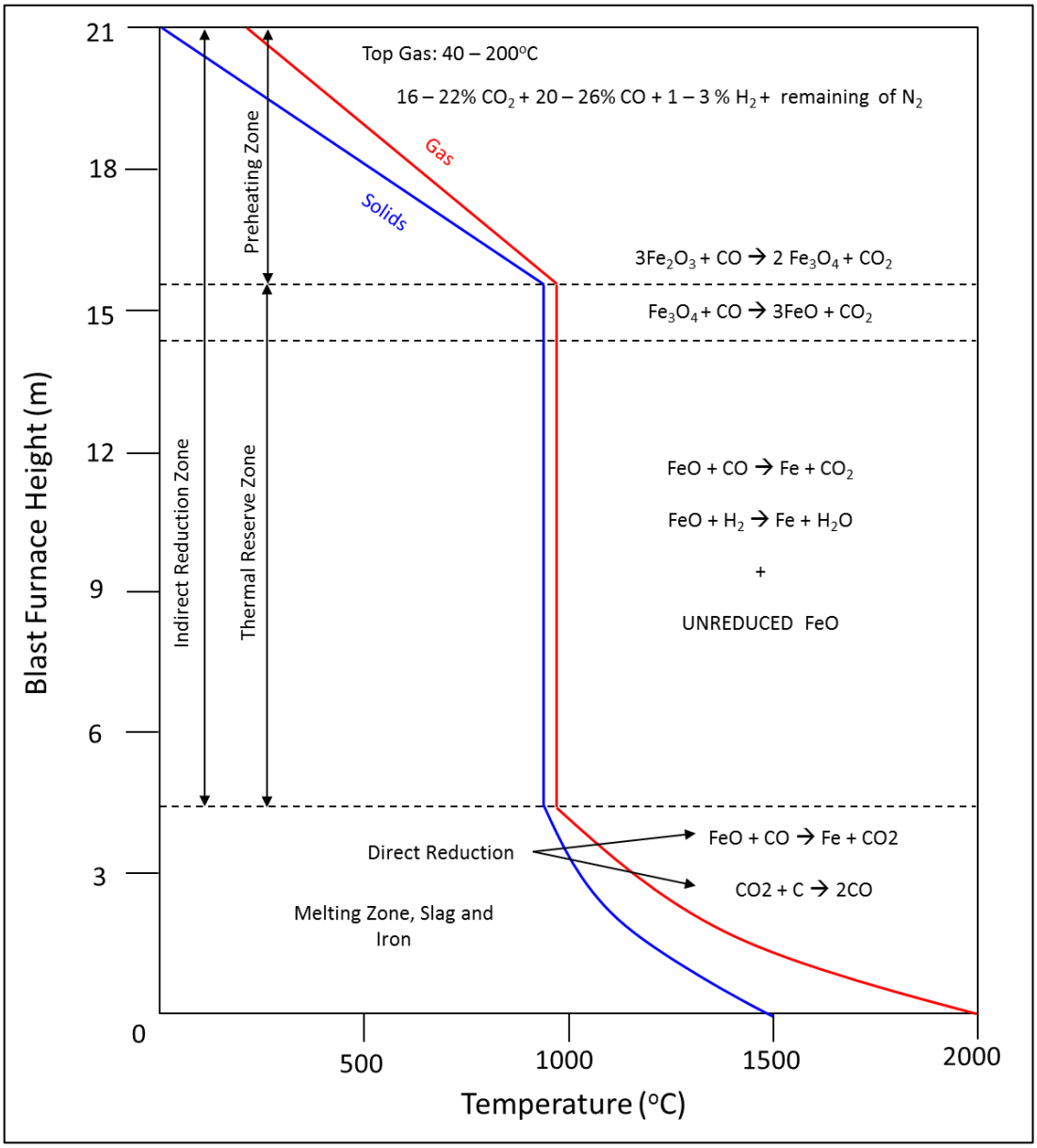

Figure 13: Schematic view of direct and indirect reduction areas in a blast furnace[7].

3.3.2. Kinetics

The study of reduction kinetics of agglomerates must encompass the ore's intrinsic mineralogical aspects, slag & induration characteristics. The contact level of gases and solid particles and certain characteristics of the system in which the reduction takes place, such as temperature and reducing gas composition are also of great importance[5,10].

For the reduction in the solid state, three steps are categorized:

1. Transport phenomena of the reducing gases (H_2 and CO) to the solid oxide and oxidized gases (H_2O and CO_2) are transported out from the reaction front.

2. The reduction reaction itself proceeds essentially at the phase boundary between solid oxide and gas.

3. As a result of the removal of oxygen from the surface of the solid phases and the accompanying transport phenomena, new solid phases such as lower iron oxides or metallic iron are being formed[(2)]

Firstly the reducing gas has to overcome an important resistance caused by the outer gas boundary layer. Difference in partial pressures is determinant to the diffusion through the outer gas boundary layer. The thickness of the boundary layer is inversely proportional to mass transfer and changes in flow rate are key drivers for its change.

After the gas boundary layer, the second transport mechanism is the gaseous diffusion into macro and micro-pores of an iron oxide. Macro (or intergranular) porosity relates to the voids in between iron ore grains whereas micro (or intergranular) porosity relates to the voids within each iron ore grain. The more porous the material the higher the reduction kinetics is and this is highly correlated to the geological characteristics or iron ores. Figure 14 illustrates the different porosity levels in both macro and microscopic views of two iron ore pellets derived from ores with different mineralogy.

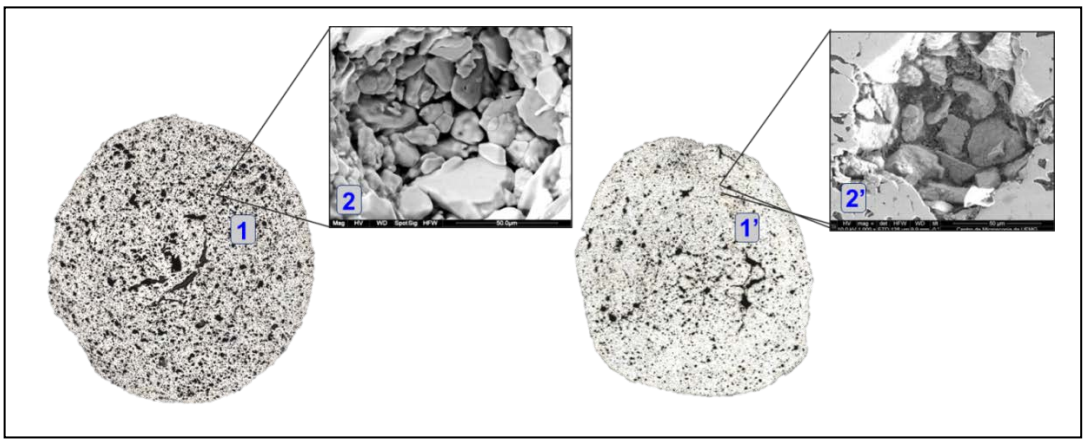

Figure 14: Different micro and macro porosities in iron ore pellets produced out of different ore minerals[(11)].

Reduction from Fe_2O_3 to metallic Fe takes place through the interfacial reaction or three-phase model, illustrated in figure 15. During the first reduction step from hematite to magnetite the crystal structure changes from hexagonal to face-centered cubic and from magnetite to wustite only the iron/oxygen ration is modified.

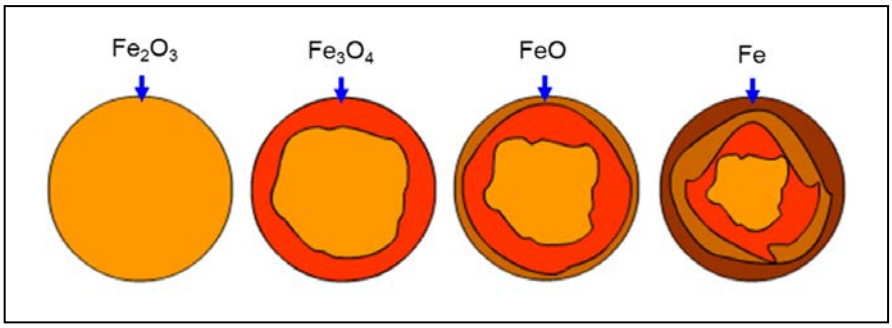

Figure 15: Topo-chemical reaction model for iron ore agglomerates.

3.4. Metallurgical influence of ferrous burden in a blast furnace operation

The blast furnace can be perceived as a dynamic system which consists of a set of inter-related hierarchical entities. Lower hierarchical entities influence and are influenced by higher hierarchical entities[12]. An example of the hierarchical levels and their relationship is depicted in figure 16, where the lower hierarchical entity is the ore's mineralogy and the higher one is the softening and melting zone and its final influence in the overall behavior of a blast furnace.

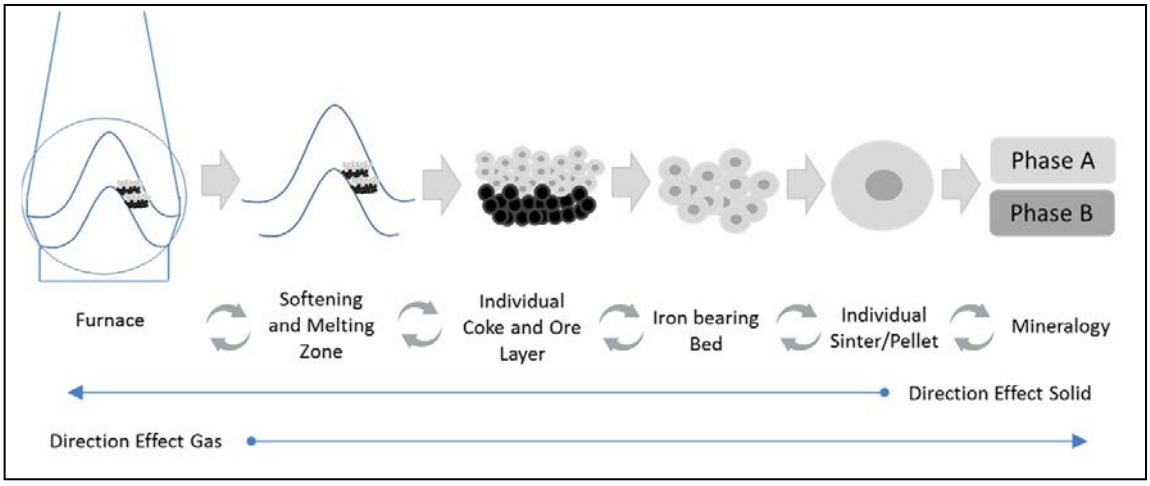

Figure 16: Hierarchical levels in a blast furnace and their relationship[12].

On a global furnace level, the burden permeability and charging pattern govern the distribution of gas, as well as heat transfer between gas and solids. However, this global furnace level influences, but is also influenced by the phenomena occurring at the deeper hierarchical level of the burden material.

As to categorize the behavior of iron ore pellets in one typical blast furnace operation, a classical zone division is adopted. Granular and cohesive zones will be the main focus of literature review as they are the subject matter of this dissertation. Dripping zone, raceway and hearth are also of great complexity and importance; however they will be described on a more generalist level. Figure 17 depicts blast furnace zone division and the metallurgical testing standards utilized for assessing the metallurgical behaviors of pellets and sinter in the granular and cohesive zones.

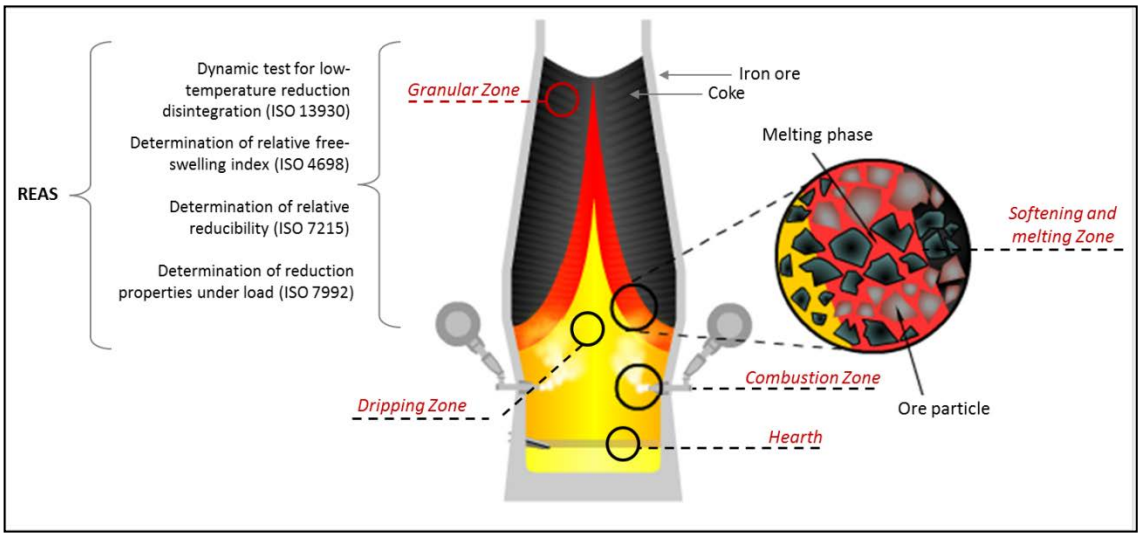

Figure 17: Typical zone division of a blast furnace and metallurgical testing standards applied in this study.

3.5. Granular zone

In the granular zone of a blast furnace all burden materials are in a solid state. It comprises intercalated layers of iron ore (mixture or pellets, sinter and lump according to the plant's operational standard) and coke. At the upper part of the granular zone, coke is inactive from a reduction point of view, however it plays an extremely significant role in heat and mass transfer, being the major responsible for the distribution of reducing gases in the stack. Permeability in the stack is a key driver for the kinetics of

reduction and the Ergun Equation describes the variables that influence pressure drop across a burden comprised of solid particles. This equation was proposed in the end of the 1940s and shows that two aspects influence delta P, one associated to viscous friction which prevails in the laminar regime and another associated to inertia which prevails in the turbulent regime[13]

$$\frac{\Delta P}{H} = \frac{150\,\mu\,(1-\varepsilon)^2 v_0}{\varepsilon^3 (\psi\ d_p)^2} + \frac{1{,}75\rho\,(1-\varepsilon)}{\varepsilon^3\,\psi\,d_p}(v_0)^2 \qquad 3.19$$

Through an analysis of the equation, the parameters that facilitate better permeability are void fraction, particle's size and sphericity (for the solid burden components) and lower viscosity, density and speed of gas. Various publications on permeability in a blast furnace stack have been made[12,14,15] and a simple but comprehensive example of the influence of a homogeneous burden size distribution is demonstrated in figure 18.

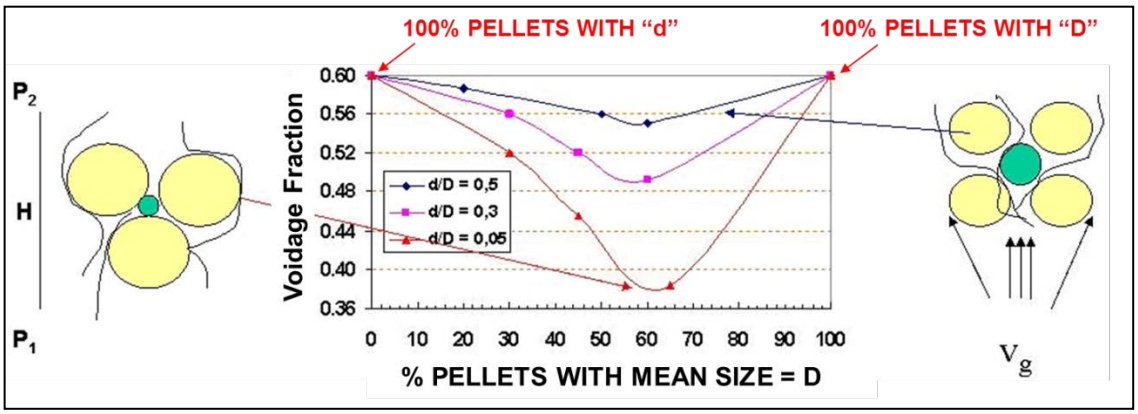

Figure 18: Influence of particles' size distribution in burden permeability[16].

The metallurgical phenomena applicable to pellets on a lower hierarchical level which can dictate different behaviors of the granular zone on a higher hierarchical level are related to degradation during reduction, reducibility and swelling.

3.5.1 Degradation during reduction at low temperatures

The major drawback of degradation during low reduction temperatures is related to fines generation, which may partly block voids in the solid burden, hindering the reducing gas passage as suggested in figure 18. Low degradation during reduction must be targeted even knowing that the biggest contributor to pressure drop is located deeper in the reactor in the cohesive zone.

As ferrous burden is fed in a blast furnace, it immediately starts the heat exchange with the upward gases, as described previously on figure 13. After moisture removal and yet at higher zones of the stack, hematite pellets undergo the first stage of reduction at the temperatures that range from 400 to 600^{o}C. The reduction of hematite into magnetite is marked by the structural lattice distortion, accompanied by anisotropic effects. The crystalline transformation from hexagonal hematite to cubic magnetite can generate a volume expansion to an extent of 25%[17,18,19]. At relatively low temperatures the single lattice elements cannot move easily and therefore the strain cracks the structure thus destroying the bonding of grains. Cracks are not only observed along the grain boundaries but can also extend inside the grain. The higher the reduction temperature the easier the elements can move and therefore less cracking is found[17].

Degradation during reduction is a phenomenon dependent on the hematite-magnetite conversion rate, residence time at a certain low temperature gradient and most importantly the bonding structure between grains. The bonds formed during the induration process of iron ore pellets can be classified into three groups: iron oxide bonds (bridge bonding), silicate bonds and calcium ferrite/ magnesium ferrite bonds[19,20,21]. Hematite bonds are the major responsible for providing pellets the high strength that enables handling, however they lose their stability when subject to reduction, whereas silicate bonds and ferrites tend to keep their structures, softening and melting later during the burden descent. This causes the major difference between the higher degradation at low reduction temperatures of acid pellets compared to fluxed pellets (either by CaO, MgO or a mix of both). The stabilization and reduction of pellets' degradation by increase of calcium oxide has been proved to work until a certain basicity level. Further increase in basicity will play minor effect on degradation due to the achievement of a cap of structural stabilization[18].

ISO (International Organization for Standardization) has developed the testing standard 13930 entitled dynamic test for low temperature reduction-disintegration[22] and it has

helped pellet suppliers and blast furnace operators to distinguish pellets according to this phenomena.

3.5.2. Reducibility

As described, at the granular zone of a blast furnace the indirect reduction takes place bringing ferrous burden components from their higher oxidation level to wüstite or metallic Fe, until softening temperatures are reached. On the deepest hierarchical level, ore mineralogy and chemistry of slag compounds formed during induration will play a significant role in the kinetics of reduction.

After the oxidizing atmosphere of a pellet induration process the majority of the iron oxide is in the form of hematite and FeO levels are below 1.0%. However, the mineralogy of various pellet feed sources can significantly differ, generating structures that are more or less favorable for reduction. Highly porous minerals like goethite and martite (porous hematite) will generate more reducible structures after induration when compared to specular hematite and magnetite.

The reducibility of different compounds present in one iron ore agglomerate has also been investigated. Results of synthetic mineral components point at the increase of reduction capacity of calcium ferrites with greater number of calcium moles and, on the other hand, to extremely poor reducibility of fayalite (Fe_2SiO_4) as per table I – 3 [23].

Table I – 3: Reducibility of synthetic mineral components of a sinter[23].

Oxide	Reducibility (%)	Silicate	Reducibility (%)
Fe_2O_3	49.4	Fe_2SiO_4	5.0
Fe_3O_4	25.5	$(Ca_{0.15}Fe_{0.85})_2SiO_4$	11.2
$Fe_{3-x}Ca_xO_4$ ($x \geq 0.04$)	30.0	$(Ca_{0.30}Fe_{0.70})_2SiO_4$	11.4
$Fe_{3-x}Ca_xO_4$ ($x \geq 0.12$)	37.6	$(Ca_{0.40}Fe_{0.60})_2SiO_4$	12.3
$Fe_{1-x-y}Ca_xO$	27.0*	$CaFeSiO_4$	12.8
$CaFe_2O_4$	49.2	$Ca_2FeSi_2O_7$	6.8
$Ca_2Fe_2O_5$	25.5		
$CaFe_4O_4$	58.4		
$Ca_3Fe_{15}O_{25}$	59.6		
$CaFe_3O_5$	51.4		

Very acid agglomerates can have the solid state diffusion as controlling mechanism of the last reduction stage, whereas fluxed agglomerates have interfacial chemical reaction as controlling stage[24]. Early softening characteristics of silicates of low

melting points (occurring mostly on acid pellets without CaO or MgO) can impose resistance to reducing gas passage thereby retarding the reaction[18,21].

For iron ore pellets, the ISO 7215 standard for determination of relative reducibility[25] is commonly utilized for quality differentiation.

3.5.3. Swelling

The first stage of reduction, from hematite to magnetite, is characterized by volume expansion and the issues related to this lattice distortion were already highlighted in the discussion over low temperature disintegration. This section will be more deeply focused on the second swelling mechanism characterized by the growth of fibrous iron (whiskers).

The problems of excessive swelling are related to the subsequent degradation or disintegration of the partly-reduced pellets, which may lose stability under the pressure of a compacted burden. This leads to the generation of fines that can hinder the furnace permeability.

Swelling of iron ore pellets occurs during the transformation of wüstite into iron, but like any transformation, this is a balance between iron nucleation and growth of these nuclei[8]. Generally the normal swelling (~20%) for the reduced pellets is a very common phenomenon in blast furnaces, but catastrophic swelling may reach over 400% under some conditions[26]. Characteristics of pellets (chemical composition, porosity and microstructure), their induration (temperature and time) and reduction conditions (reduction temperature, flow rate) influence the swelling phenomenon[26,27].

- Pellet induration characteristics: homogeneous firing and sufficient energy for the bridge bonding of ore grains are required for low swelling indexes.

- Reduction atmosphere: at H2 atmospheres no abnormal swelling is noticed whereas CO rich atmospheres lead to whisker formation.

- Reduction temperature: critical temperatures for swelling are at the range of 900 to 1000^{o}C.

- Chemical composition of pellets: the increase of overall gangue contributes to higher slag formation and reduction of swelling. For the achievement of low-slag pellets without the risk of the catastrophic growth of whiskers during reduction, fluxing agents CaO and MgO contribute to better stability of the agglomerate. Figures 19 (Burghard diagram) and 20 denote the effects of overall slag, binary basicity and MgO contents on swelling.

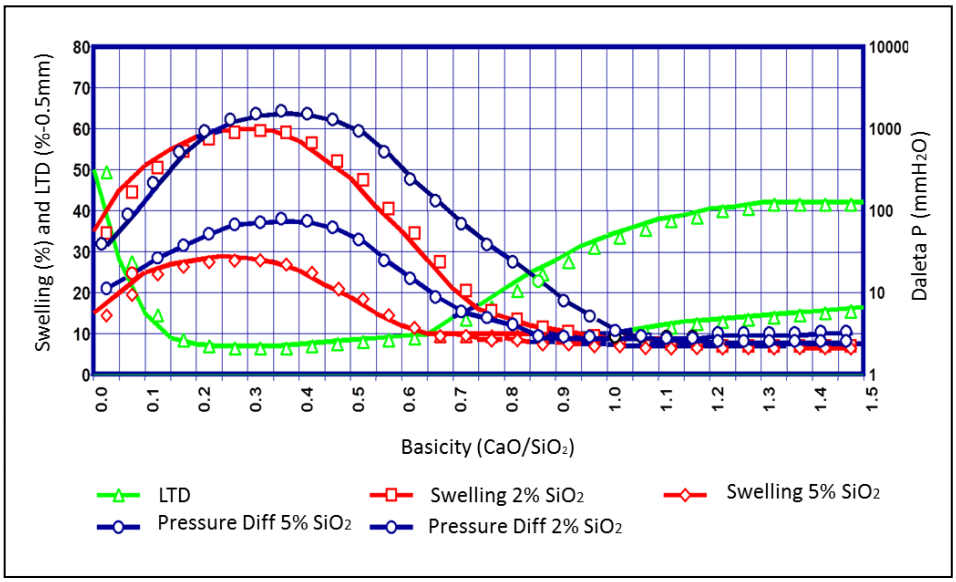

Figure 19: Burghard diagram for swelling and Delta P as function of silica content and basicity.

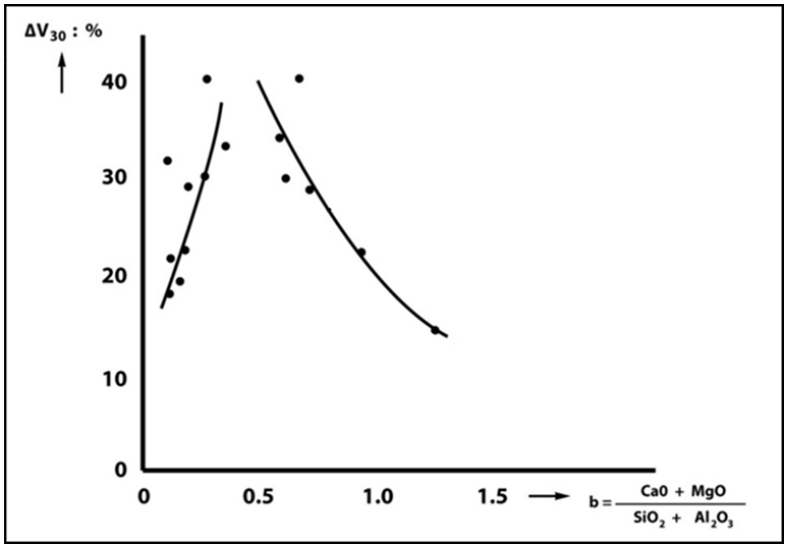

Figure 20: Influence of quaternary basicity in swelling index[8].

ISO has defined one metallurgical standard test for characterization of pellets in relation to their swelling tendency based on volume prior and after reduction conditions that favors the phenomena: ISO 4698 determination of relative free-swelling index[28].

As so far disclosed, permeability in the granular zone is core for smooth blast furnace operations. Another ISO methodology also aims at distinguishing metallurgical property of pellets encompassing aspects of degradation at first steps of reduction, growth of fibrous iron, shrinkage and behavior near softening: ISO 7992 – reduction under load[29].

It is valid to state that no ISO methodology serves the purpose of simulation; however they offer a very good standardized way to differ pellets on their metallurgical behaviors.

3.6. Cohesive (softening and melting) zone

As the ferrous burden continues its descent in the shaft, it will reach softening and melting temperatures. A common approach defines the upper and lower boundaries of the cohesive zone as two isotherms (e.g. 1200 – 1500^{o}C). However, temperature is not an objective criterion for describing the limits of the softening and melting zone. Since the permeability distribution is the aspect of key importance at a global level, it is more obvious to define the boundaries of the softening and melting zone based on this aspect[12]. In this zone the metallic burden loses its permeability and gas flow occurs only through the coke layers[30]. On a low hierarchical level, the high temperature properties of the ferrous burden largely control the shape, width and position of the cohesive zone. The latter is also affected on a higher hierarchical level by the burden distribution, in particular ore to coke ratio and temperature distribution in the blast furnace. It is important to have the roof of the cohesive zone deep in the blast furnace as to prevent gas flow close to the wall and to minimize coke rate. It is also of great importance to have a thin cohesive zone since it is the major contributor to pressure drop. This can be achieved with smallest gradient of temperatures between the start of softening and end of melting stages[30,31,32].

The permeability loss is basically caused by the deformation of particles through the pressure of the burden column, occupying the voids in the bulk. Different phenomena

occur at the same time: the softening and melting of the oxide phase and the softening and melting of the metallic iron phase.

Softening and melting of the oxide phase is extremely influenced by the slag composition and the morphology of the compounds formed. The presence of iron oxide (wustite) also plays a very significant role in the phenomena due to the low liquidus temperature of compounds comprising FeO.

Softening of metal phase is very dependent on the thickness of the metallic shell and its capacity to resist the direct contact with coke particles, which leads to the cementitization phenomena.

If a stepwise description of the softening, melting and dripping of the ferrous burden would be established, the first phenomena to trigger the process would be the melting of the oxide phase with lowest melting point within the agglomerate, which will act as a “lubricant” to the other ore particles. At this stage reduction kinetics is compromised as the liquid slag film imposes difficulty to the transport phenomena of gases. When the burden reaches the cohesive zone of a blast furnace, reduction will already have taken place in a way that a film of metallic Fe around the ore will be present. The metallic Fe film is called metallic shell, which at this moment is the major responsible for confining the mixture of solid and liquid oxides together. The strength of the iron shell will tend to be compromised by effects taking place at both of its extremities. On its internal side the increasing temperatures will lead to higher participation of liquid phases, which tend to penetrate the iron shell as this movement reduces the overall free energy. On its external side the continuous carburization leads to the formation of cementite, which generates cracks in the iron shell structure. The softening will be finally defined when the metallic burden can no longer resist the action of mechanical forces and the iron shell cracks open, promoting the exudation phenomena of liquid phases[12,30].

Various studies have been conducted to evaluate the influence of slag components in softening and melting characteristics of pellets[12,21,30-41]. The addition of FeO up to 20% mass in a design of experiment containing CaO-SiO2-MgO-Al2O3 synthetic slags significantly decreases the softening and melting temperatures of the system[34]. Acid pellets without MgO have overall inferior softening and melting characteristics due to the formation of FeO-rich low melting fayalitic liquidus slag. The increase in basicity exhibited increased softening temperatures and low softening-melting range due to the formation of burden slag with high liquidus temperature[21,35].

High MgO bearing pellets at both levels of binary basicity (CaO/SiO_2) increase overall softening and melting properties, due to high melting point of slag which keeps the pores open for the reduction to continue[21].

Alumina in the ore lowers the temperature at which primary melt forms in sinter. It would pose difficulties to permeability and continuation of indirect reduction[36].

Softening and melting experiments are not standardized by ISO due to their complexity. They can differ significantly in the ways of accessing the phenomena of a blast furnace cohesive zone. For tests which evaluate a bulk behavior such as the REAS[36] utilized in this dissertation, the interaction between different burden components at high temperatures can be studied[30,31,37,38,39,40,41]. Previous studies considering the interaction of acid & basic and acid & MgO fluxed pellets[30,38,39] point at similar softening temperatures, but the same did not apply for dripping and meltdown temperature each of the pellet types individually. The addition of DRI to a mixed burden has the increase of the cohesive zone's width as an important side effect, however at the same time its blending with pellets/lump ores improves dripping temperature[31,40,41]. Burden interaction and melt exudation phenomenon is influenced by the reduction characteristics of pellets, morphology of iron shell, slag distribution, its basicity and viscosity. A mechanism of burden interaction encompasses four steps: sintering of solid phases at interface of pellets, incipient liquid slag formation, interaction of liquid at interface and interaction of core of material[41].

3.7. Dripping zone

In the dripping zone the droplets of iron and slag descend towards the hearth. It can be divided into active coke and inactive coke (dead man) zones. In the active coke zone, the carbon of the coke will reduce the remaining iron oxides already in the liquid phase. This mechanism will also lead to carburization of the dripping metal. The largest quantity of the coke will descend for further consumption in the raceway and a small part will move into the dead man (or inactive coke zone). The dead man is formed by the remaining coke that is not consumed in the raceway. It will slowly be refreshed by dissolution into the molten iron, which facilitates the last minute reduction of remaining FeO in the slag.

3.8. Raceway

The combustion zone (or raceway) is the area where the hot blast containing oxygen is injected through the various tuyeres of a blast furnace. Hot blast at very high speed will generate a semi-void area where most of coke and PCI coal are gasified and oxidized, increasing the temperature to over 2,000^{o}C.

3.9. Hearth

The hearth area comprises the lowest part of the blast furnace. Its main function is the temporary storage of hot metal and slag for controlled timeframes before the tapping process. The dead man extends itself to this zone and it has the important role of sustaining the burden load. At the same time it also has to be permeable for the liquid phases to be drained smoothly through to the tapping hole(s).

4. Materials and methods

As to assess the metallurgical characteristics of Samarco pellets and their interaction with a typical Western European Sinter, an extensive set of laboratory methodologies were used at both Samarco Ponta Ubu – Brazil and SGA, Liebenburg – Germany, which are described in this section.

For an evaluation of only intrinsic properties of Samarco pellets and Western European sinter, it was decided to produce both agglomerates in pilot plants. This decision has helped to eliminate any misleading interpretation of quality results caused by standard deviation from an industrial pellet or sinter plant operation.

4.1. Pellet production in a pilot scale

As intakes for blast furnace pellets, Samarco utilizes bentonite, limestone and anthracite. Bentonite improves pelletizing efficiency by promoting additional binding characteristics during green balling. Limestone will control the pellets' basicity levels for adequate metallurgical characteristics and improved firing conditions through the

generation of slag (which is not the major driving force for fired pellets' resistance, but improves the bridge bonding of pellet feed grains). Anthracite will enhance induration by providing more homogeneous firing of pellets from inside out through its ignition.

Firstly the raw materials to be used as feed mix for pellet production were cautiously sampled and characterized according to their chemical and physical characteristics. An x-ray fluorescence apparatus (XRF) was used for the complete chemical analysis of pellet feed, anthracite, bentonite and limestone. Figure 21 depicts the XRF apparatus at Samarco Mineração.

Figure 21: XRF apparatus for chemical characterization of raw materials.

The overall quality aspects of pellet feed, anthracite limestone and bentonite are presented in table I – 4. Specific testing on inferior calorific value, volatile matter and ash content was made in the anthracite sample. For the pellet feed, an important mineralogical characterization through optical microscopy was made as to quantify the participation of main ore types and silica in its composition. The latter characterization is extremely important as mineralogy plays significant role in the agglomerate's final metallurgical properties. Figure 22 depicts the optical microscopy apparatus for mineralogical characterization of pellet feed and table II – 4 presents the mineralogical results.

Table I – 4: Characterization of raw materials for pellet production.

	Pellet Feed	Limestone	Anthracite	Bentonite
Fe%	66.2	-	4.43	-
FeO%	0.47	-	-	-
SiO_2%	1.69	4.78	51.12	59.41
Al_2O_3%	0.41	0.52	30.17	15.94
CaO%	0.09	49.25	2.9	1.31
MgO%	0.03	3.52	1.5	2.54
P%	0.048	-	-	-
LOI%	2.93	40.8	-	-
Fixed Carbon%	-	-	71.59	-
Volatiles%	-	-	12.37	-
Ash%	-	-	16.04	-
Calorific value (cal/g)	-	-	6658	-
+ 100 #	0	11.4	12	95% <200 #
- 100 + 200 #	0.4	17.5	17	
- 200 + 325 #	2.2	15.8	12.5	
- 325#	90	55.3	58.5	

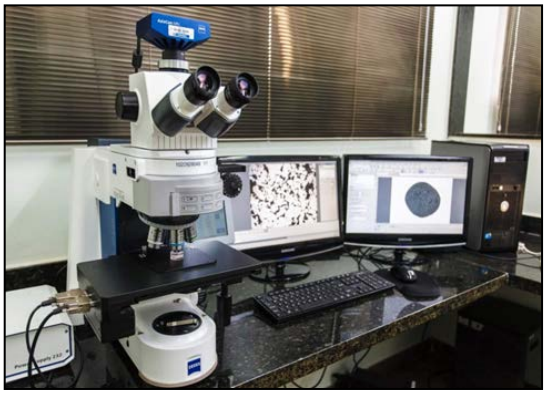

Figure 22: Optical microscopy apparatus.

Table II – 4: Mineralogical characterization of Samarco's pellet feed through optical microscopy.

Mineral type	Percentage
Specular Hematite	51.38%
Porous hematite	30.59%
Goethite	14.81%
Magnetite	3.12%
Free quartz	0.10%
mixed quartz	0.00%

All characterization results presented good adherence to the usual qualities utilized in industrial scale, therefore the samples were considered suitable for the undertaking of pilot tests.

4.1.1. Pressure grinding - roller press

The pilot pressure grinding consists of two counter-rotating rolls mounted in frictionless bearings, enclosed in a frame. Pressure is applied to one of the rolls by means of a hydro-pneumatic spring system, while the other roll is held in a fixed position in the frame. The “free” or “floating” roll is allowed to slide (or float) on frictionless pads, reacting to the forces acting on the roll by the material and the spring system. Feed to the rolls is done through a hopper mounted above them. This apparatus is in line with similarly designed industrial equipment present in between the filtering and mixing stages at each of Samarco’s four pellet plants. Figure 23 depicts the pilot roller press apparatus.

Figure 23: Samarco’s pilot roller press.

The pressure grinding roller press has the role of adjusting size and specific surface of the pellet feed particles for improved balling properties. Figure 24 shows the change in size distribution of a typical pellet feed from Samarco when subject to this process stage. Figure 25 depicts the microscopic aspect of the ore grains with 1700cm^2/g compared to 2400cm^2/g when subject to scanning electron microscopy analysis.

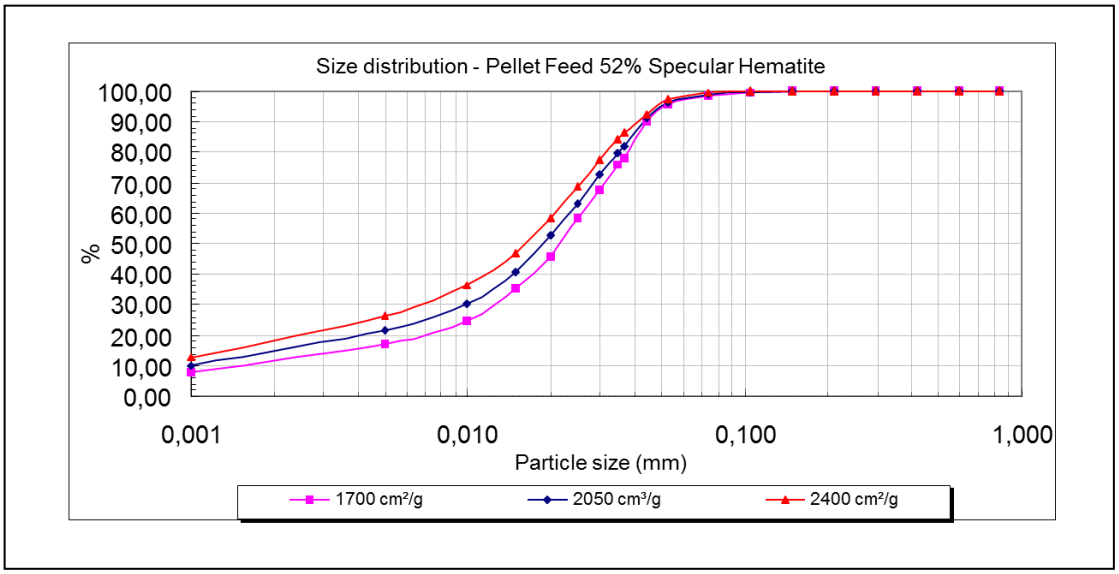

Figure 24: Change in size distribution of Samarco's pellet feed when subject to the pilot roller press[42].

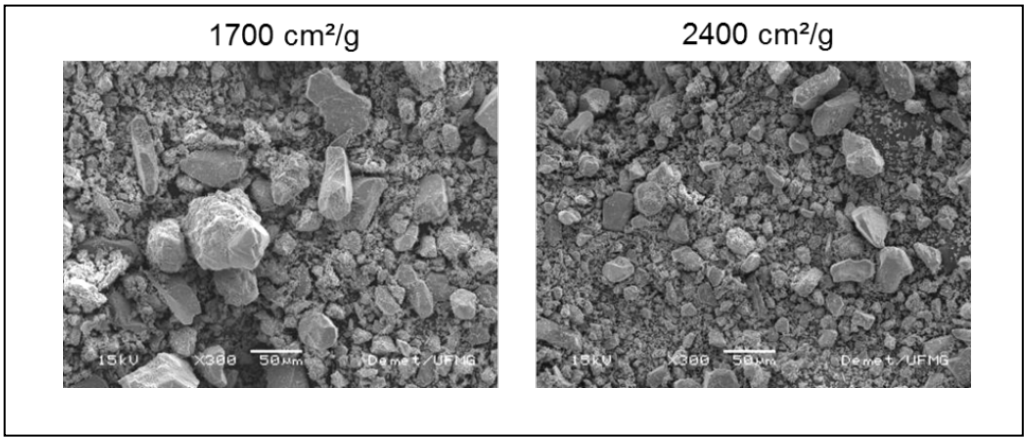

Figure 25: Change in the aspect of the iron ore particle's size through SEM analysis[42].

4.1.2. Pilot mixing

Mixing is a very important step during the preparation of raw materials. The amounts described on table I – 4 are homogeneously mixed through a batch-type Eirich intensive mixer. Homogeneity in the distribution of solid fuel, fluxing agent, binder and iron ore particles is essential for an efficient balling and induration processes. Good mixing will therefore cope with the achievement of homogeneous quality of the fired

pellets. Table III – 4 describes the percentage of intakes mixed on a dry basis and figure 26 depicts the pilot mixing equipment.

Table III – 4: Percentage of mixed intakes on a dry basis.

Pellet type	Participation in the feedmix (% Dry basis)			
	Pellet Feed	Bentonite	Anthracite	Limestone
PBFMB45	96.6%	0.4%	1.4%	1.7%
PBFSTD	94.8%	0.4%	1.4%	3.4%
PBFHB	94.1%	0.4%	1.4%	4.1%

Figure 26: Samarco's batch-type pilot mixer.

4.1.3. Pilot disc

The balling process will enable the formation of green pellets. At Samarco, iron ore particles must have typically 10.5% moisture for an efficient balling. These particles involved by a water film start touching each other and liquid bridges are formed due to the surface tension of water. Due to the rotating movement of the disc, the union of several water coated particles will take place, generating the first agglomerates. The residence time of the agglomerate in the pelletizing disc enable the liquid bridges to become a network that holds the particles together. Water capillarity and the effective action of bentonite enable the growth of the agglomerate until the desired size distribution. Figure 27 depicts a schematic view of the water surface tension in a green pellet.

On this specific pilot test, balling productivity and final size distribution were not a matter of concern. The standard pot test utilizes a fixed ratio 50% between 16 and 12.5mm and 50% between 12.5 and 9mm and main objective was replicating the quality of fired pellets of Samarco's portfolio. The disc's slope, rotating speed, feeding rate and position were chosen to provide the most homogeneous green pellets for the induration stage. Figure 28 depicts Samarco's pilot balling disc.

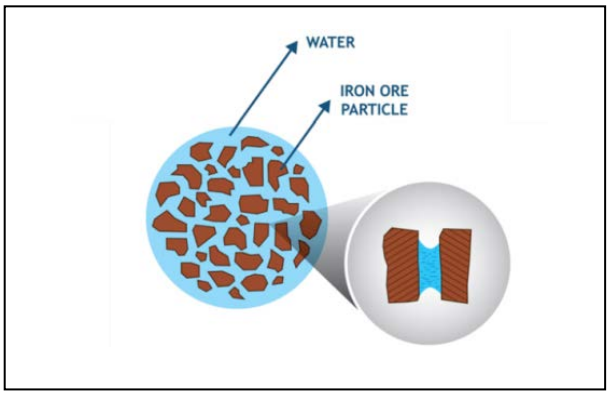

Figure 27: Schematic view of green pellet formation.

Figure 28: Samarco's pilot disc.

4.1.4. Pilot induration machine

Samarco's pot grate is designed to simulate the thermal cycle utilized industrially in the induration process of green pellets. It has been utilized for extensive R&D work throughout the company's history and has been already described elsewhere[42]. Figure 29 depicts the equipment and its main components.

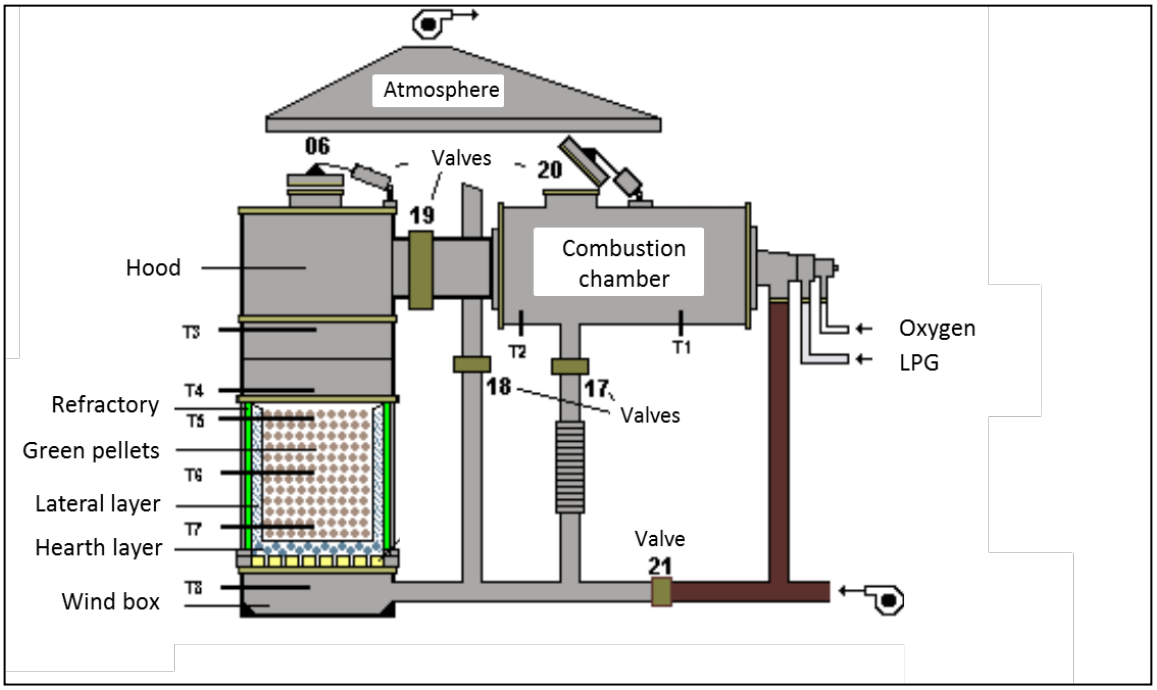

Figure 29: Schematic view of the pot grate furnace.

The major components of the pot grate are:

Combustion chamber: where liquefied petroleum gas is ignited for the heating of process gas. The heated airstream is injected in the pot either on updraft or downdraft flows, depending on the stage of induration to be simulated.

Pellet pot: is the recipient where the green pellets are placed for the induration simulation. The Pot has refractory lining and three thermocouples in different height levels for the monitoring of temperature throughout the process.

Wind box: is situated underneath the pot, where occurs the passage of hot air responsible for the updraft drying, cold air responsible for the cooling and the gases deriving from the downdraft drying and firing.

Hood: is placed above the pot and its function is to conduct the heated air to the top of the pellet burden during downdraft drying and firing stages and conduct the updraft air from the updraft drying and cooling stages to the furnace's exhausting system.

Control system: is a computer system that allows the simulation of residence time of pellets in the drying, firing and cooling zones, as a function of production rhythm and thermal profiles established in each process stage.

Temperature measurement system: is comprised of a set of thermocouples for the measurement of temperatures in all regions of the furnace. The thermocouples T4, T5, T6, T7 and T8 measure the temperatures of hood, burden layers and wind box, respectively.

Control valves: are responsible for adjusting the gas flow for the simulation of the induration process.

Figure 30 depicts Samarco's pot grate furnace and its peripherals.

Figure 30: Pot grate apparatus.

4.1.4.1. Preparation of green pellets for induration in the pot grate

The preparation of the pot is an important stage of the testing process. As to minimize the effects of the size distribution of pellets in the gaseous flow, the pot is prepared as follows:

Hearth layer, with a height of 7cm, is filled in with indurated pellets of 16mm diameter.

A lateral protection layer is also made through the use of pellet screenings (pellet chips) with size distribution from 3.15 to 8mm.

Green pellets produced in the pilot balling disc are classified in two size ranges (50% between 16 and 12.5mm and 50% between 12.5 and 9mm) and homogenized thereafter. The homogeneous mix is placed in the pellet pot.

4.1.4.2. Induration of green pellets in the pot grate

After the preparation of the burden, the green pellets will undergo the induration process according to the defined setup.

The temperature profile of the superior pellet layer (thermocouple T5), intermediate layer (thermocouple T6), inferior pellet layer (thermocouple T7) and wind box (thermocouple T8) are monitored during induration. Figures 31, 32 and 33 show the actual results during the production of PBFMB45, PBFSTD and PBFHB, respectively.

During the production of any of the pellet types, the difference of temperatures in superior, intermediate and inferior pellet layers is intrinsic of the simulation of a traveling grate process. The superior pellet layer is exposed to the higher temperatures and is kept for the most extended time in the same temperature range. At the end of the induration the inferior pellet layer presents the lower temperature.

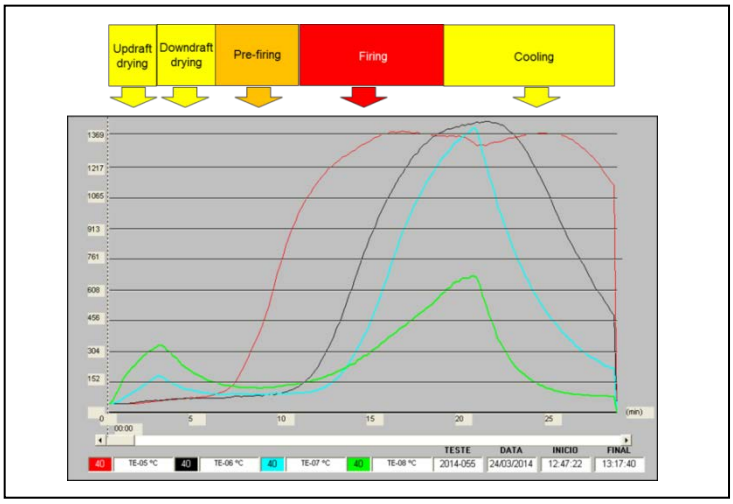

Figure 31: Temperature profile of the pellet pot layers during induration test of PBFMB45.

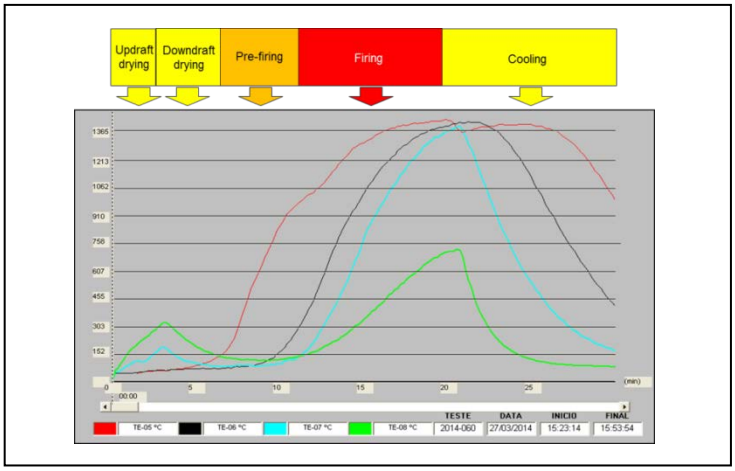

Figure 32: Temperature profile of the pellet pot layers during induration test of BFSTD.

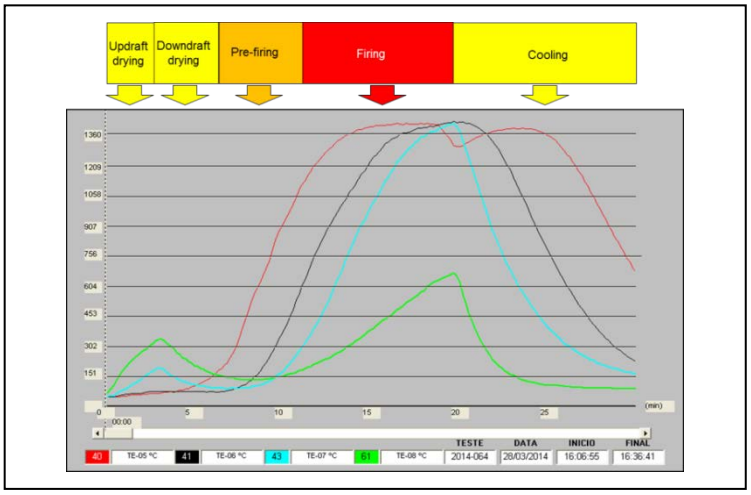

Figure 33: Temperature profile of the pellet pot layers during induration test of PBFHB.

4.2. Chemical characterization of pellets

Chemical characterization of the indurated pellets was conducted according to ISO standards. The chemical analysis was made through the use the Plasma ICP/OES apparatus depicted in figure 34.

Figure 34: Plasma – ICP/OES apparatus.

4.3. Physical characterization of pellets

Physical testing methodologies were also utilized for assessing the capacity to endure handling of the three pellet types produced at pilot scale.

4.3.1. Determination of crushing strength

This standard indicates a method to determine the crushing strength of fired iron ore pellets. It measures the value of the compressive load applied to an individual pellet to cause breakage in a compression test. A compressive load is applied to 100 pellets of size -12.5 +10mm separately, at a constant platen speed between 10mm/min and 20mm/min, until the pellet is broken. The crushing strength is the maximum load attained in the test. Figure 35 depicts a cold compression strength machine at Samarco's laboratory.

Figure 35: Cold compression strength testing apparatus.

4.3.2. Determination of the tumble and abrasion indices

This standard indicates a method to evaluate the resistance to degradation by impact and abrasion in a rotating drum. It measures the tumble strength and abrasion index of iron ores. A 15kg test portion is placed in a tumble drum and rotated at 25rpm, for a total of 200 revolutions. The product material is screened and the tumble index is expressed as the mass percentage of material greater than 6.3mm, and the abrasion index as the mass percentage of material smaller than 0.5mm. Figure 36 depicts a tumble drum at Samarco's physical characterization laboratory.

Figure 36: Tumble drum testing apparatus.

4.4. Metallurgical testing methodologies for pellets

The metallurgical testing standards were conducted for an assessment of the behavior of the three pellet types in the granular and cohesive zones of a blast furnace.

4.4.1 Dynamic test for low-temperature reduction-disintegration

This standard indicates a method to test the disintegration pellets during reduction in a rotation tube at a temperature of 500ºC. In the process, a 0.5kg test portion is heated in a 10rpm rotating tube at a temperature of 500ºC, using reducing gas at a flow rate of 20l/min, consisting of 20% of CO, 20% of CO_2, 2% of H_2 and 58% of N_2 for 60 minutes. Then, the test portion is cooled to a temperature below 100 ºC and screened with test screens of 6.3mm, 3.15mm and 0.5mm. The low-temperature disintegration (LTD) values are calculated as a quantitative measure of the degree of disintegration of an iron ore sample that has been reduced while tumbling: the percentage masses of material greater than 6.3mm, smaller than 3.15mm and smaller than 0.5mm, respectively, are related to the total mass of the test portion after reduction. Figure 37 depicts an LTD testing apparatus at Samarco's metallurgical laboratory.

Figure 37: Low-temperature disintegration testing apparatus at Samarco's metallurgical laboratory.

4.4.2. Determination of relative reducibility

This standard indicates a method to determine the reducibility in relative terms of pellets. It measures the extent to which oxygen has been removed from iron oxides. In the process, a 0.5kg test portion of iron ore is heated under a flow of inert gas at a rate of 5l/min. When the temperature approaches 900ºC, the flow rate is increased to 15l/min for 30 minutes. The mass of the test portion is measured and the gas is replaced by reducing gas, consisting of 30% of CO and 70% of N_2 at a flow rate of 15l/min. After 3 hours, the mass is measured again and nitrogen inserted at a flow rate of 5l/min until the test portion is cooled to 100ºC. The degree of reduction is calculated from the loss in mass and the total iron content of the test portion. Figure 38 depicts a reducibility testing apparatus at Samarco's metallurgical laboratory.

Figure 38: Reducibility testing apparatus at Samarco's metallurgical laboratory.

4.4.3. Determination of relative free-swelling index

This standard indicates a method to determine the relative free-swelling index of pellets during reduction under isothermal heating in an unconstrained state using a gaseous reductant. In the process, a test portion of 18 pellets is heated using inert gas at a flow rate of 10 l/min. When the temperature approaches 900ºC the flow rate is increased to

15l/min and a reducing gas consisting of 30% of CO and 70% of N_2, replaces the inert gas at the same flow rate for 60 minutes. After that, the test portion is cooled to a flow rate of 5l/min and the free-swelling index is calculated as percentage, using the difference between the final and initial volumes. Figure 39 depicts a swelling testing apparatus at Samarco's metallurgical laboratory.

Figure 39: Swelling testing apparatus at Samarco Mineração's metallurgical laboratory.

4.4.4. Determination of reduction under load

This standard indicates a method to evaluate physical stability of pellets measuring the change in the differential gas pressure across a bed of pellets and the change in the height of the bed during reduction under load. In the process, a 1.2kg test portion of iron ore is heated with a load of 50kPa applied on the pellet layer and inert gas at a flow rate of 50l/min. When the temperature approaches 1050ºC, the flow rate is increased to 83l/min and the reducing gas, consisting of 40% of CO, 2% of H_2 and 58 % of N_2, is introduced. From the beginning of passing the reducing gas, it is calculated the differential gas pressure and the height of the test bed at an 80% degree of reduction. The furnace that performs the reduction under load test has the same configuration of picture 39 from the outside, however with a different assembling of a retort on the inside.

4.5. Sinter production in a Pilot Scale

This study aims at understanding not only the metallurgical behavior of Samarco pellets alone, but also when they are mixed with a typical Western European sinter at proportions usually observed in industrial blast furnaces. For this purpose a representative sample form a typical Western European industrial sinter was reproduced in the pilot plant of SGA in Germany. In this specific case, the blend of ore fines and other intakes, productivity and final quality were all selected according to industrial characteristics of Western European sinter plants. For a typical ore blend in a Western European sinter, ores from Brazil (north and south systems), Canada, Mauritania, as well as BF return fines, were selected in the proportions described in table IV – 4.

Table IV – 4: Mix of sinter feed and BF returned fines utilized for the production of the typical Western European sinter sample.

Ore type	Participation in blend
Brazilian Sinter Feed (North System)	40%
Brazilian Sinter Feed (South system)	35%
BF Return fines	10%
Canadian Concentrate	8%
Mauritanian Concentrate	7%

Similarly to the pellet case, all intakes were fully characterized according to their chemical and physical qualities through ISO standards. Results are presented in tables V – 4 and Table VI – 4.

Table V – 4: Quality characteristics of the sinter fines utilized for the production of the typical Western European sinter sample.

Designation		Brazilian sinter feed (North System)	Brazlian sinter feed (South System)	BF return fines	Canadian concentrate	Mauritanian Concentrate
Chemical analysis						
Fe_{tot}	[%]	65,32	63,79	56,01	65,64	65,36
FeO	[%]	0,20	0,76	7,86	11,26	26,88
SiO_2	[%]	2,42	5,47	5,33	4,39	7,26
Al_2O_3	[%]	1,14	0,78	1,44	0,18	0,55
CaO	[%]	0,06	0,34	11,95	0,45	0,41
MgO	[%]	0,07	0,17	0,65	0,47	0,55
P	[%]	0,016	0,047	0,031	0,006	0,013
S	[%]	0,005	0,005	0,032	0,007	0,023
Na_2O	[%]	0,030	0,004	0,019	<0,005	0,051
K_2O	[%]	0,025	0,015	0,050	<0,005	0,081
Mn	[%]	0,670	0,150	0,460	0,132	0,030
TiO_2	[%]	0,056	0,059	0,084	0,036	0,170
V	[%]	0,004	0,005	0,005	0,004	0,002
L.O.I	[%]	1,82	1,69	0,53	1,64	0,38
Size distribution						
+25 mm	[%]					
+20 mm	[%]					
+18 mm	[%]					
+16 mm	[%]		1,4 / 1,4			
+12.5 mm	[%]	5,7 / 5,7	1,0 / 2,4			
+10 mm	[%]	0,6 / 6,3	1,6 / 4,0	0,0 / 0,0	0,0 / 0,0	0,1 / 0,1
+8 mm	[%]	1,9 / 8,2	2,6 / 6,6	0,3 / 0,3	0,0 / 0,0	0,0 / 0,1
+6.3 mm	[%]	3,4 / 11,6	5,9 / 12,5	10,2 / 10,5	0,0 / 0,0	0,1 / 0,2
+5,0 mm	[%]	5,1 / 16,7	6,4 / 19,0	27,4 / 37,8	0,0 / 0,0	0,1 / 0,3
+4,0 mm	[%]	1,1 / 17,8	2,1 / 21,1	13,5 / 51,3	0,0 / 0,0	0,0 / 0,3
+3.15 mm	[%]	7,4 / 25,2	7,0 / 28,1	12,7 / 64,0	0,0 / 0,0	0,1 / 0,4
+2.5 mm	[%]	9,5 / 34,7	8,0 / 36,1	14,5 / 78,6	0,1 / 0,1	1,1 / 1,5
+1.0 mm	[%]	12,3 / 47,0	8,1 / 44,3	9,7 / 88,3	2,1 / 2,2	7,4 / 8,8
+0.5 mm	[%]	7,6 / 54,6	5,2 / 49,5	4,8 / 93,1	5,4 / 7,6	13,6 / 22,4
+0.315 mm	[%]	7,2 / 61,7	3,1 / 52,6	2,2 / 95,3	13,8 / 21,5	13,9 / 36,4
+0.200 mm	[%]	5,9 / 67,6	5,0 / 57,7	1,5 / 96,8	22,0 / 43,4	14,8 / 51,2
+0.160 mm	[%]	3,0 / 70,5	3,6 / 61,3	0,0 / 96,8	0,0 / 43,4	0,0 / 51,2
+0.100 mm	[%]	4,6 / 75,1	7,5 / 68,8	1,3 / 98,2	37,1 / 80,5	19,2 / 70,4
+0.063 mm	[%]	3,0 / 78,1	0,6 / 69,4	0,5 / 98,6	14,3 / 94,8	9,4 / 79,8
+0.040 mm	[%]	1,7 / 79,8	16,7 / 86,1	0,3 / 98,9	3,4 / 98,2	6,2 / 85,9
+0.025 mm	[%]	2,5 / 82,3	4,5 / 90,7	0,2 / 99,1	0,6 / 98,8	4,3 / 90,2
+0 mm	[%]	17,7 / 100,0	9,3 / 100,0	0,9 / 100,0	1,2 / 100,0	9,8 / 100,0

Table VI – 4: Quality characteristics of the raw materials utilized for the production of the typical Western European sinter sample.

Designation		Limestone	Olivine	Coke breeze	Burnt lime
Chemical analysis					
Fe_{tot}	[%]	0,25	6,25	1,32	0,25
FeO	[%]	0,15	5,31	-	<0,1
SiO_2	[%]	0,96	41,00	6,82	1,79
Al_2O_3	[%]	0,20	0,61	3,36	0,29
CaO	[%]	54,90	0,43	0,95	94,70
MgO	[%]	0,50	47,50	0,20	1,16
P	[%]	0,003	0,002	0,037	0,005
S	[%]	0,020	0,014	0,700	0,052
Na_2O	[%]	0,010	0,030	0,170	0,060
K_2O	[%]	0,050	0,045	0,220	0,060
Mn	[%]	0,030	0,084	0,007	0,054
TiO_2	[%]	0,010	0,013	0,160	0,013
V	[%]	<0,001	<0,001	0,007	<0,001
L.O.I	[%]	43,02	1,34	86,05	1,54
Size distribution					
+25 mm	[%]				
+20 mm	[%]				
+18 mm	[%]				
+16 mm	[%]				
+12.5 mm	[%]			0,3 / 0,3	
+10 mm	[%]	0,0 / 0,0	0,0 / 0,0	1,1 / 1,4	
+8 mm	[%]	0,0 / 0,0	0,1 / 0,1	1,7 / 3,2	
+6.3 mm	[%]	0,0 / 0,0	0,3 / 0,5	4,9 / 8,1	
+5,0 mm	[%]	0,1 / 0,1	1,3 / 1,7	8,8 / 16,9	
+4,0 mm	[%]	0,2 / 0,2	1,1 / 2,9	8,1 / 25,0	
+3.15 mm	[%]	2,3 / 2,6	2,5 / 5,3	9,9 / 34,8	
+2.5 mm	[%]	21,3 / 23,9	4,1 / 9,4	15,6 / 50,4	
+1.0 mm	[%]	28,9 / 52,7	8,4 / 17,8	15,9 / 66,4	
+0.5 mm	[%]	15,4 / 68,1	7,3 / 25,1	9,4 / 75,8	
+0.315 mm	[%]	9,0 / 77,1	23,1 / 48,3	4,4 / 80,2	
+0.200 mm	[%]	6,2 / 83,3	14,6 / 62,9	4,0 / 84,2	
+0.160 mm	[%]	0,0 / 83,3	0,0 / 62,9	2,1 / 86,3	
+0.100 mm	[%]	4,8 / 88,1	17,3 / 80,2	3,8 / 90,1	
+0.063 mm	[%]	1,2 / 89,3	6,9 / 87,1	2,7 / 92,9	
+0.040 mm	[%]	0,5 / 89,8	4,1 / 91,1	2,1 / 95,0	
+0.025 mm	[%]	0,7 / 90,5	2,2 / 93,3	1,6 / 96,6	
+0 mm	[%]	9,5 / 100,0	6,7 / 100,0	3,4 / 100,0	

4.5.1. Apparatuses utilized in the pilot sintering plant

Ignition hood: uses a combination of air and natural gas for igniting the top layer of the sinter mix in the sinter pot, enabling the combustion zone to be initiated.

Sinter pot: a refractory lined pot with perforated bottom in which the sinter mix is placed. Gases will be soaked through the bed enabling the sintering process.

Suction chamber & waste gas fan: are responsible for the downdraft suction of gases through the sinter cake, enabling the combustion zone to travel through the sinter pot's height.

The overall process setups are described in VII – 4. Figure 40 depicts a schematic view of the apparatus.

Table VII – 4: Sinter pot overall design and process characteristics.

Pot Grate	450 mm, height 600 mm
Bed Height	520 mm, including 20 mm hearthlayer
Ignition Time	90 seconds
Ignition Temperature	1220 ^{o}C
Ignition Suction	increasing from 40 to 160 mbar
Sintering Suction	160 mbar
Sintering treatment for return fines generation	tumbling (70 revolutions)
Return fines screening	6.3mm

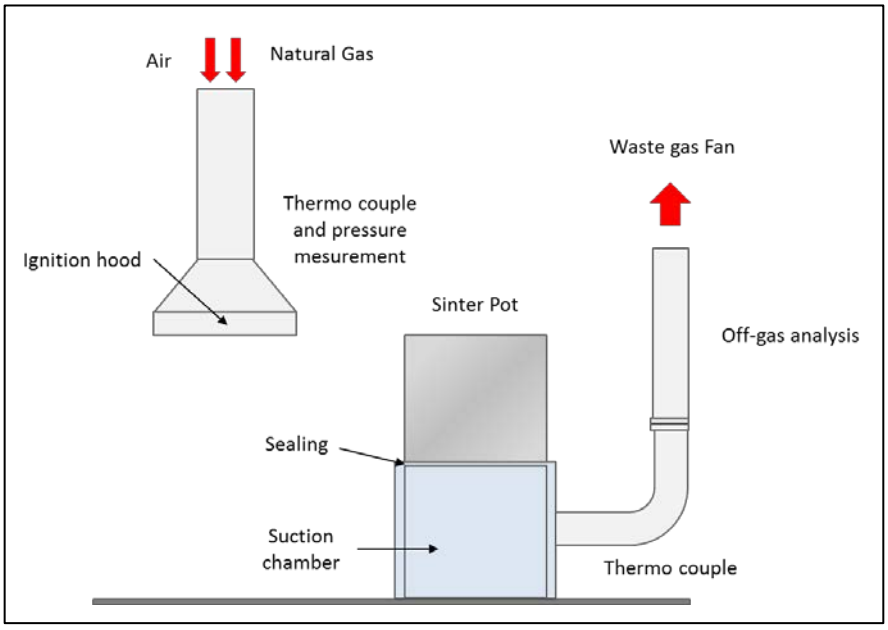

Figure 40: Schematic view of a sinter pot.

4.5.2. Process description

Burnt lime was added to improve the sintering performance at 0.8%. Initial tests were performed to adjust a balanced return fines ratio of 0.95 - 1.05. At balanced return fines ratio and correct FeO-content, the sinter feed moisture was varied to achieve optimum productivity. The ore blends were prepared as follows:

- mixing of all ores and additives in a Cyclos mixer for 4 minutes at natural moisture

- Addition of water

- Mixing for another 2 minutes

- Rerolling in a drum for 3 minutes. As drum a conventional cement mixer drum type is used without mixing tools (shovels) and equipped with two lifters of 3 cm width. After the sinter mixture was formed, the material was placed in the sinter pot for ignition. As the ignition takes place, the waste gas fan promotes a pressure differential which “soaks” atmospheric air through the sinter cake, allowing the combustion zone to travel through the sinter pot. Figure 41 depicts the assembled sinter pot and ignition hood and sinter pot right after the ignition process and table VIII – 4 describes the sinter pot process characteristics.

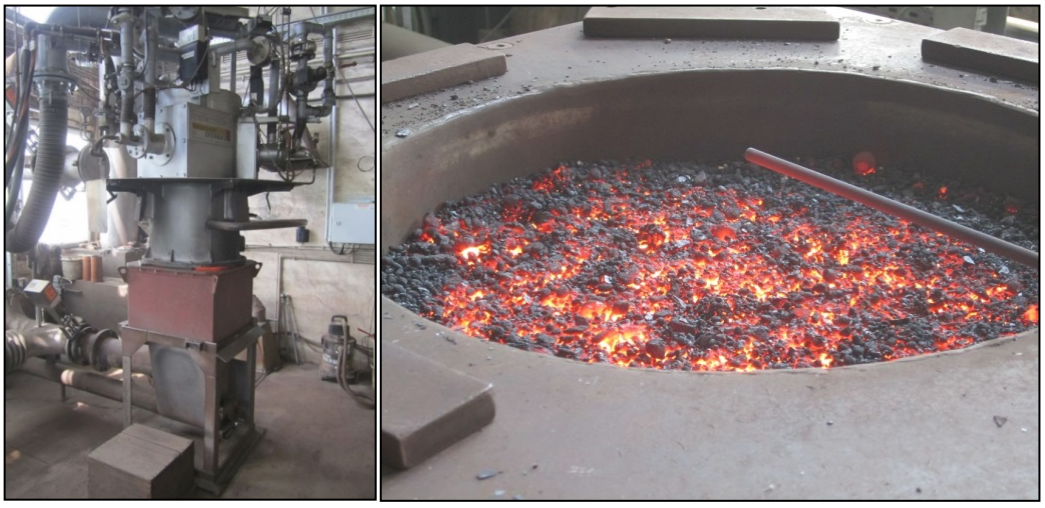

Figure 41: Sinter pot with ignition hood and pot after ignition.

Table VIII – 4: Process characteristics during pilot production of the typical Western European Sinter sample.

Sintering conditions										
suction at ignition / sintering		[mbar]	40 to 120 / 160							
ignition time / temperature		[sec.] / [°C]	90 / 1220							
net bed height / hearthlayer		[mm] / [mm]	500 / 20							
sinter treatm., tumbling and screening		[rev] / [mm]	70 / 6,3							
Mixture										
Samarco Pellet screenings		[pts] / [%]	**0.00**	**/**	**0.00**					
Brazilan Sinter N. System		[pts] / [%]	40.00	/	32.29					
Brazilian Sinter S. System		[pts] / [%]	35.00	/	28.25					
BF return fines		[pts] / [%]	10.00	/	8.07					
Canadian Concentrate		[pts] / [%]	8.00	/	6.46					
Mauritanian Concentrate		[pts] / [%]	7.00	/	5.65					
		subtotal	*100.00*		*80.73*					
Limestone		[pts] / [%]	19.95	/	16.10					
Olivine		[pts] / [%]	1.66	/	1.34					
Sand		[pts] / [%]	1.27	/	1.03					
Burnt lime		[pts] / [%]	0.99	/	0.80					
		[pts] / [%]	**123.88**	**/**	**100.00**					
test No.			S17633	S17634	S17635	S17636	S17639	S17641	S17638	S17640
sinter mixture		[pts]	100.00	100.00	100.00	100.00	100.00	100.00	100.00	100.00
water		[pts]	7.00	9.50	9.55	9.55	9.70	9.90	10.10	10.40
Coke		[pts]	4.00	4.50	5.40	5.60	5.60	5.60	5.60	5.60
return fines	(dry)	[pts]	RF-Test	32.00	32.00	32.00	32.00	32.00	32.00	32.00
sinterfeed	(wet)	[pts]	111.00	146.00	146.95	147.15	147.30	147.50	147.70	148.00
moisture content of sinter feed		[%]		5.7	5.6	5.6	5.8	6.0	6.2	6.5
Sintering data										
ignition temperature		[°C]		1220	1220	1220	1220	1220	1220	1220
ignition energy		[MJ/t f.s.]		199	204	201	202	205	199	200
sintering temp. 40% bed height		[°C]		n.b.	n.b.	n.b.	n.b.	1320	n.b.	1335
volume of waste gas										
at 60% of test time		[Nm³/h]		275	270	265	235	275	285	280
at end of test		[Nm³/h]		650	640	760	740	775	615	735
temperatures at end of test										
grate bar		[°C]		570	615	625	525	590	645	600
waste gas		[°C]		475	530	525	605	480	465	485
sintering rate		[mm/min]		19.5	19.8	18.9	19.2	20.3	19.5	19.4
sintering time = t [Tmax + 1 min]		[min]		25.6	25.3	26.5	26.0	24.6	25.6	25.8
coke consumption		(kg/t FS)		51.8	62.4	64.6	64.7	65.4	65.4	64.6
total energy [ignition and sintering]		[MJ/t f.s.]		1728	2043	2105	2111	2133	2127	2106
shrinkage of sinter cake		[dH %]		5.0	11.0	8.0	10.4	8.2	6.4	5.4
return of sintered fines		[%]		86.9	86.6	86.7	86.5	85.7	85.7	86.7
Yield		[%]		57.0	72.2	73.2	74.6	73.9	74.3	70.5
return sintered fines balance [RO/RI]		[%]		167.0	107.9	104.0	98.1	100.4	98.8	114.3
final sint. productivity at [RO/RI=100]		[t/m²·24h]		34.9	34.6	33.5	34.0	35.4	35.0	34.6
Magnetite content (presample)		[%]			*15.2*	*17.5*	*19.1*	*20.2*	*21.3*	*20.0*
FeO content (presample)		[%]			*5.5*	*6.5*	*6.9*	*7.3*	*7.5*	*7.2*
Remarks: ***evaluation of chem., phys. and metallurg. propert						z		***		
Size distribution of sintermixture			> 3.15 mm	< 1.0 mm	< 0.1 mm	< 0.04 mm				
Ores		[%]	26.4	56.1	24.7	14.2				
Ores + additives		[%]	21.8	55.8	23.1	14.1				
Ores + additives + coke		[%]	22.4	54.7	22.4	13.6				
Ores + additives + coke + return fines		[%]	28.9	46.9	18.2	10.6				

Figure 42: Sinter cake before crushing.

4.6. Metallurgical testing of pellets, sinter and their mixtures through the softening and melting apparatus (REAS)

The REAS test enables investigation of the reduction, softening, melting and dripping behavior of the blast furnace burden: pellets, sinters, and lump ores as well their mixtures with the particle size in the range 10–12.5 mm.

When the column of burden materials descends through a blast furnace it starts to soften and melt due to increasing temperature and progressive reduction. As a result of the softening and melting of the burden, gas permeability of the blast furnace decreases in the cohesive zone. This results in an increase of pressure drop in the lower part of the furnace. For an efficient operation, it is important to have the cohesive zone deep into the Blast Furnace. This can be achieved by charging the materials that possess superior high temperature characteristics and smaller softening-melting temperature interval. An appropriate selection of the burden materials in relation to their softening and melting behavior is therefore of great importance for a stable operation.

The REAS test gives indications of blast furnace process conditions in the following zones:

- Shaft, where indirect reduction of iron oxides with CO takes place;

- Cohesive zone, where softening and melting of the burden material occur.

- Active coke zone, where direct reduction with carbon from coke and dripping of the liquid over coke slits takes place.

The REAS test set-up has been described elsewhere[37] and consists of the main sections for gas supply, online analysis of the input and off gas, furnace control, furnace itself and data recording. The furnace is electrically heated, with a maximum operating temperature of about 1600°C. The maximum temperature reached in the sample is between 1510°C and 1540°C, depending on the sample nature and test duration.

An outer retort with opening diameter of 110mm and an inner retort with opening diameter of 92mm both made of Alsint (99.7% Al_2O_3) and gas-tight are mounted within the furnace. The inner retort serves as a holder for the test sample. The perforated bottom of the sample holder allows the passage of input gas to the sample as well dripping of liquid phases from the retort to the melt collector. The test sample is packed as a 60mm high column between two graphite layers into the sample holder. As the objective of the test is the evaluation of metallic burden materials, graphite is used in replacement of coke as source of carbon for direct reduction. The graphite layers have a thickness of 25mm.

The temperature of the sample is measured with a Pt–Pt /Rh thermocouple positioned at half of its height. Another Pt–Pt/Rh thermocouple mounted inside the furnace measures the furnace temperature and serves as a sensor for the furnace temperature program. The pre-heated input gas is introduced to the sample through the space between the two retorts and it reaches the sample passing through the holes in the bottom of the sample holder. The change in the input gas composition is automatically done by a previously defined gas program. A constant load of 1 kg/cm^2 on the sample is designed to represent the weight of the burden column. During testing various data are recorded and stored on a computer. Temperature in the furnace and temperature in the sample are continuously measured and online displayed during the test. The inlet and off gas are online analyzed for their CO and CO_2 contents. These analyses serve as the base data for calculation of reduction index (%) and reducibility (%/min). Shrinkage of the sample (%) and differential pressure over the sample (mmWG) are recorded in order to evaluate softening behavior of the sample. Also, the total mass dripped off during the test is continuously measured with the help of a digital balance.

The REAS test consists of two phases: the indirect reduction in which the sample is reduced with a reduction gas and the phase of direct reduction where the partially reduced sample undergoes further reduction by the carbon from the graphite.

Before the beginning of the test and data acquisition, the sample is heated under nitrogen to 450°C. When this temperature is reached, the phase of indirect reduction begins by the introduction of a reducing gas in the test. In the indirect reduction phase, the sample is heated from 450 to 900°C at a rate of 10°C/min. Then, the temperature is kept constant at 900°C for 100 min as a tentative reproduction of the thermal reserve zone of a Blast Furnace. The initial composition of reducing gas is 25% CO, 15% CO_2, 60% N_2. At 55 min of test time the reducing gas composition is changed to 35% CO, 5% CO_2, 60% N_2. The increase of CO% in the input gas, aims at reproducing the change of the gas composition during the descent of the burden in the blast furnace shaft. After 150 minutes indirect reduction ends, reduction gas is turned off and only nitrogen is fed in the testing retort.

During the phase of direct reduction, the temperature is constantly increased at a rate of 5°C/min until the end of the test. Due to increasing temperature and progressive reduction, the sample starts to soften, whereby the differential pressure over the sample increases. The flow rate of the input gas through the sample retort during the test is kept at 1800l/h until the differential pressure of 200mmWG is reached. At this moment, a gas bypass is opened and the gas (nitrogen) volume fed to the sample is reduced, corresponding to a differential pressure of approximately 25mmWG. This prevents blowing out of molten material. Upon completion of the test, the furnace and the sample remainder are left to cool down under nitrogen flow. Table IX – 4 summarizes the data recorded in the REAS. Figures 43 and 44 depict the schematic view and an actual picture of the testing apparatus.

Table IX – 4: Data recorded through the conduction of the REAS softening and melting

Data	Unit
1. Furnace temperature	(° C)
2. Sample temperature	(° C)
3. Total gas flow	(l/h)
4. CO-content of the inlet gas	(% by vol.)
5. CO-content of the outlet gas	(% by vol.)
6. CO2-content of the inlet gas	(% by vol.)
7. CO2-content of the outlet gas	(% by vol.)
8. Shrinkage of the sample	(%)
9. Differential pressure	(mmWG)
10. Differential pressure /actual sample height	(mmWG)
11. Reducibility	(%/min)
12. Reduction index	(%)
13. Dripped mass	(g)

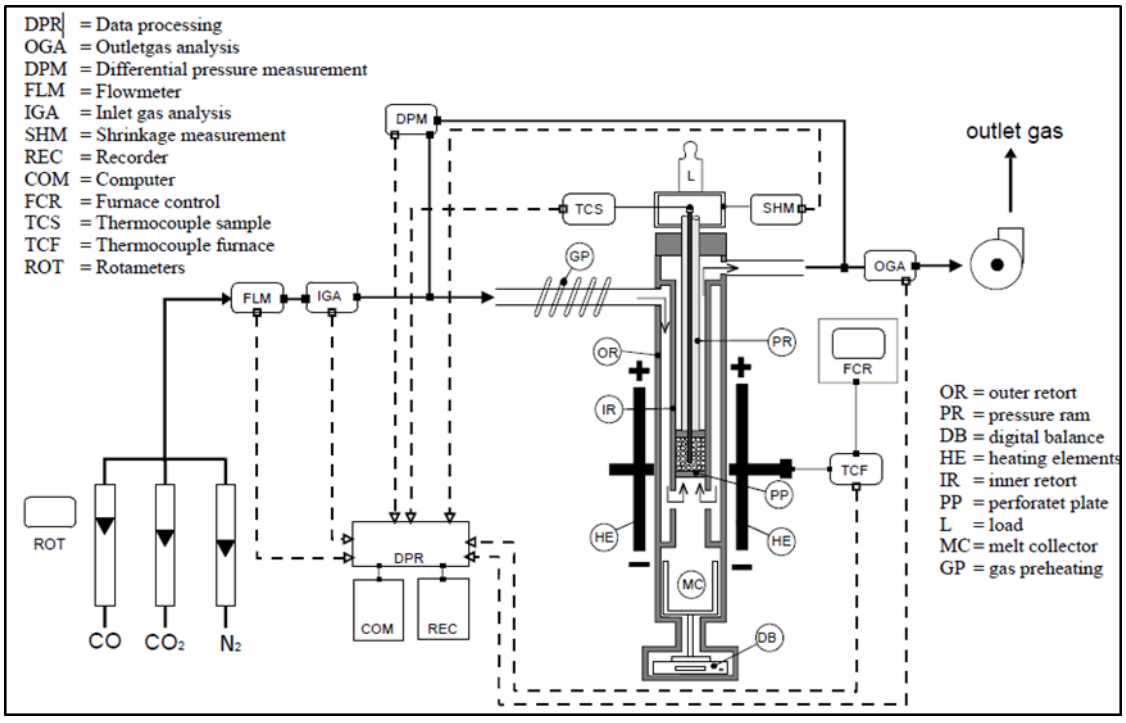

Figure 43: Schematic view of the REAS testing apparatus.

Figure 44: REAS testing apparatus at SGA.

In order to understand the metallurgical characteristics of Samarco's pellet portfolio during softening, melting and dripping, as well as its interaction with a typical Western European sinter, a set of ten REAS tests were conducted. Pellets and sinter were firstly tested individually and afterwards mixed in the ratios 20%/80% and 40%/60%, respectively. These burden percentages are in line with industrial records of utilization of Samarco pellets in European blast furnaces. Table X – 4 depicts the design of experiment.

Table X – 4: Design of experiment for the REAS test.

REAS - Softening and Melting test			
Agglomerate type	**100%**	**20% Pellet 80% Sinter**	**40% Pellet 60% Sinter**
High Basicity Pellet (PBFHB) CaO/SiO_2 = 1.0	x	x	x
Standard Basicity Pellet (PBFSTD) CaO/SiO_2 = 0.8	x	x	x
Medium Basicity Pellet (PBFSTD) CaO/SiO_2 = 0.45	x	x	x
Typical Western European Sinter	x		

4.7. Microscopy characterization

As to understand the phenomena that lead to different metallurgical behavior of different pellet types and sinter, a thorough microstructural investigation has been made in the oxides (pellets and sinter) and also partly reduced pellets after metallurgical testing. Apart from the already described optical microscope, also the scanning electron microscope (SEM) was used for phase, morphology and chemical (EDS) characterization. Figure 45 depicts Samarco's SEM used in the study.

Figure 45: Scanning electron microscope at Samarco's laboratories.

5. Results and discussions

5.1 Chemical and physical characteristics of Samarco pellets and typical West European Sinter

At Samarco's industrial process, the concentrate production is uniform in chemical and sizing aspects. The product differentiation takes place in the pellet plants where adjustments of limestone dosage will provide binary basicities of 0.45, 0.8 and 1.0 to PBFMB45, PBFSTD and PBFHB, respectively. The three pellet types therefore have similarly low percentages of acid gangue and deleterious elements but will differ in calcium oxide and Fe levels. The typical Western European sinter produced in pilot scale is comprised of a major participation of Brazilian sinter feed and smaller contribution of Canadian and Mauritanian concentrates. It has significantly higher gangue content and consequently lower Fe% if compared to pellets. Higher gangue in sinter is expected and at a certain extent required as it has major contribution to the binding mechanism of this agglomerate. The difference of FeO percentages is also noticeable between the three pellet types and sinter. The full oxidizing atmosphere of a pellet induration process will promote nearly all the ore to the highest oxidation level (Fe_2O_3), even if magnetite concentrates are used. The sinter production comprises a semi-fusion which is partly oxidizing and partly reducing, depending on the position of the material in relation to the combustion zone on a sinter strand. For this reason, the sinter cake is not entirely reoxidized into Fe_2O_3 and, in fact, percentages of FeO from 7 to 10% are targeted as this item is also related to the agglomerate's strength and metallurgical behavior. Table I – 5 presents the difference in chemistry of the iron oxides evaluated in this study.

Table I – 5: Chemical characterization of Samarco blast furnace pellets and typical Western European Sinter.

	MB45	**STD**	**HB**	**Sinter**
Fe (%)	67.20	66.82	66.53	56.26
FeO (%)	0.17	0.17	0.14	7.26
SiO2 (%)	1.92	1.93	1.94	5.97
Al2O3 (%)	0.50	0.51	0.51	1.04
CaO (%)	0.90	1.56	1.92	11.60
MgO (%)	0.11	0.16	0.19	1.03
P (%)	0.049	0.050	0.050	0.03
S (%)	0.002	0.003	0.004	0.02
Na2O (%)	0.019	0.020	0.020	0.02
K2O (%)	0.009	0.008	0.008	0.04
Mn (%)	0.07	0.06	0.07	0.29
TiO2 (%)	0.05	0.05	0.05	0.07
V2O5 (%)	0.00	0.00	0.00	0.00
B2 (-)	0.49	0.80	0.99	1.94

Although different basicities of pellets will lead to different slag compositions and microstructural aspects, the physical characteristics of Samarco's three blast furnace products are similar. This is possible because the biggest driver for pellets' strength is associated to the bridge bonding phenomena, or "welding" of iron ore particles. In the case of sinter, slag volume, basicity and targeted FeO levels are of great importance for strength. Figure 46 depicts the homogeneous cold compression strength of the three blast furnace pellet types produced in pilot scale even with their different basicity levels. In this case they were not compared to sinter as this ISO standard is only applicable to pellets.

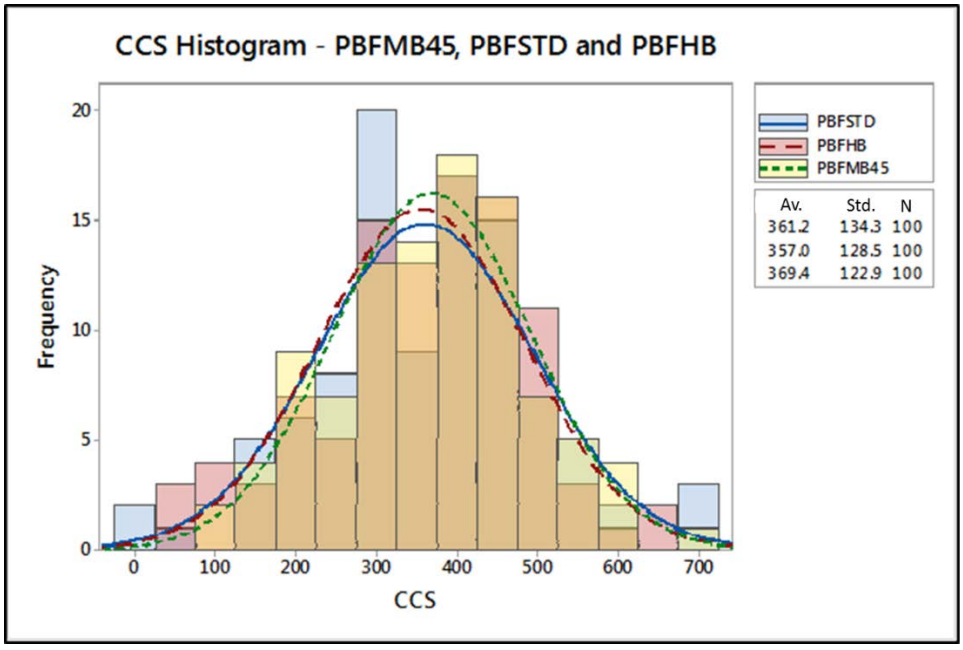

Figure 46: Cold compression strength of Samarco's three pellet types in the size range 16 to 12mm.

In the tumble results, it can be noticed the higher capacity of pellets to absorb impacts of low magnitude when compared to sinter. Based on the CCS and tumble results it is reasonable to state that pellets tend to preserve high yield of on-size material (above 6.3mm) to be fed in the blast furnace, even when the fines generated through seaborne transportation are considered. The generation of abrasion fines (below 0.5mm) was similar between sinter and the three pellet types. Figure 47 depicts the tumble +6.3mm and abrasion -0.5mm results for pellets and sinter.

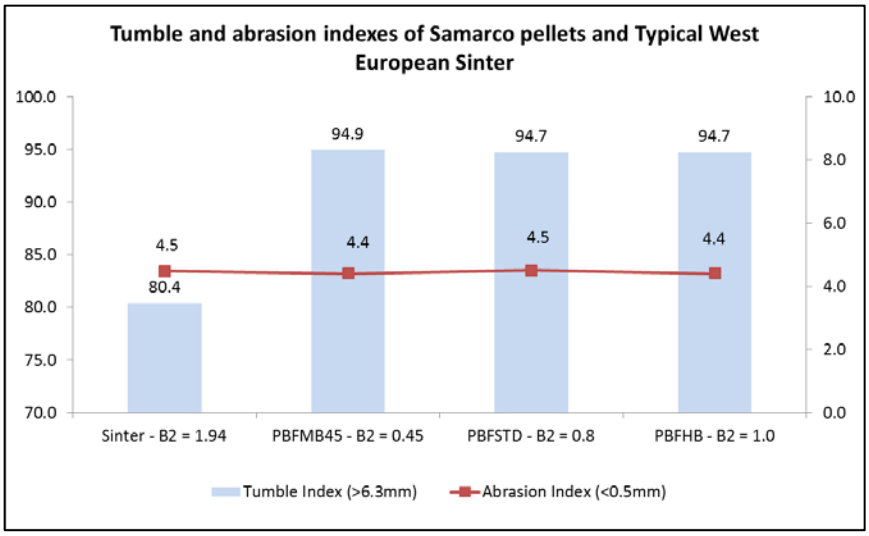

Figure 47: Tumble and abrasion indexes of Samarco blast furnace pellets and typical Western European Sinter.

5.2 Microstructure of oxide pellets

One representative sample from each pellet type was carefully chosen by having the most proximal CCS result from the average of the lot produced in the pilot plant. These samples were embedded in bakelite resin and polished until a clear crossed section was formed for image analysis. Figure 48 depicts an image of the three pellet types for the start of the microscopy analysis.

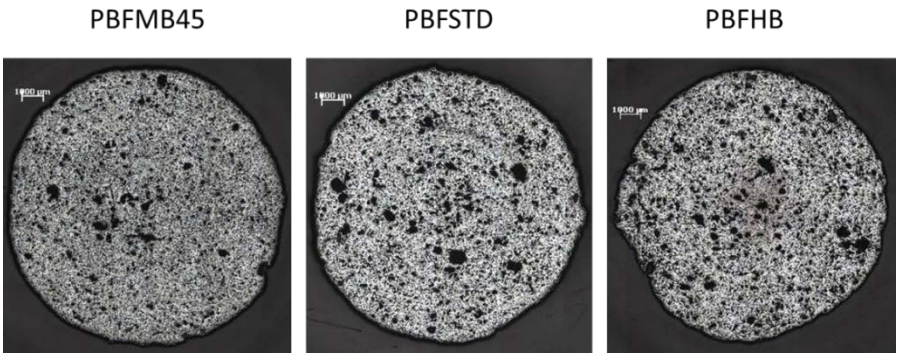

Figure 48: Embedded pellet samples for microscopy analysis.

5.2.1 PBFMB45

Figure 49 depicts an image of the transversal section of PBFMB45 and reveals its macrostructure. It is possible to identify a large quantity of macro-pores spread

throughout all regions of the sample. From the macrostructure it is also possible to observe the absence of magnetite and cracks in the pellet.

Figure 49: Macrostructure of a crossed section of PBFMB45.

Figure 50 depicts the microstructure of PBFMB45 in a mosaic fashion with magnifications of 500x and 1000x from the pellet's shell, middle and core sections. The images with 500x magnification reveal a structure rich in porosity and grains with morphologies resembling the ones from pellet feed. The lower limestone addition in this product leads to fewer formation of calcium silicates and, due to this aspect, higher intergranular porosity is observed. At 1000x magnification the predominance of hematite grains with high intragranular porosity is noticed, however some compact grains are also observed. This is in line with the typically higher participation of porous ores in Samarco's pellet feed blend. For both magnification levels homogeneous inter-granular porosity from shell to core was observed.

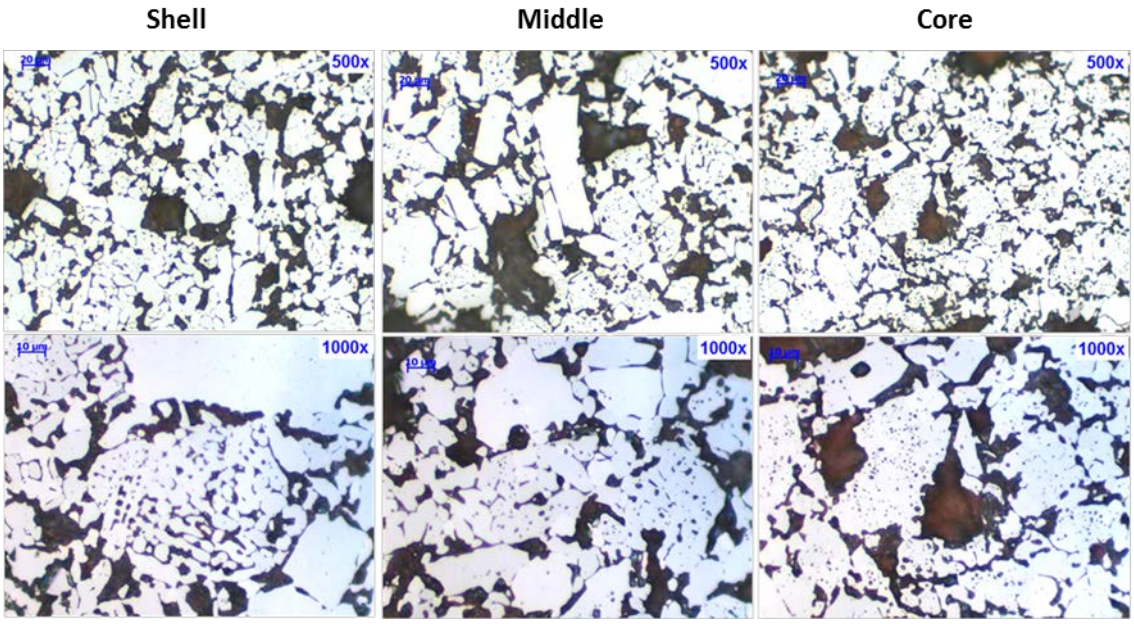

Figure 50: Microstructure of PBFMB45 at 500x and 1000x magnifications in an optical microscope.

Through SEM analysis examples of inter-granular and intra-granular porosities are observed at figure 51 (A) and (B). Semi-reacted silica grains were also identified, even with the lower presence of silicates in the grain borders (C).

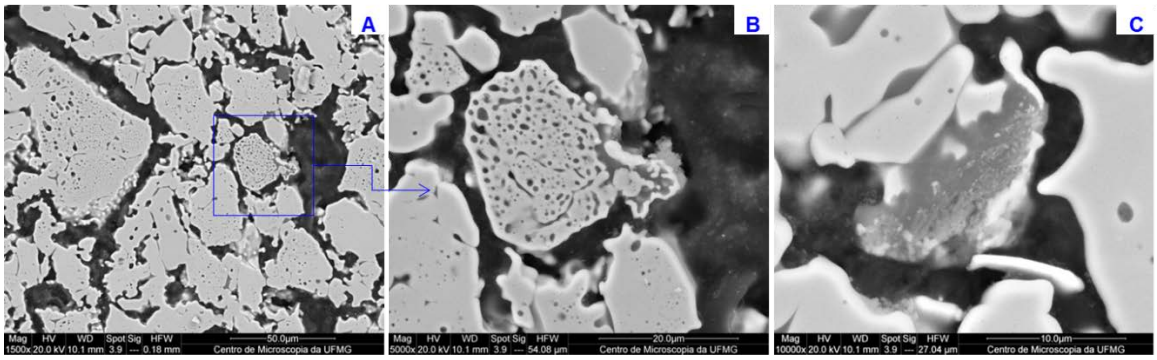

Figure 51: SEM analysis of PBFMB45 and intra-granular porosity (A) & (B) and semi-reacted silica grain (C).

More examples of intra-granular porosity are depicted in figure 52. The lower quantity of calcium silicates allied to the inferior growth of grains makes PBFMB45 the most porous of the pellets in Samarco's blast furnace portfolio. As noticed in the SEM analyses, the bridging between grains is very homogeneous, which causes this product to have similar cold compression strength to PBFSTD and PBFHB.

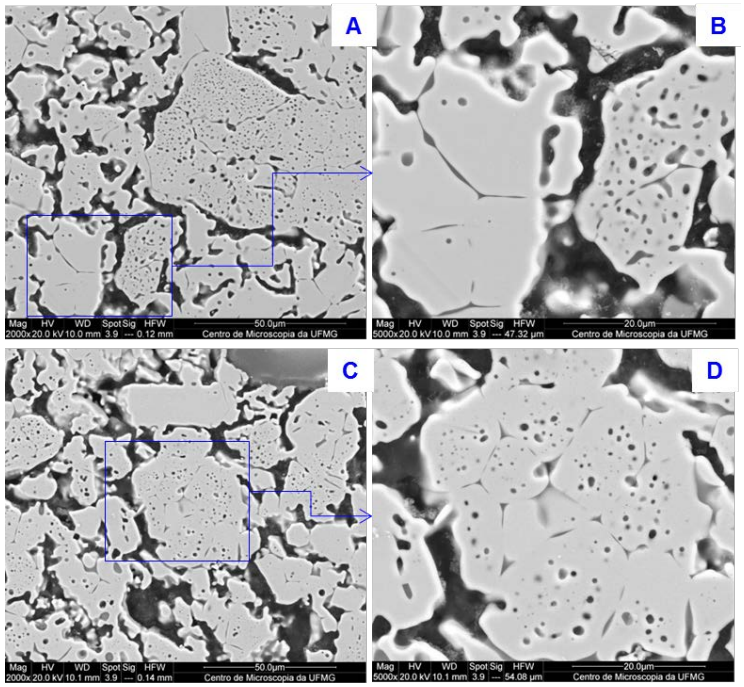

Figure 52: Intra-granular porosity and bridge-bonding of PBFMB45.

Table II – 5 summarizes the contents of pores, hematite, magnetite, silicates and ferrites in the PBFMB45 sample in its shell, medium and core sections.

Table II – 5: Quantitative analysis of PBFMB45's microstructure.

PBFMB45					
	Pores	Hamatite	Magnetite	Silicates	Ferrites
Shell	52.01	45.95	0	1.95	0.05
Middle Section	52.95	44.91	0.08	1.7	0.11
Core	49.89	48.71	0.64	0.75	0
Average	**51.62**	**46.52**	**0.24**	**1.47**	**0.05**

5.2.2 PBFSTD

Figure 53 depicts the image of the transversal section of PBFSTD and reveals its macrostructure. Macro-pores are present in all of the pellet's crossed section and no magnetite is observed.

Figure 53: Macrostructure of a crossed section of PBFSTD.

Figure 54 depicts the microstructure of PBFSTD in a mosaic arrangement and magnification of 500x and 1000x. This product presents larger grain sizes and lower level of inter-granular porosity when compared to PBFMB45. The higher limestone addition of PBFSTD in comparison to PBFMB45 will lead to the formation of intergranular melting phases in larger quantities. These phases have important role of transport medium for the growth of iron oxide crystals. The analysis did not detect magnetite in the sample nor micro-cracks caused by the tension of phase transformations.

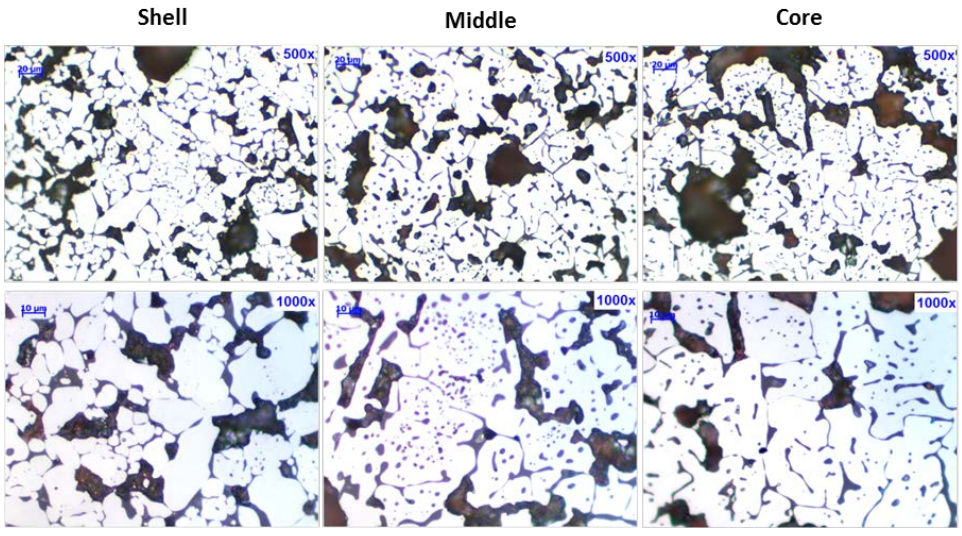

Figure 54: Microstructure of PBFSTD at 500x and 1000x magnifications in an optical microscope.

SEM analyses from figure 55 depicts the occurrence and distribution of silicates and pores, as well as consolidated bridge bonding formations of PBFSTD.

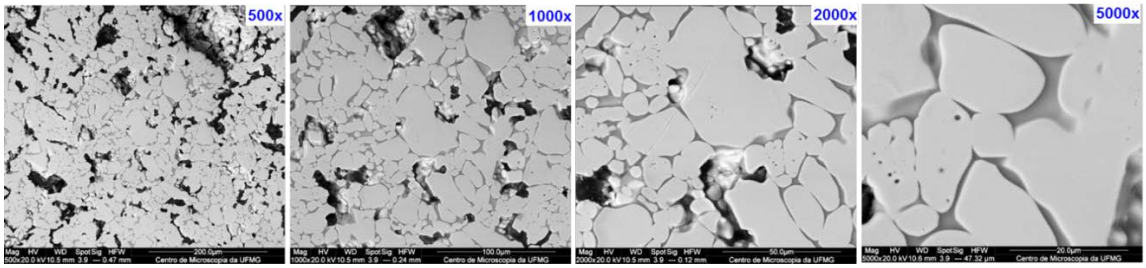

Figure 55: Distribution of silicates and pores, as well as bridge-bonding of PBFSTD.

Table III – 5 summarizes the contents of pores, hematite, magnetite, silicates and ferrites in the PBFSTD sample in its shell, medium and core sessions.

Table III – 5: Quantitative analysis of PBFSTD's microstructure.

PBFSTD					
	Pores	Hamatite	Magnetite	Silicates	Ferrites
Shell	52.65	44.42	0.14	2.56	0.19
Middle Section	47.71	49.4	0.22	2.48	0.12
Core	46.79	49.93	1.58	1.26	0.1
Average	**49.05**	**47.92**	**0.65**	**2.10**	**0.14**

5.2.3 PBFHB

Figure 56 depicts the image of the transversal section of PBFHB and reveals its macrostructure. As well as in the other pellet types, macro-pores are present throughout the pellet's crossed section. Magnetite, which has a dark gray color aspect in comparison to hematite, is present in the core of the sample.

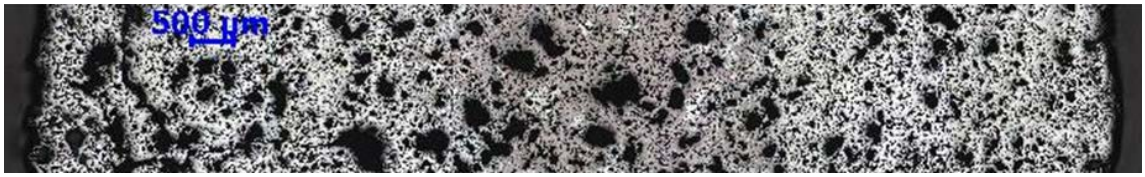

Figure 56: Macrostructure of a crossed section of PBFHB.

The mosaic at figure 57 presents magnification of 500x and 1000x of PBFHB's shell, middle and core sections. The highest growth of grains of all pellet types is noticed, with also homogeneously round structure. As expected, magnetite was present in the core of the of the pellet sample in both magnification scales. The higher presence of silicates and ferrites percolated through pores, reducing their numbers.

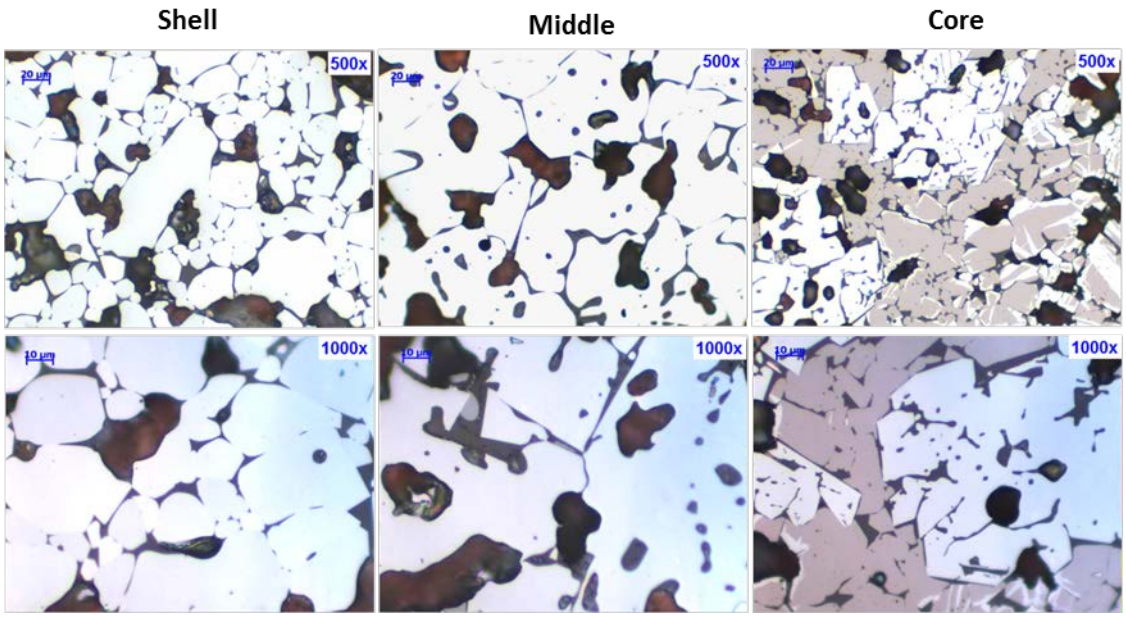

Figure 57: Microstructure of PBFHB at 500x and 1000x magnifications in an optical microscope.

Figure 58 depicts SEM analysis of PBFHB, of 500x, 1000x and 2000x which corroborate the results found in optical microscopy: larger and rounder grains with

lower intergranular porosity and higher presence of silicates when compared to the other pellet types.

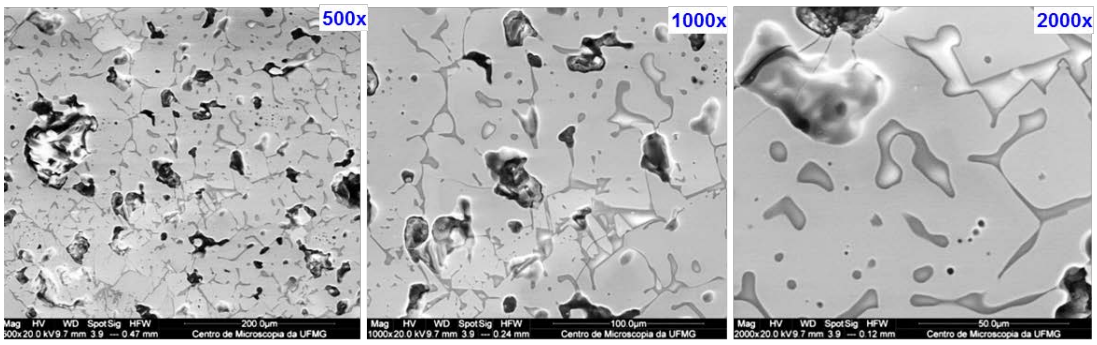

Figure 58: Distribution of silicates and pores, as well as bridge-bonding of PBFHB.

Table IV – 5 summarizes the contents of pores, hematite, magnetite, silicates and ferrites in the PBFHB sample in its shell, medium and core sessions.

PBFHB					
	Pores	Hamatite	Magnetite	Silicates	Ferrites
Shell	37.99	58.16	0.13	2.93	0.76
Middle Section	42.41	47.26	6.96	2.72	0.53
Core	45.49	40.58	11.5	1.84	0.21
Average	**41.96**	**48.67**	**6.20**	**2.50**	**0.50**

5.2.4 Summary of macroscopic differences of Samarco's three blast furnace pellet types

Figure 59 depicts the comparison of the three pellet types at the 1000x magnification and clearly shows the tendencies of reduction in porosity, increase in size and roundness of grains and calcium-silicate participation as basicity increases from 0.45 to 1.0.

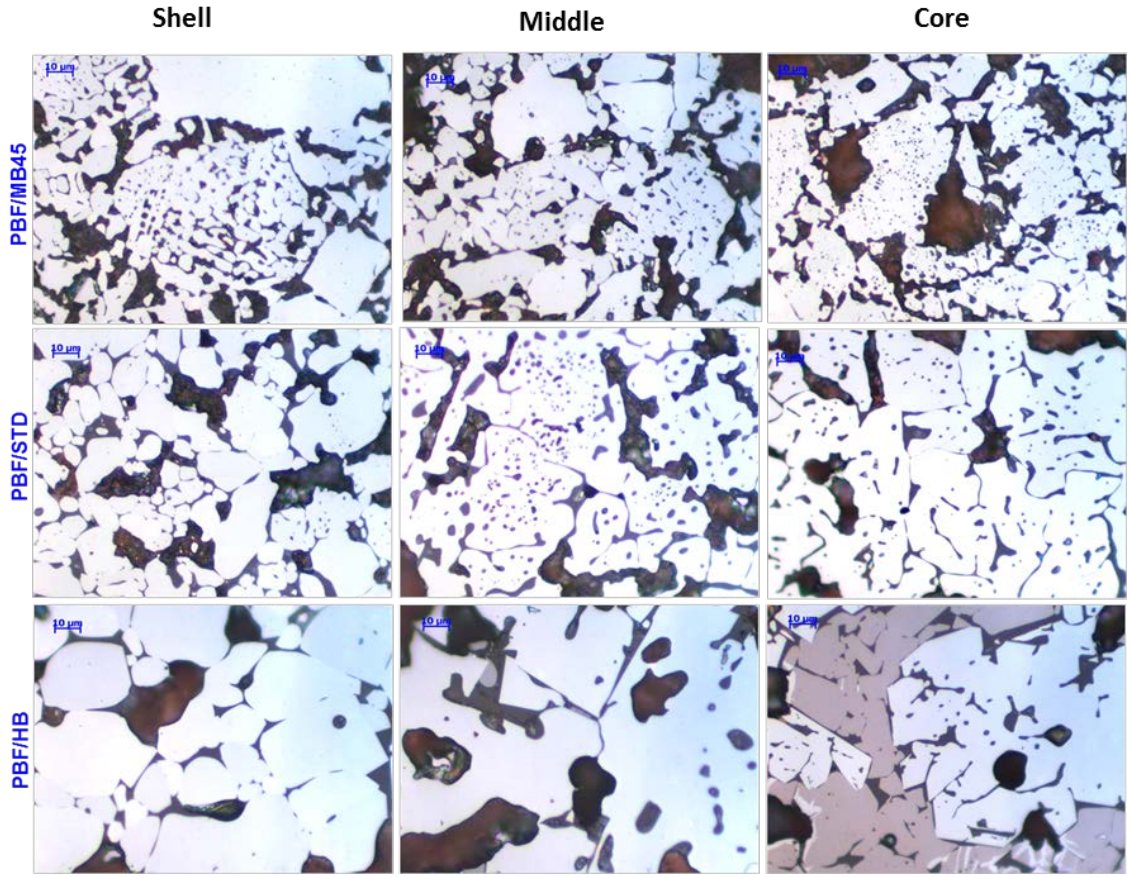

Figure 59: Shell, middle and core sections of Samarco's three pellet types at 1000x magnification.

Figure 60 depicts reduction of inter-granular porosity with the increase of pellet basicity through a 2D quantification algorithm applied in an optical microscope.

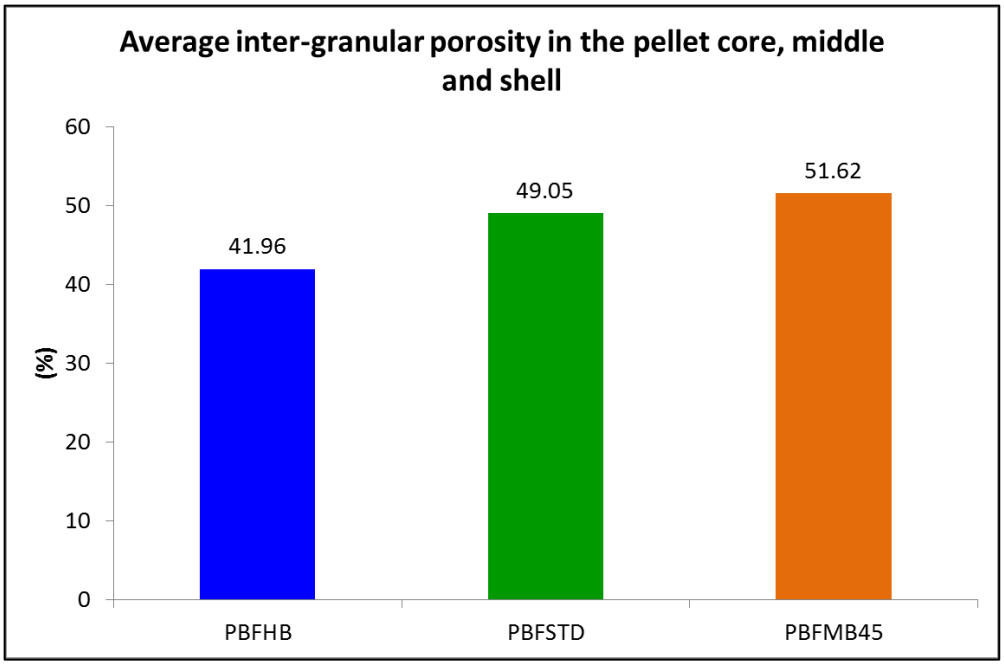

Figure 60: Inter-granular porosity through image analysis.

Figures 61 and 62 combined depict in quantitative means the growth of grains when basicity is increased, through the measurement of grain area in squared micrometers and grain absolute numbers per pellet section (shell, middle and core).

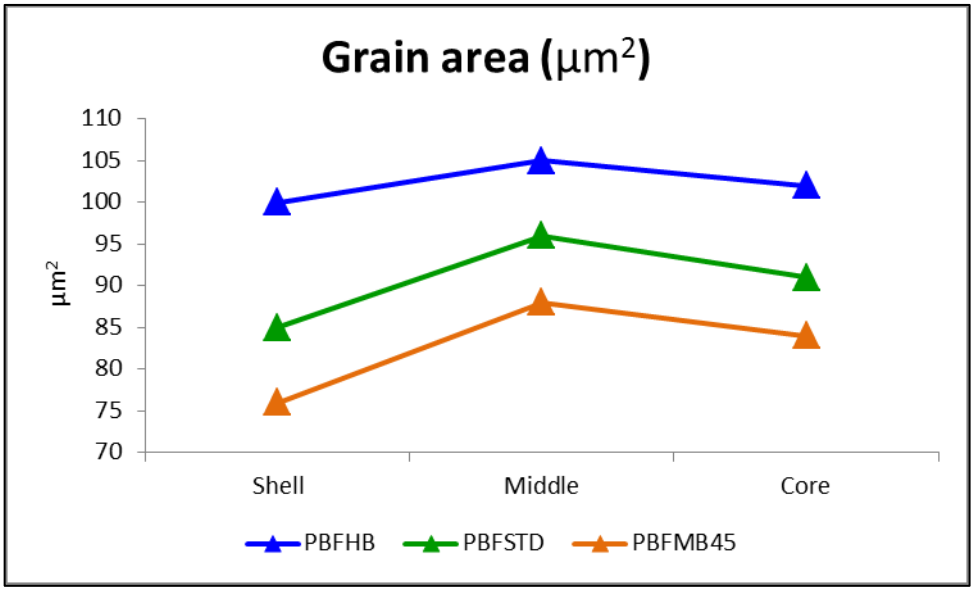

Figure 61: Grain area quantification through image analysis.

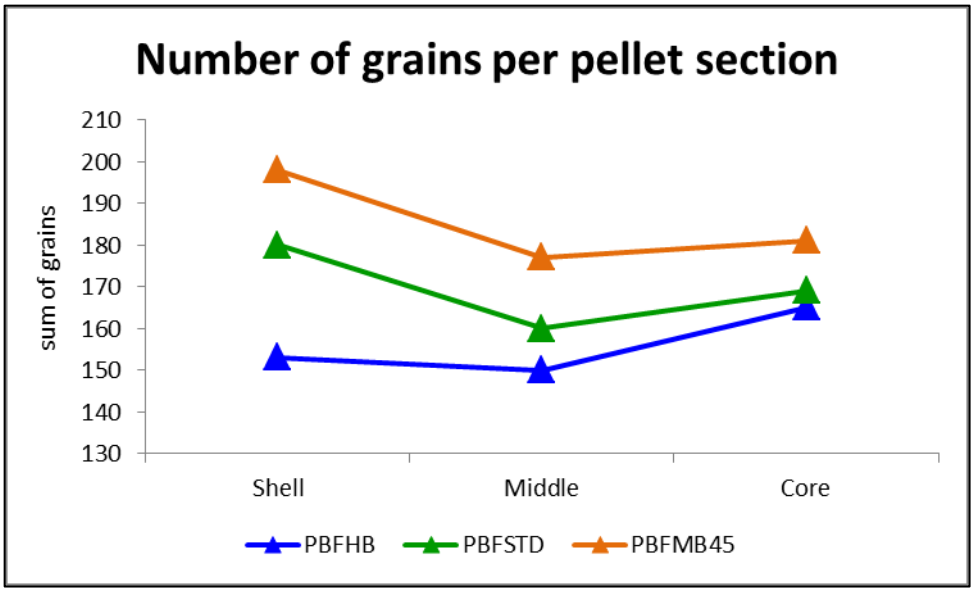

Figure 62: Grain quantification through image analysis.

5.3 Metallurgical characteristics of pellets in a blast furnace's granular zone

5.3.1 Low Temperature Disintegration

Before the knowledge on pellets' metallurgical proprieties was refined, their resistance to degradation during reduction was believed to depend solely on homogeneous induration and high cold compression strength. However, even when the agglomerates are subjected to very appropriate firing conditions they can still differ significantly in their capacities to endure degradation when exposed to the reducing atmosphere at low temperatures in a blast furnace (between 400 and 600^{o}C), especially in the case of low slag pellets. The ISO LTD test aims at differentiating pellets according to this metallurgical quality. The test characteristics compared to an actual blast furnace operation in relation to CO partial pressure and temperature are depicted in the iron-oxygen-carbon diagram of figure 63.

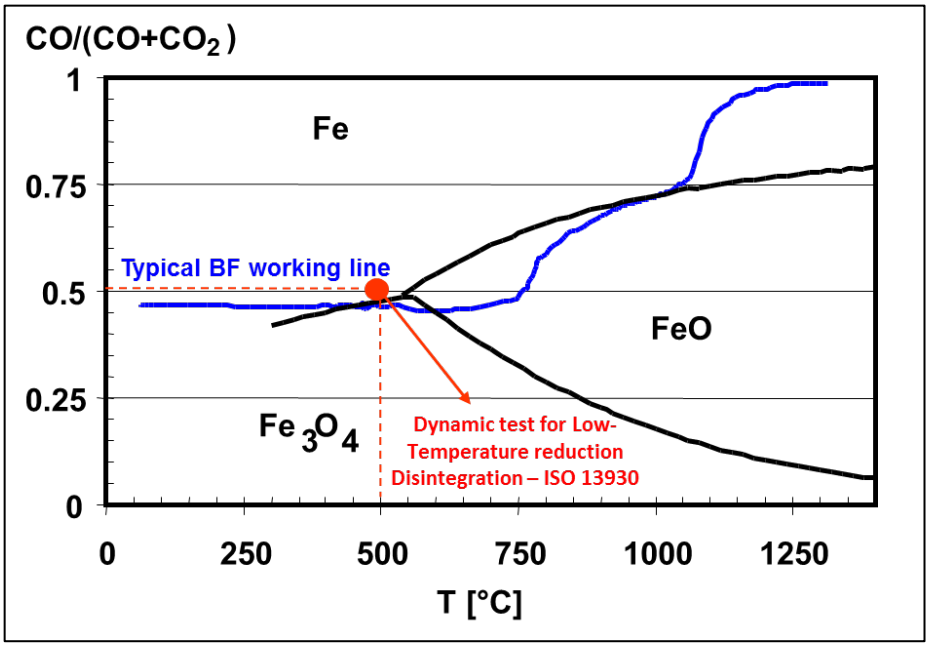

Figure 63: Comparison of the LTD test and an industrial blast furnace operation in relation to CO partial pressure and temperature on an iron-oxygen-carbon diagram.

Low LTD numbers depend very much on the agglomerate's slag composition. At this low temperature range nearly all gangue components are still in solid state, whereas the ore is facing significant lattice distortion as it undergoes the first reduction stage. Silicates and ferrites therefore act as a supporting frame preventing exaggerated fines generation, as the tension caused by the HC – CFC transformation of Fe_2O_3 into Fe_3O_4 takes place. As mentioned in the literature review session, lattice distortion can cause up to 25% swelling in the initial phase of reduction. In the case of Samarco's portfolio, all the three pellet types have superior LTD properties; however the increased percentages of silicates and ferrites from PBFMB45 to PBHB will result in slightly improved trends on this metallurgical characteristic. Figure 64 illustrates one example of SEM analysis at 2000x magnification and the difference in the presence of silicates in the three pellet samples.

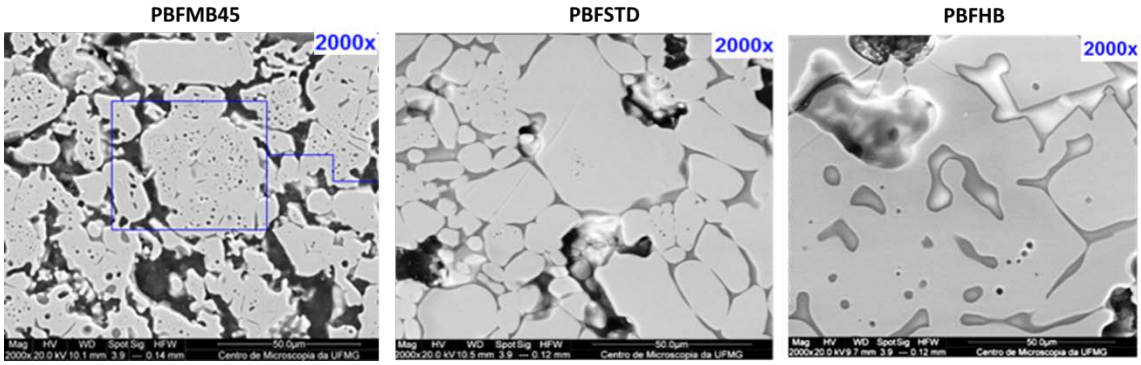

Figure 64: Difference of grain morphologies, porosity and percentage of silicates in the three blast furnace pellet samples at 2000x magnification.

Figure 65 presents a tangible graphical comparison of percentages of silicates and ferrites in the three pellet types of Samarco performed through 2D image analysis in an optical microscope.

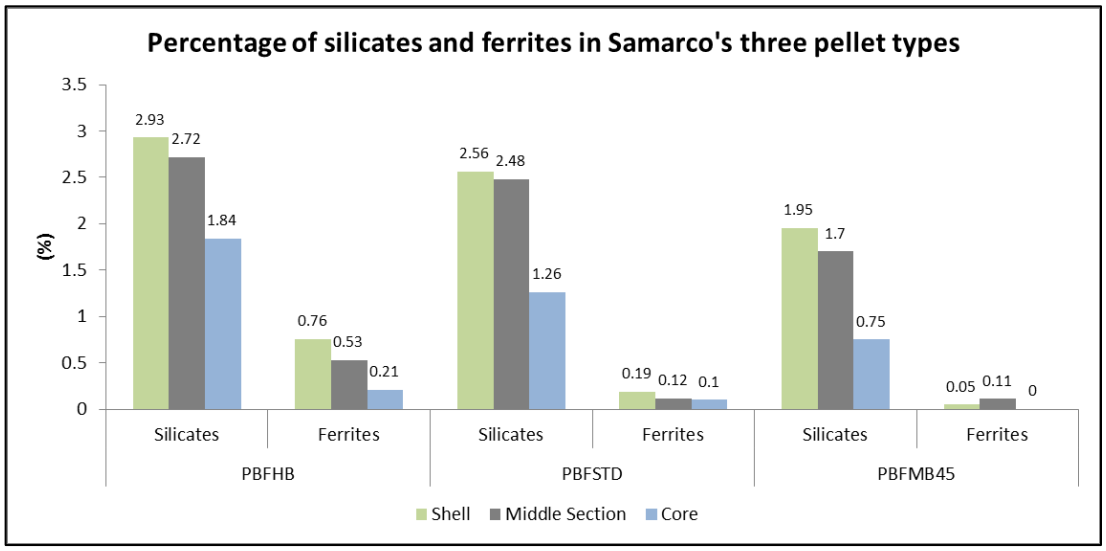

Figure 65: Quantitative assessment of the presence of silicates and ferrites in the three blast furnace pellet samples through 2-D image analysis.

Figures 66 and 67 finally present the low degradation results of Samarco pellets, for both on-size pre-reduced pellets (%>6.3mm) and ultra-fines (%<0.5mm).

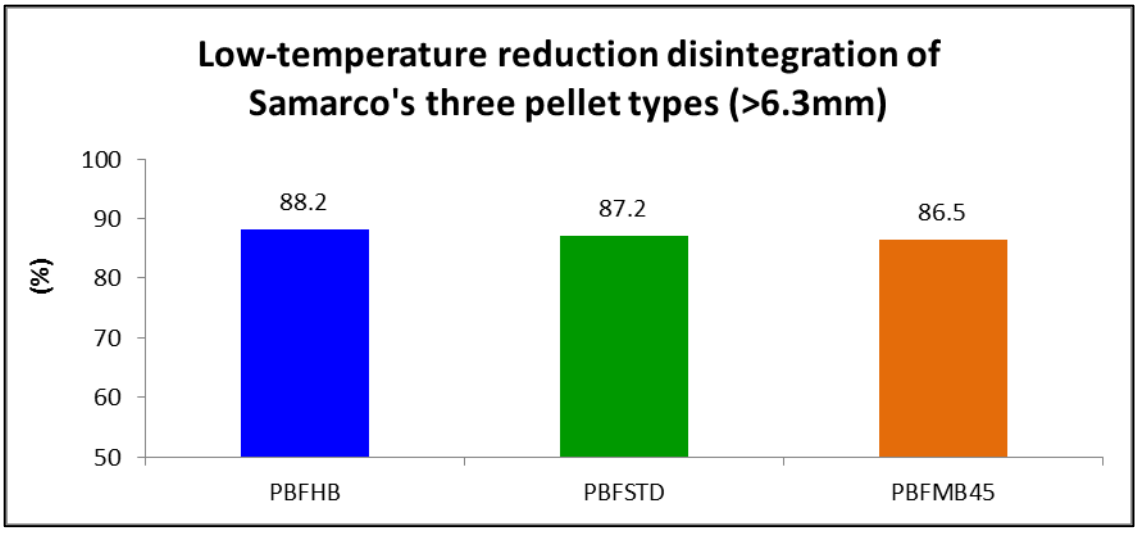

Figure 66: ISO low-temperature reduction degradation result. Percentage of pellets above 6.3mm.

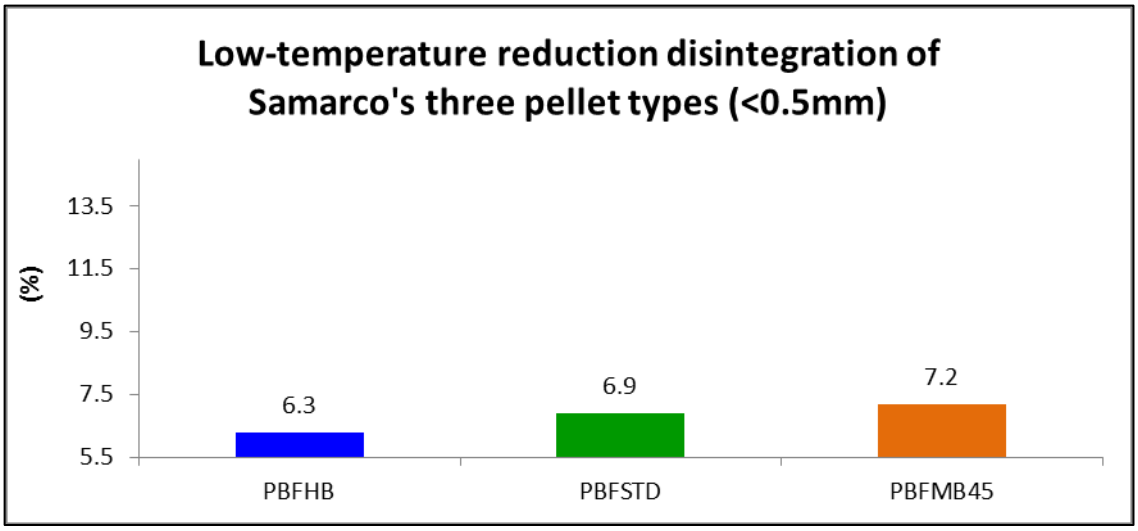

Figure 67: ISO low-temperature reduction degradation result. Percentage of pellets above below 0.5mm.

5.3.2 Swelling

The last stage of reduction from wüstite to metallic Fe can be followed by the growth of fibrous iron, especially in the case of low-slag pellet types with low binary basicity and absence of MgO. Figure 68 depicts examples of whiskers.

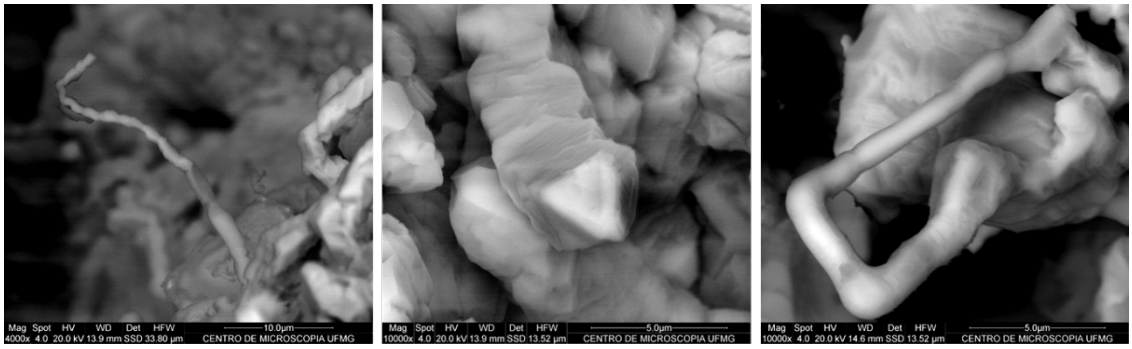

Figure 68: Examples of whisker formations in Samarco pellet samples.

Moderate swelling does not negatively impact an industrial blast furnace process; however the loss of stability of the agglomerate and further dust generation can impact the permeability of its granular zone. The comparison of the ISO standard for swelling utilized in this study and an actual blast furnace operation in relation to CO partial pressure and temperature is depicted in the iron-oxygen-carbon diagram of figure 69. It can be seen that the test is undertaken in a much more aggressive setting than the industrial process as to distinguish different pellets according to this metallurgical characteristic.

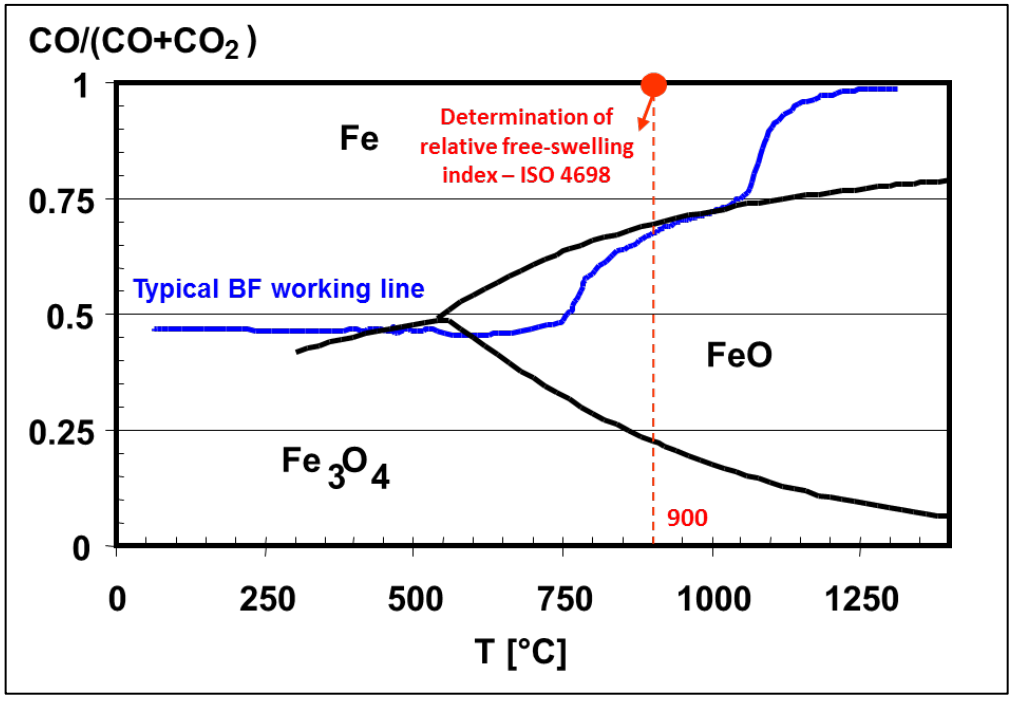

Figure 69: Comparison of the swelling test and an industrial blast furnace operation in relation to CO partial pressure and temperature on an iron-oxygen-carbon diagram.

All of Samarco pellets are in the acceptable range of ISO swelling and, in line with literature, the progression to higher basicities will work in favor of the lower occurrence of whiskers, as depicted in figure 70. As described in the microscopy analysis, PBFHB and PBFSTD presented larger recrystallized hematite grains with higher participation of silicates in their boundaries, whereas PBFMB45 presented smaller hematite grains with larger intra-granular and inter-granular porosities or “open pores” with lower participation of silicates in the overall agglomerate matrix. Due to these characteristics, Samarco’s CaO fluxed pellets seemed to follow a reduction behavior more similar to the topo-chemical theoretical model when compared to Samarco’s middle-basicity pellet. In PBFMB45 the iron formation predominated as filaments “whiskers” causing a more pronounced swelling phenomena when compared to PBFSTD and PBFHB.

Higher swelling index and lower melting temperatures of slag are characteristics that are usually perceived together and this is the case for Samarco pellets, as it will be described in the softening and melting session.

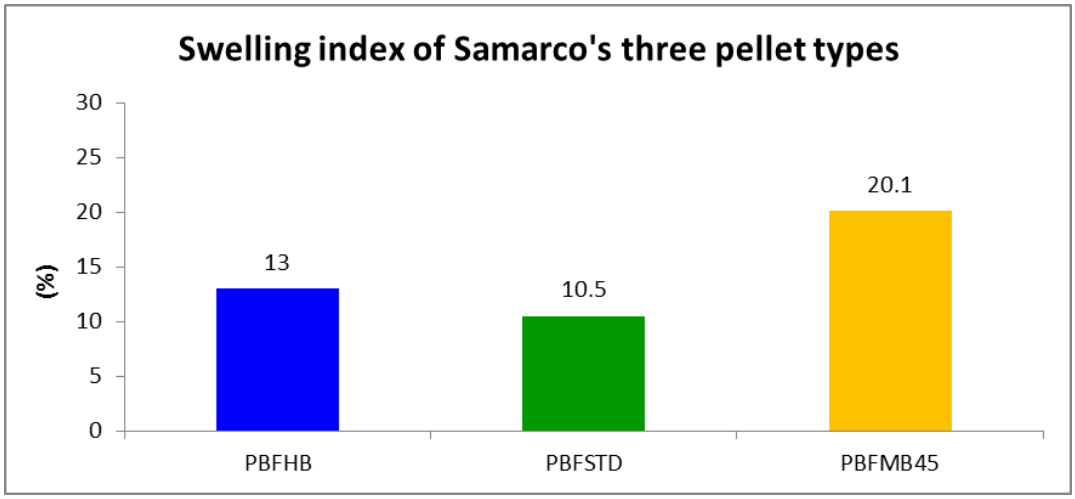

Figure 70: Swelling index of Samarco’s three blast furnace pellet types.

5.3.3 Reduction under load

The ISO reduction under load test comprises an evaluation of pellets’ swelling susceptibility coupled with their capacity to endure deformation at a reducing atmosphere with high CO partial pressure, temperature of 1050^{o}C, and pressure of 50kPa. These conditions correspond to the lower levels of the granular zone; however the pellets are subject to them already at the very beginning of the test. Figure 71

depicts the reduction under load test compared to an actual blast furnace operation in an iron-oxygen-carbon diagram.

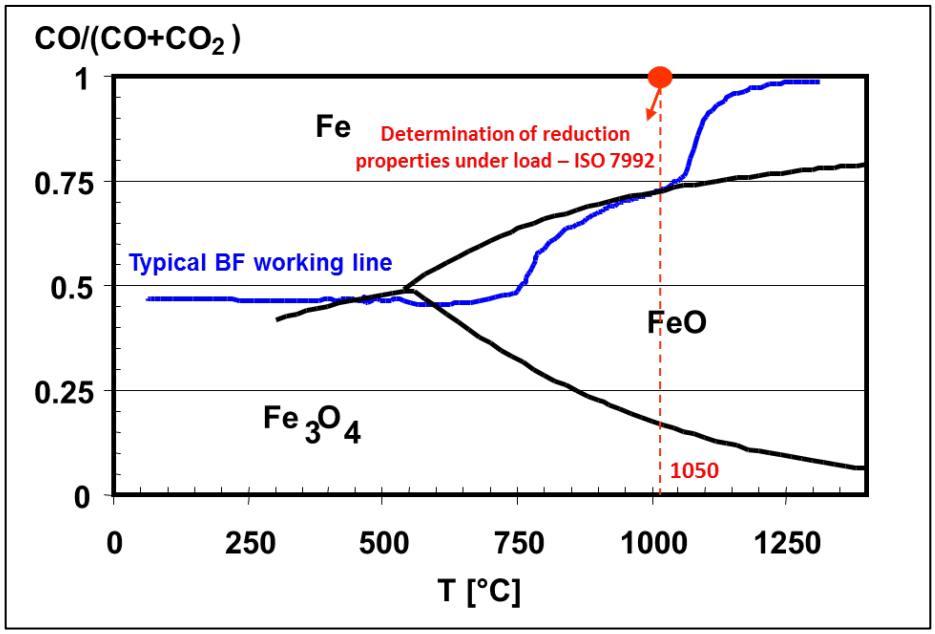

Figure 71: Comparison of the swelling test and an industrial blast furnace operation in relation to CO partial pressure and temperature on an iron-oxygen-carbon diagram.

Figure 72 depicts the bed height contraction and the pressure difference in mmWG when the three pellets of Samarco's BF portfolio are subject to the reduction under load test. On bed height, it is noticeable that PBFSTD and PBFHB contract from the beginning of the test whereas PBFMB45 swells until 15 minutes before contracting. This phenomenon is very in line with what was already described in the LTD session. CaO fluxed pellets will have the tendency to better withstand the first lattice distortion caused by the Fe_2O3 – Fe_3O_4 transformation, whereas PBFMB45 will be more prone swell when subject to the very beginning of reduction. The lower gangue of PBFMB45 represent lower supporting frame against destroying pressure forces from the conversion between hematite into magnetite. At 15 minutes the pressure differential hadn't yet been significantly increased for PBFMB45, which means that the first mechanism of swelling doesn't hinder the bulk permeability in the test and the same can be assumed to an industrial reactor. The extremely aggressive reduction condition of the RUL test when compared to a smooth descent of the pellets in a blast furnace burden will cause the reduction reactions to take place on a much faster pace within the retort tube. After 15 minutes of test it is reasonable to state that for the CaO fluxed

pellet types the outer shell of the agglomerate will already start undergoing the last stage of reduction and, in case of PBFMB45, bed contraction will be intensified as growth of whiskers takes place abruptly already deeper in the agglommerate's radius, due its higher intergranular porosity. Swelling and occupation of voids between pellets caused excessive increase of pressure differential in PBFMB45 when compared to PBFSTD and PBFHB.

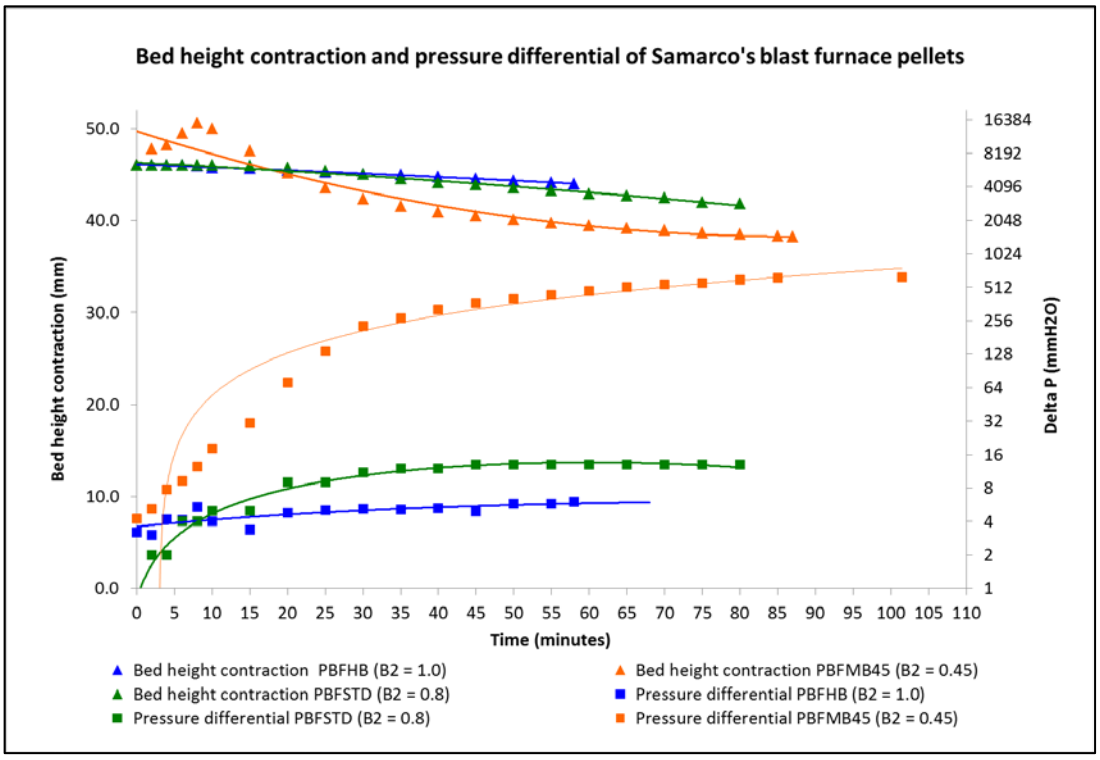

Figure 72: Bed height contraction and pressure differential of Samarco's blast furnace pellets.

Figure 73 depicts the comparison of bed contraction and reduction degree. Again it is noticeable that until 15 minutes of test, the reduction degree of the three product types follow the same pace and afterwards it is better as binary basicity increases. Two factors explain this phenomenon: first and most importantly the better permeability of the bulk through lower swelling and second the presence of slag compounds richer in calcium which have more reducible characteristics.

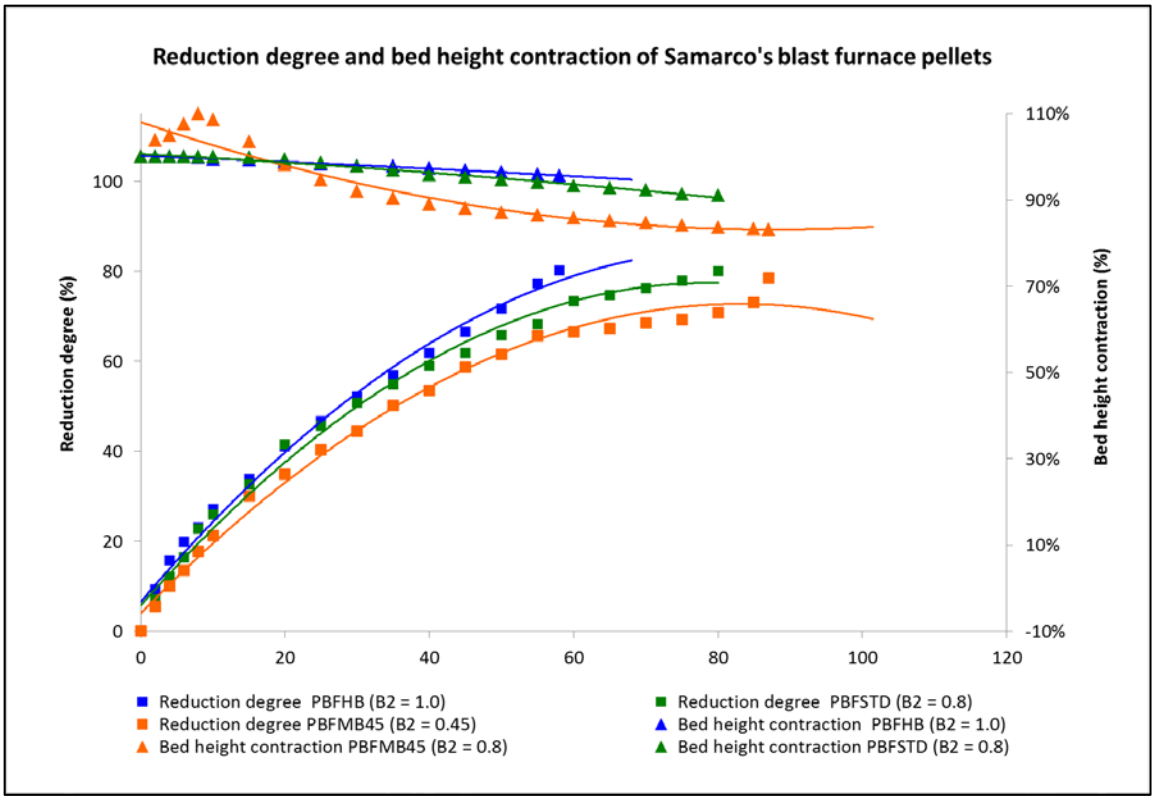

Figure 73: Reduction degree and bed height contraction of Samarco's blast furnace pellets.

Figure 74 depicts the visual aspect of the three product types after the conclusion of the test (degree of reduction equals to 80%). It can be seen that the deformation through swelling, followed by the shrinkage phenomenon is more noticeable at the lower basicity pellet type.

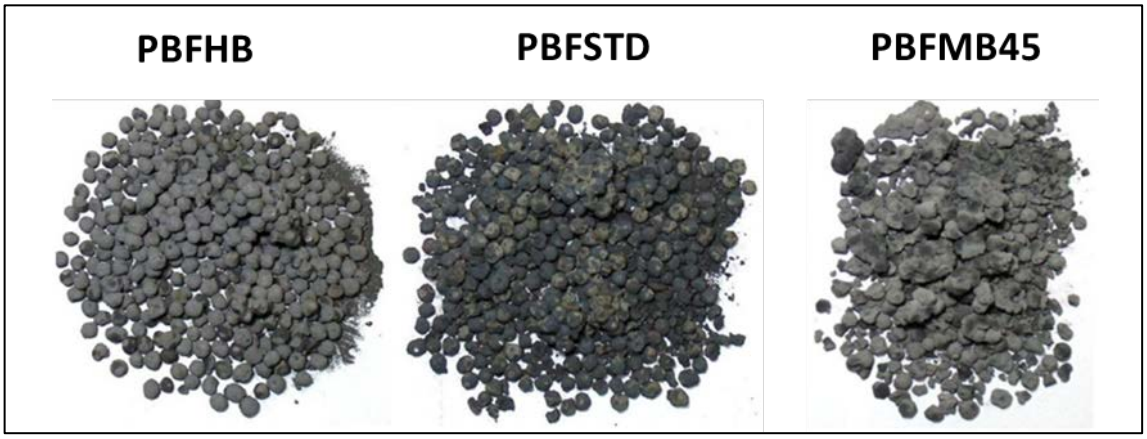

Figure 74: Visual aspect of the pre-reduced samples of Samarco's blast furnace pellets after the Reduction under Load test.

Partially-reduced samples of the three pellet types were embedded in bakelite for SEM characterization. Figure 75 infers how the topo-chemical reduction took place in the fluxed pellet types on a fairly homogeneous way whereas the medium basicity pellet presented a more deformed aspect and less symmetrical reduction behavior. The black aspects in the core of the partly-reduced PBFSTD and PBFHB samples are due to the loss of material during resin embedding, which indicates that large quantities of very friable structure (wüstite) was present in this area. Their shell presents however a very metallized aspect. PBFMB45 had partial stability loss (deformed aspect) caused by intense swelling coupled with the 50kPa pressure of the test.

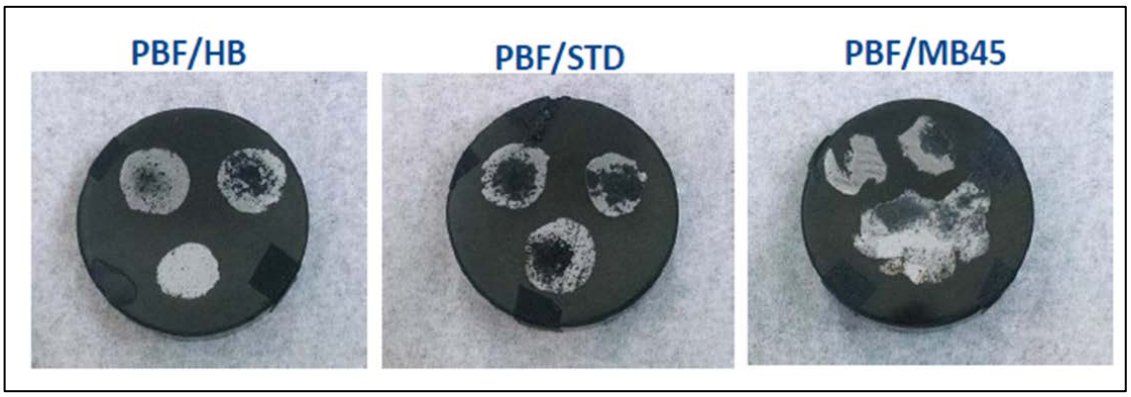

Figure 75: Embedded samples of Samarco's blast furnace pellets after the Reduction under Load test.

Figure 76 depicts the SEM analysis at 500x magnitude from the shell, middle and core of the three partially-reduced pellets. It can be noticed that the fluxed pellet types present more slag phases dispersed in the Fe matrix with yet some small percentages of wüstite. The morphology of grains are round although heterogeneous from shell to core. The medium basicity pellet type presented round and large grain morphology with silicate (slag) puddles in their borders. It also presented whisker-like morphology on its middle section and this evidences that fibrous iron indeed grew in more regions than just the pellet shell.

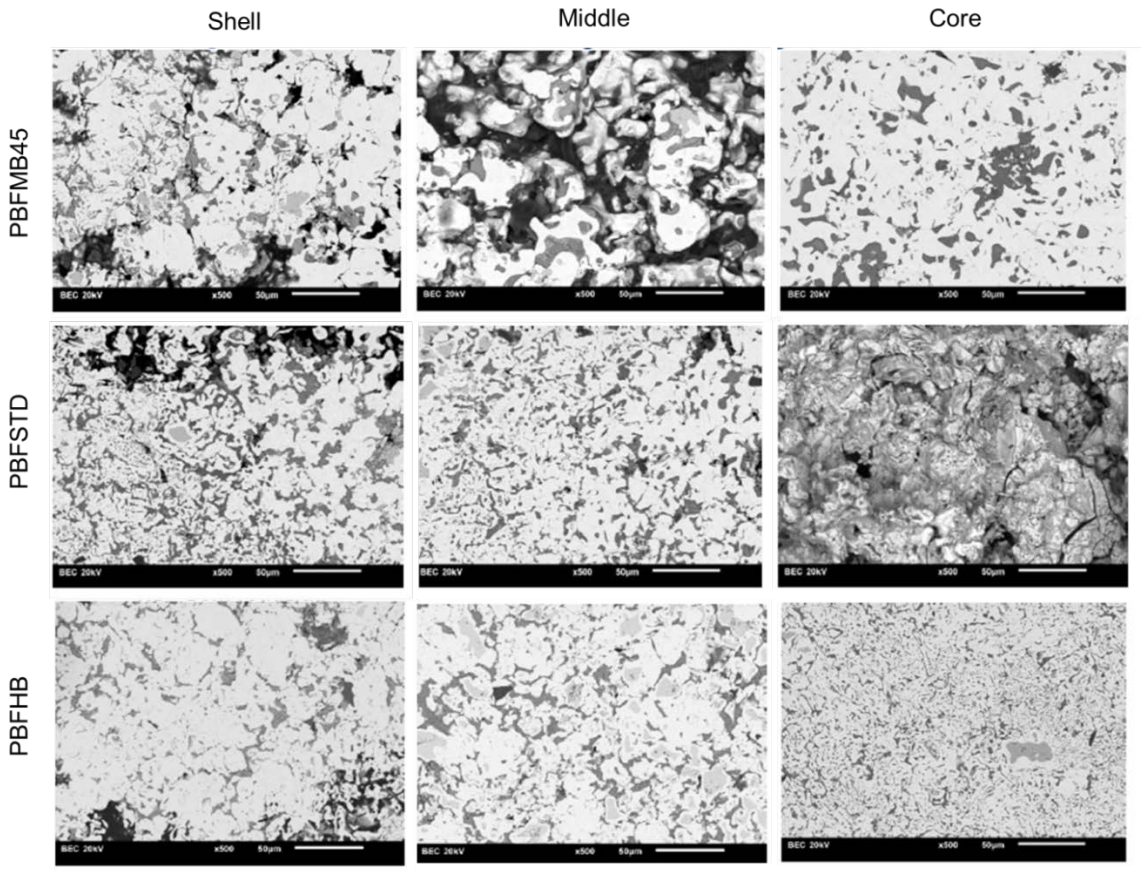

Figure 76: SEM analyses at 500x magnification of the crossed sections of PBFMB45, PBFSTD and PBFHB.

5.3.4 Reducibility

Reducibility of iron ore pellets results from a combination of intrinsic mineralogical properties of the iron ore and factors attributed to slag composition and induration characteristics. In relation to iron ore mineralogy, the Alegria Mining complex, where Samarco's run of mine (ROM) is explored, is known for its various mineralogical associations. The mineralogical diversity of the Alegria mining pits led Samarco's engineers to perform a thorough investigation and classification of itabirites according to mineralogical associations along with their distinct behavior in the beneficiation process. The major ore types which will afterwards be subdivided 15 itabirite categories are: specular hematite, porous hematite (martite), goethite and magnetite. Figure 77 depicts the four main mineral types of the Alegria Complex and also their estimated participation in a typical pellet feed processed in Ponta Ubu, when it is subject to quantitative image analysis under an optical microscope.

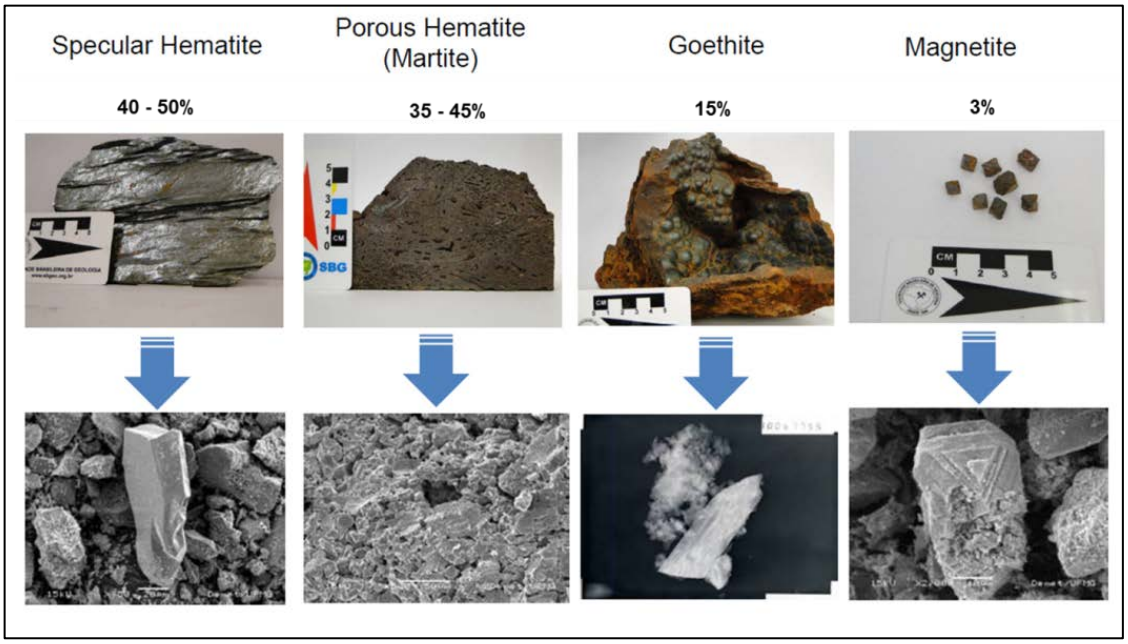

Figure 77: Typical mineralogical blend of Samarco's pellet feed.

The participation of the various ore types in Samarco's concentrate will influence diverse aspects of the downstream processing chain: beneficiation, pelletizing and reduction behavior in a blast furnace. As far as reducibility is concerned, figure 78 elucidates that compact ores as specular hematite and magnetite will lead also compact iron oxide grains in pellets and, conversely, goethite and porous hematite will contribute to the formation of porous oxide grains in pellets after the induration process.

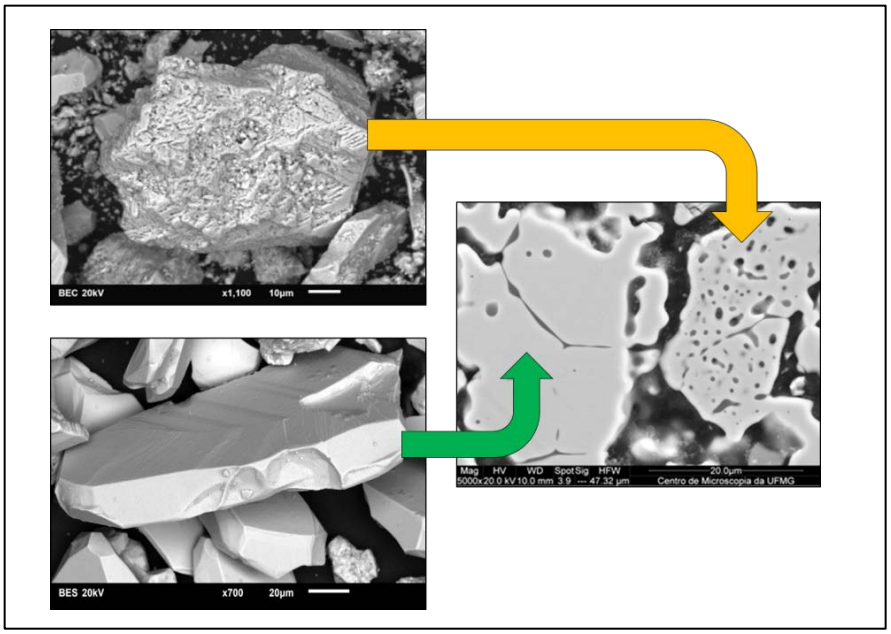

Figure 78: Morphology comparison of iron ore grains before and after the induration process.

The reducibility of Samarco pellets is usually high due to the intrinsic ore characteristics of Alegria Complex, which is the same for the three blast furnace types produced. However, the increments of basicity from the lowest level (PBFMB45) to (PBFHB) will lead to higher reduction index results under ISO 7215, as per depicted in figure 79.

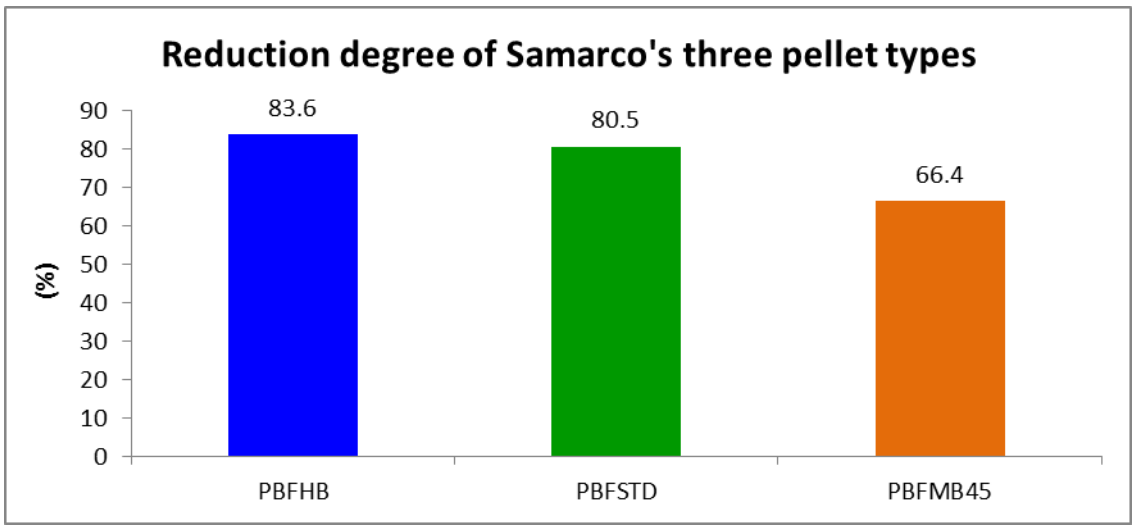

Figure 79: Reduction degree of Samarco's three blast furnace pellets.

The explanation for this phenomenon is in the fact that ferrites and silicates with higher molar participation of calcium oxides are, up to certain limits, more subject to fast reduction, as already described by table I – 3 in the literature review section. In this specific metallurgical test it is however important to mention that swelling of pellets with lower basicity will also affect the bulk permeability and hinder reducibility as a whole, as ISO 7215 is undertaken under more aggressive conditions when compared to an actual blast furnace operation (Figure 80).

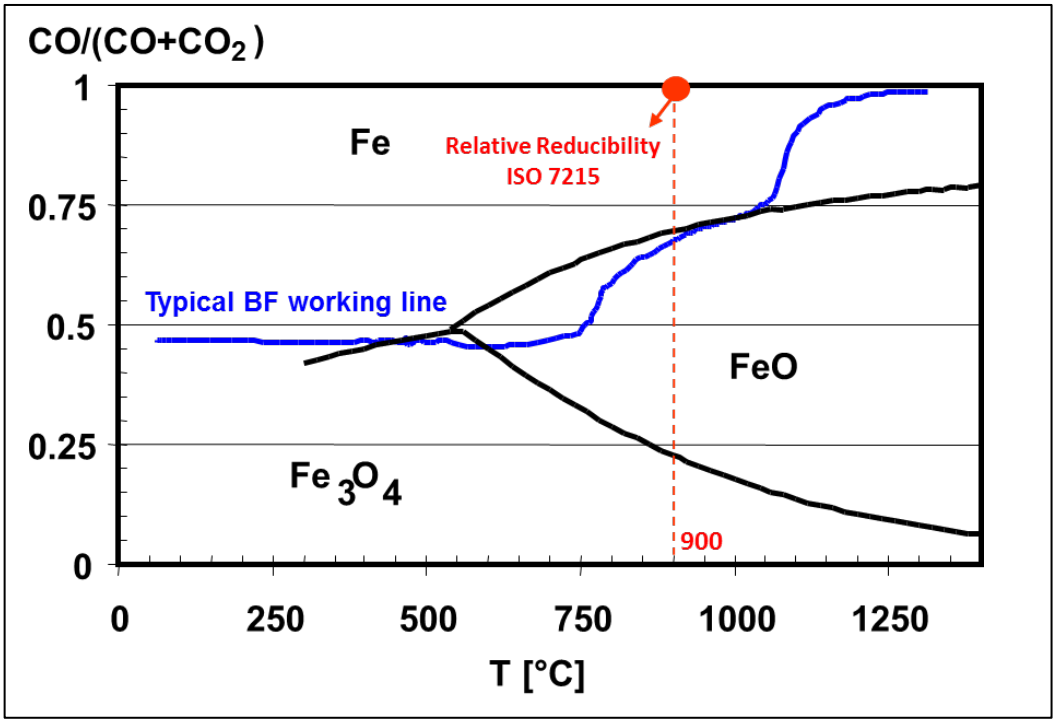

Figure 80: Comparison of the reducibility test and an industrial blast furnace operation in relation to CO partial pressure and temperature on an iron-oxygen-carbon diagram.

A prove of the occurrence of swelling and compromised bulk permeability is given in figure 81 where cold compression strength of the partly reduced pellets after ISO 7215 is reduced with the reduction of the pellet basicity level.

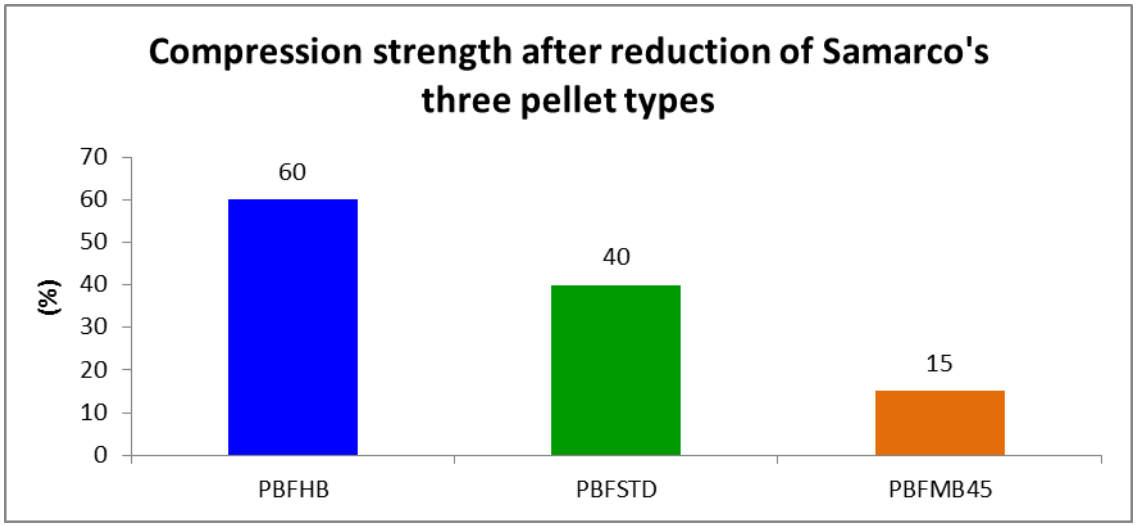

Figure 81: cold compression strength of Samarco's three blast furnace pellet types after the ISO 7215 reducibility test.

5.4 Metallurgical characteristics of pellet-sinter mixes in the cohesive zone

5.4.1 Main differences of pellets and Standard EU sinter under microscopy

Five 15mm samples of the Western European Sinter were chosen for analysis and microstructural comparison with pellets. The objective of this microstructural characterization is to provide elements for further investigation of the differences between these two agglomerate types during reduction, softening and melting through the REAS method.

Figure 82 depicts the samples prior and after the bakelite embedment and polishing.

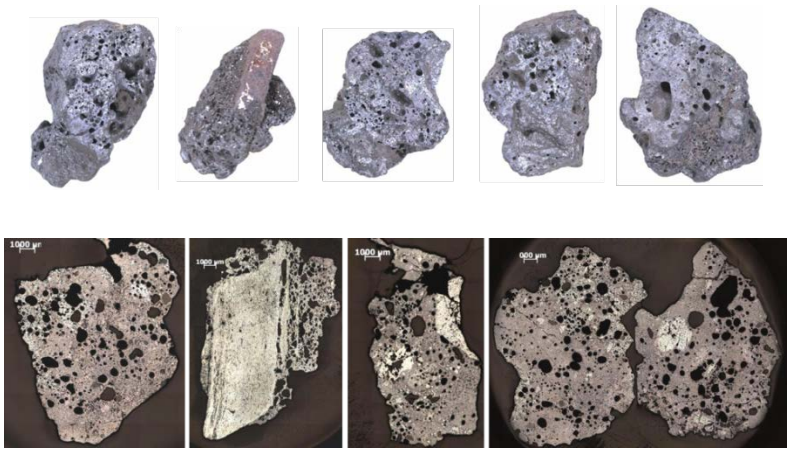

Figure 82: Samples of Western European Sinter prior and after resin embedding.

Figure 83 depicts the different macro-aspects of one embedded sinter sample compared to Samarco's PBFMB45.

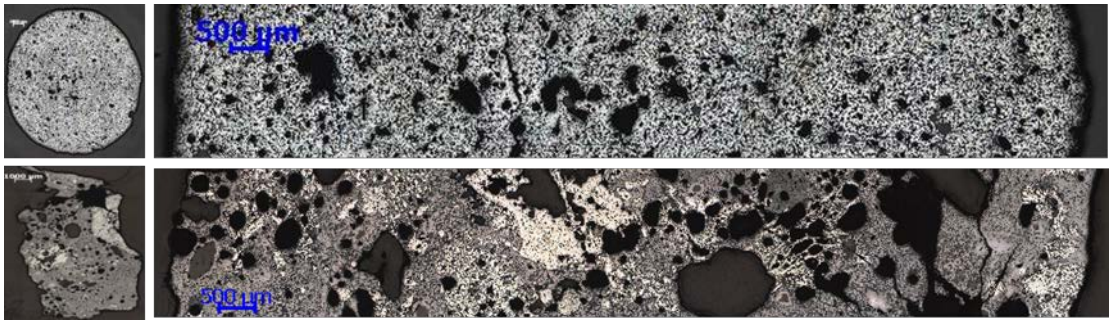

Figure 83: Macro-aspect comparison of a sinter sample compared to a pellet sample.

Figure 84 depicts an average quantitative analysis of pores, hematite, magnetite, silicates and ferrites of the five embedded sinter samples compared to Samarco's three pellet samples.

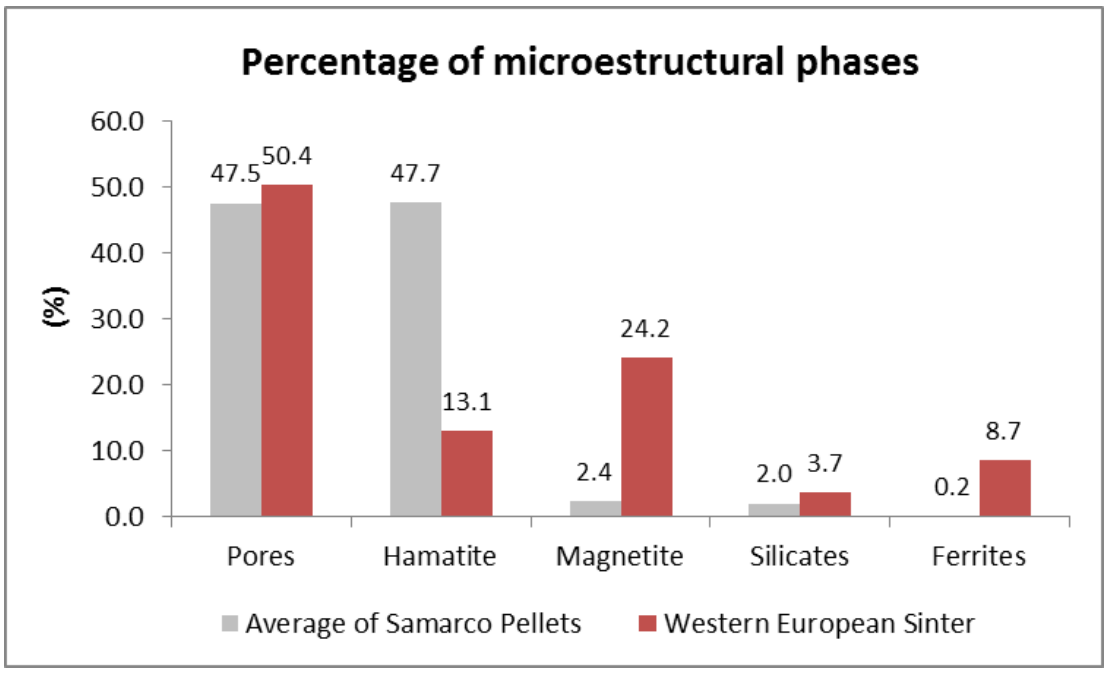

Figure 84: Average quantitative analysis of pores, hematite, magnetite, silicates and ferrites of the 5 sinter samples compared to the 3 pellet samples.

Through a joint evaluation of figures 83 and 84 it can be seen that although the quantification of pores is similar between the agglomerate types, their distribution and sizes are more homogeneous in the pellet sample when compared to the sinter sample. Hematite is predominant in the pellet type whereas a mixture of mostly secondary hematite and magnetite are present in the sinter sample. The presence of silicates and ferrites are much larger in the sinter sample due to its higher addition of fluxing agents.

5.4.2 Morphological differences between the components of pellets and Sinter

5.4.2.1 Hematite

Figure 85 depicts the major morphological differences between the hematite phases found in Samarco pellets and in the Western European sinter sample. The hematite of pellets presents round grains with silicates in their borders, especially in the more fluxed types. Due to the lower and more finely dispersed gangue amount from pellets in comparison to sinter, their grain sizes are smaller and more homogeneous. It is also possible to find a mixture of porous and compact grains. The sinter sample has hematite with different morphologies: cubic, precipitated in the form of dendrites within the silicates, romboedric and also rounded-cubic. These different morphologies are related to the heterogeneous temperature gradient reached during sintering and cooling stages of the agglomerate. Due to the higher levels of fluxes in the sinter, there are favorable conditions for the growth of grains from ferrous phases in sinter when compared to pellets.

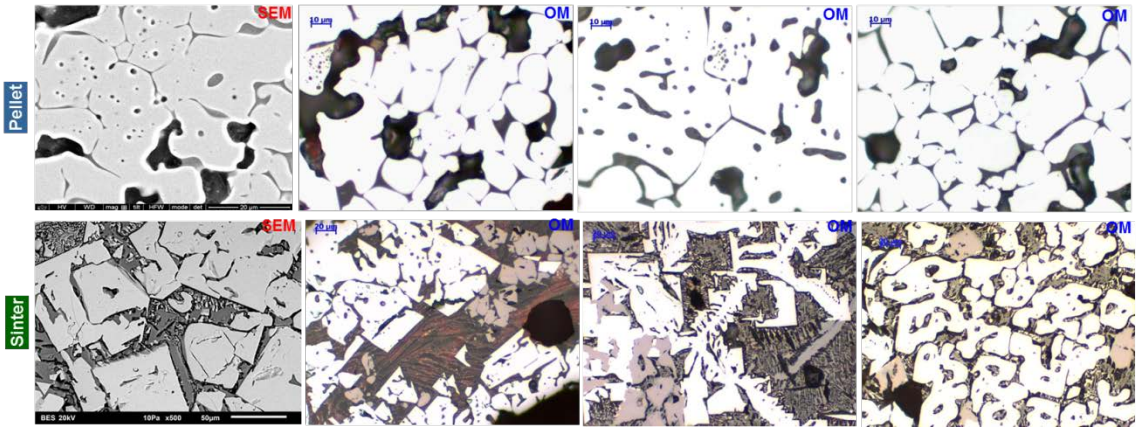

Figure 85: Comparison of morphological characteristics of hematite in Samarco pellets and typical Western European Sinter.

5.4.2.2 Magnetite

In pellets, the occurrence of magnetite is low compared to sinter, as grains are at a major percentage re-oxidized during the induration process. If small amounts of residual magnetite are found, they are mostly located in the pellet core due to the difference of oxygen partial pressure between the pellet's core and shell at the end of the induration stage. Figure 86 depicts the aspect of residual magnetite in the core of an iron ore pellet sample. In sinter, elevated percentages of magnetite are found in association with silicates and Ca/Mg ferrites. There is also precipitation of magnetite phases in dendrite form, due to certain cooling conditions.

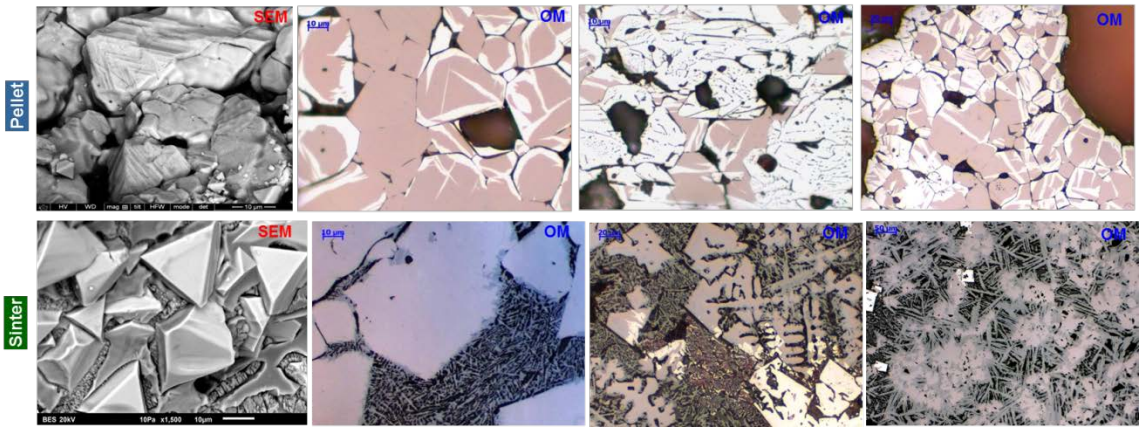

Figure 86: Comparison of morphological characteristics of magnetite in Samarco pellets and typical Western European Sinter.

5.4.2.3 Silicates

Silicates in pellets are present in the boundaries of hematite or magnetite grains. During induration they can migrate to the interior of pores, helping the consolidation of sintering reactions and crystal growth of the iron oxides. The higher gangue content of sinter will also lead to much higher percentage of silicates when compared to pellets. In sinter, they are mostly classified as complex silicates, with the presence of various elements (e.g. Ca, Mg, Al) and other precipitated phases in their interior. Figure 87 depicts the comparison of the silicate morphologies between pellets and sinter.

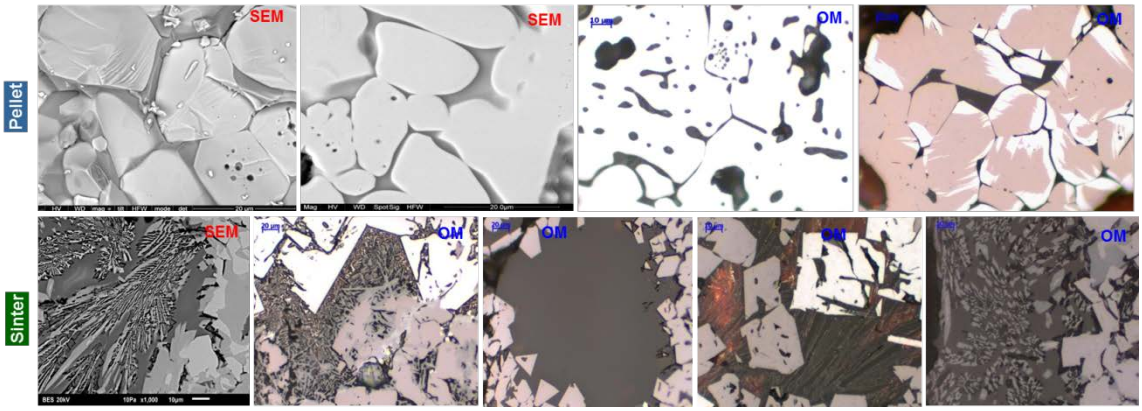

Figure 87: Comparison of morphological characteristics of silicates in Samarco pellets and typical Western European Sinter.

5.4.2.4 Ferrites

In Samarco pellets ferrites are present in very low percentages, as calcium ferrites tend to dissolve and calcium will migrate to the interior of silicates during the induration process. When ferrites are found, they tend to be the magnesium-ferrite type which is a phase that remains stable throughout all induration stage. The increase in participation of ferrites is noticed in Samarco pellets produced with higher limestone dosages. Sinter has an elevated percentage of ferrites, once again due to the higher addition of calcium and magnesium oxides. They can be associated to hematite, magnetite or precipitated in the interior of silicates. Ferrites can occur at different morphologies, being deposited in the grain boundaries or spread over the microstructure in acicular (needle-like) structures. Figure 88 depicts the comparison of the ferrite morphologies between pellets and sinter.

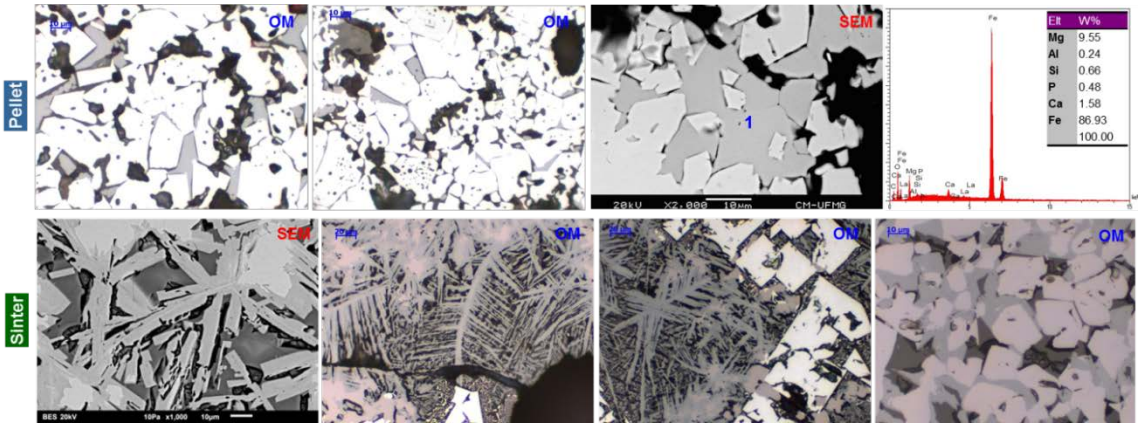

Figure 88: Comparison of morphological characteristics of ferrites in Samarco pellets and typical Western European Sinter.

5.4.2.4 Porosity

Pellets have more homogeneity in size and distribution of pores when compared to sinter. Intra-granular porosity is high due to already explained ore characteristics and part of the inter-granular porosity is generated by the ignition of solid fuel finely dispersed in the agglomerate's matrix. In the sinter sample the pores, mostly deriving from the ignition of solid fuel, present intense migration of silicates to their cores due to the much higher gangue content in comparison to pellets. Figure 89 depicts the comparison of pore morphologies between pellets and sinter.

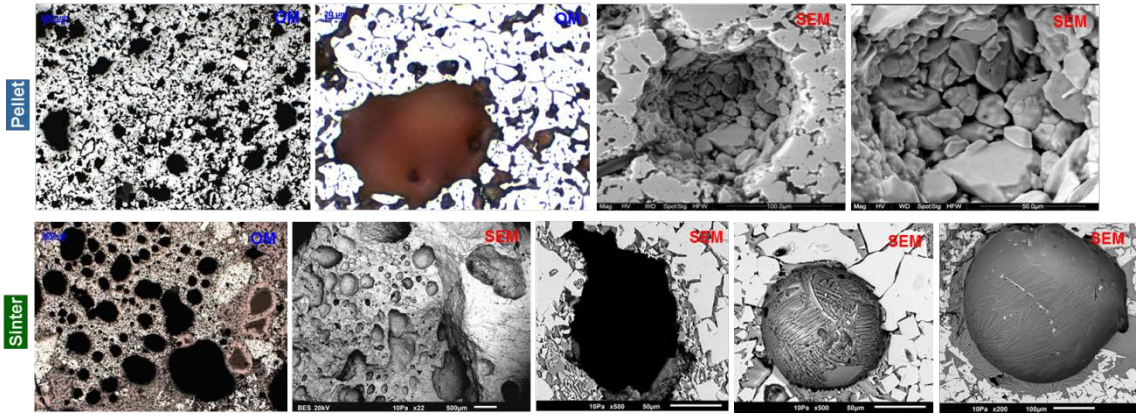

Figure 89: Comparison of morphological characteristics of pores in Samarco pellets and typical Western European Sinter.

5.4.3 REAS Test Results

A total of 10 REAS tests were conducted using the burden components individually and in pre-defined pellet/sinter ratios: 20%/80% and 40%/60%. The pellet/sinter percentages were chosen according to an assessment over the operations of Western European integrated steel plants with Samarco pellets.

From all metallurgical testing standards utilized in this study, the REAS is the most proximal to an actual blast furnace operation, as depicted in the iron-oxygen-carbon diagram of figure 90.

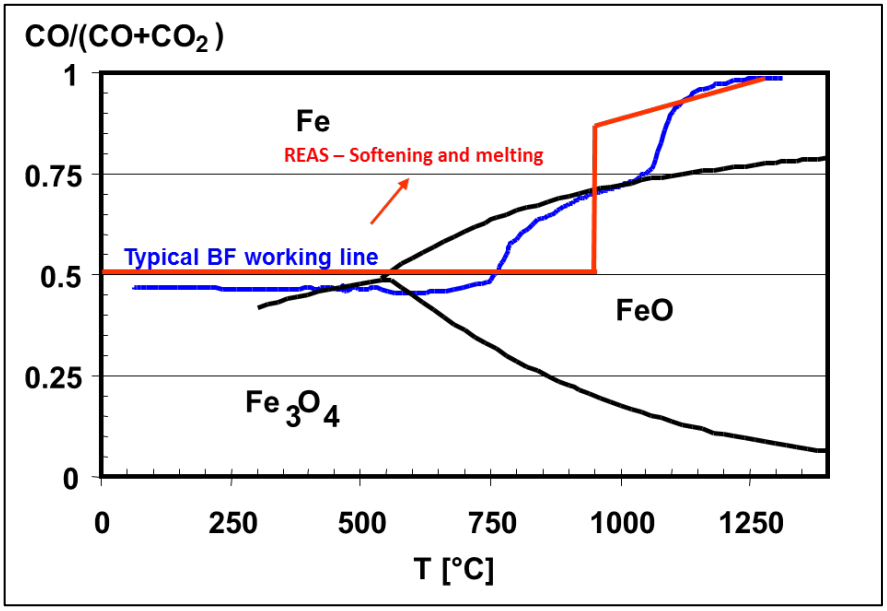

Figure 90: Comparison of the REAS test and an industrial blast furnace operation in relation to CO partial pressure and temperature on an iron-oxygen-carbon diagram.

For better compilation and analysis, the testing results of different burden materials were divided in two categories: reduction behavior during indirect & direct reduction phases and softening & melting behavior.

5.4.3.1 Reduction behavior during indirect and direct reduction phases

The REAS test has pre-established reference points for comparison of different ores throughout its various stages. The series of graphs presented in this section represent the first 150 minutes of test, in which only the indirect reduction of burden materials is assessed. At figure 91 an example of Reduction Index (%) and reducibility (%min) versus time is plotted. In the Reduction Index curve, the chosen reference points are Reduction Index at start of isothermal phase (t = 60 minutes) and Reduction index at the end of indirect reduction (t = 150 minutes). In the Reducibility curve, the chosen reference points for comparison are Max Reducibility 1 and Max Reducibility 2, which account for the reduction steps from hematite to magnetite and from magnetite to wüstite, respectively.

Both curves have a significant change in their patterns at 55 minutes of the test due to the change of reducing gas composition (25% CO2, 15% CO into 35% CO, 5% CO2), which represents the burden descent in a Blast Furnace shaft.

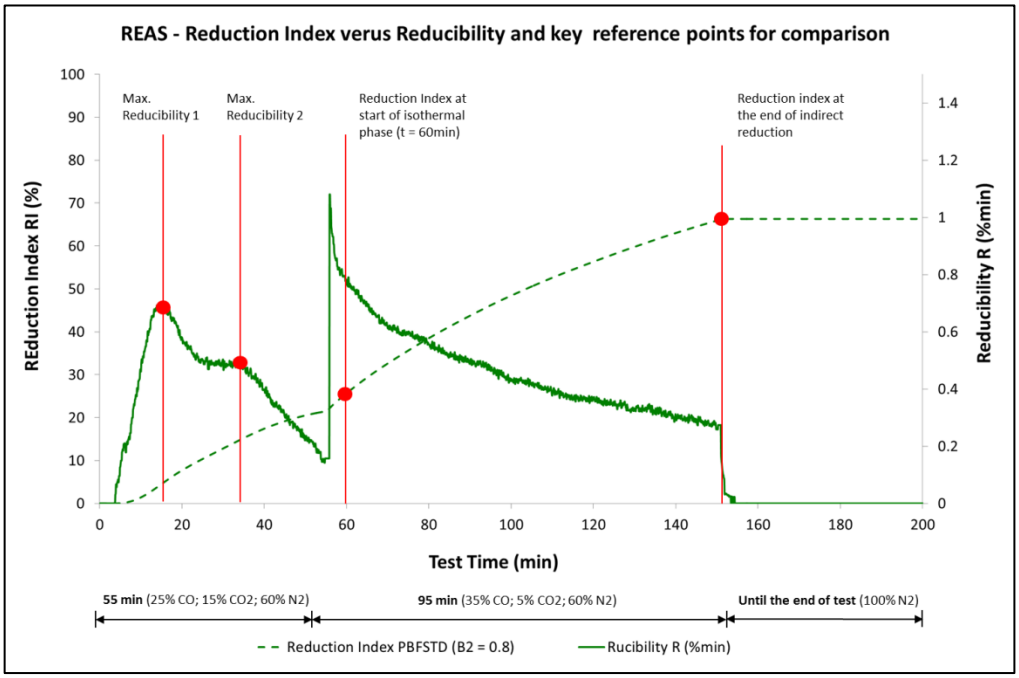

Figure 91: Example of reduction index and reducibility curves as well as their reference points in the REAS test.

Figure 92 describes the reduction index of the three pellet types and sinter separately. Figures 93, 94 and 95 describe the reduction index resulted from the interaction of the mixtures of each pellet type with the Standard Western European sinter at 20%/80% and 40%/60% proportions.

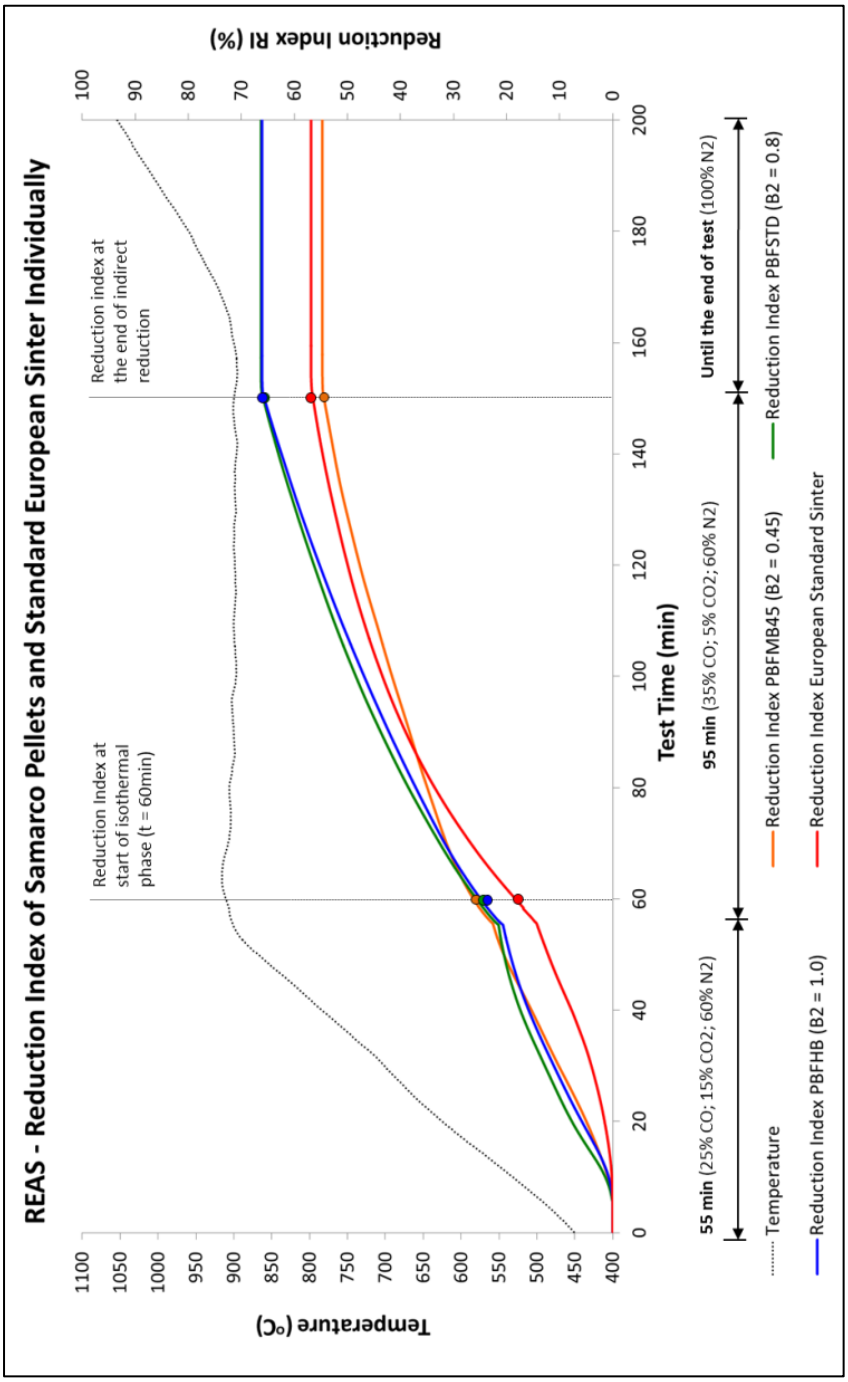

Figure 92: Reduction index of Samarco pellets and typical Western European Sinter sinter separately.

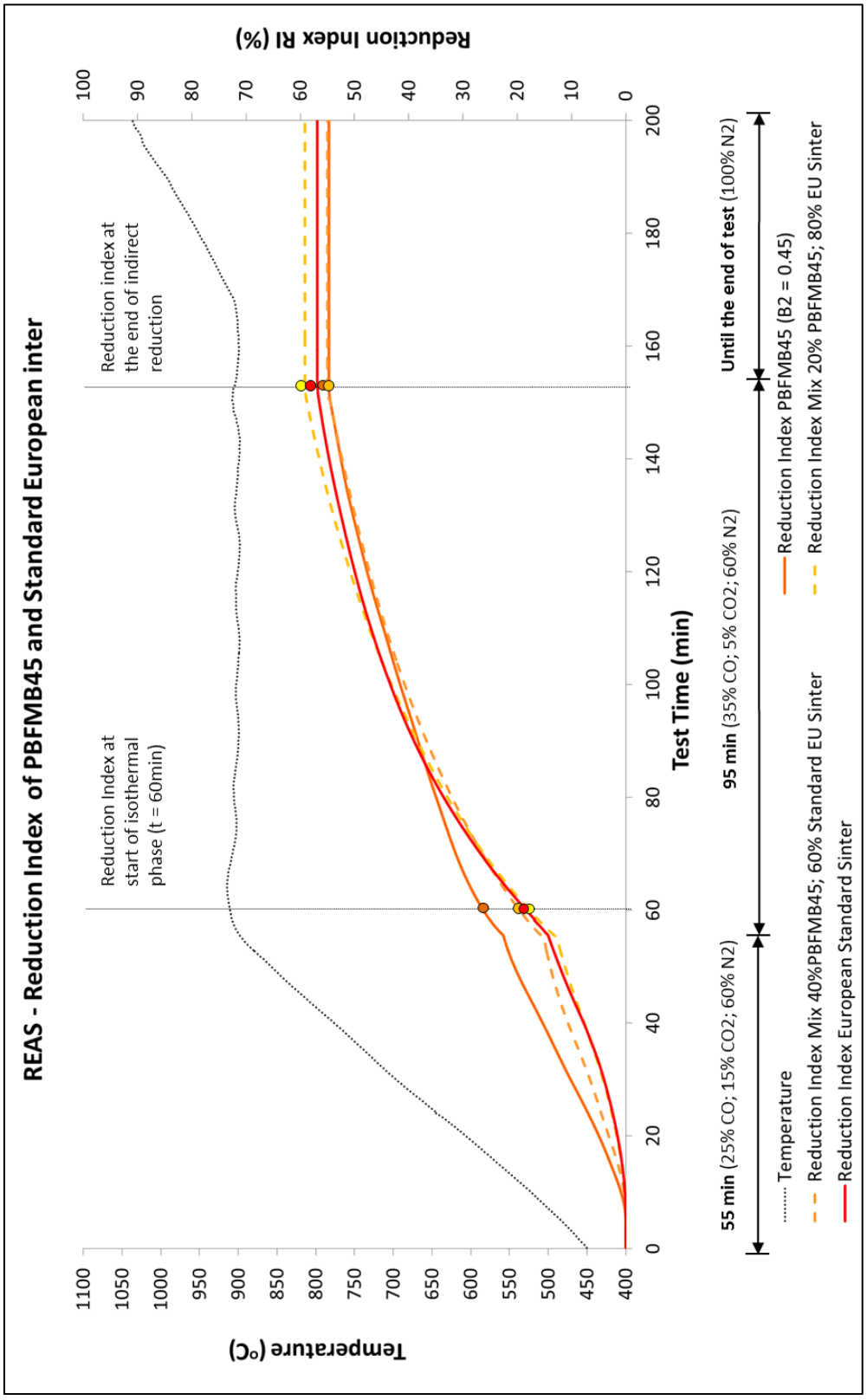

Figure 93: Reduction index of PBFMB45 and typical Western European sinter separately as well as their mixtures at 20%/80% and 40%/60%

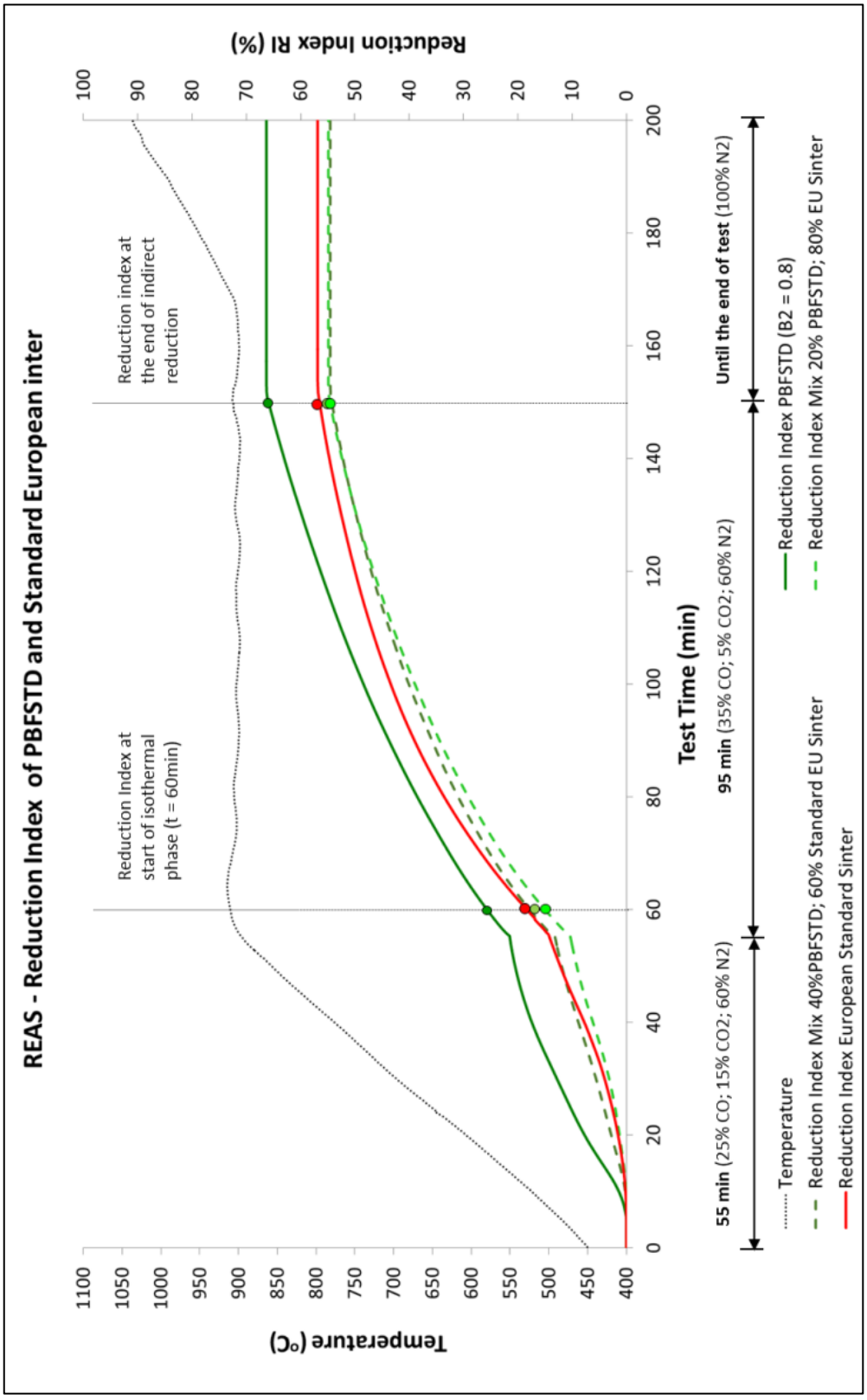

Figure 94: Reduction index of PBFSTD and typical Western European sinter separately as well as their mixtures at 20%/80% and 40%/60%.

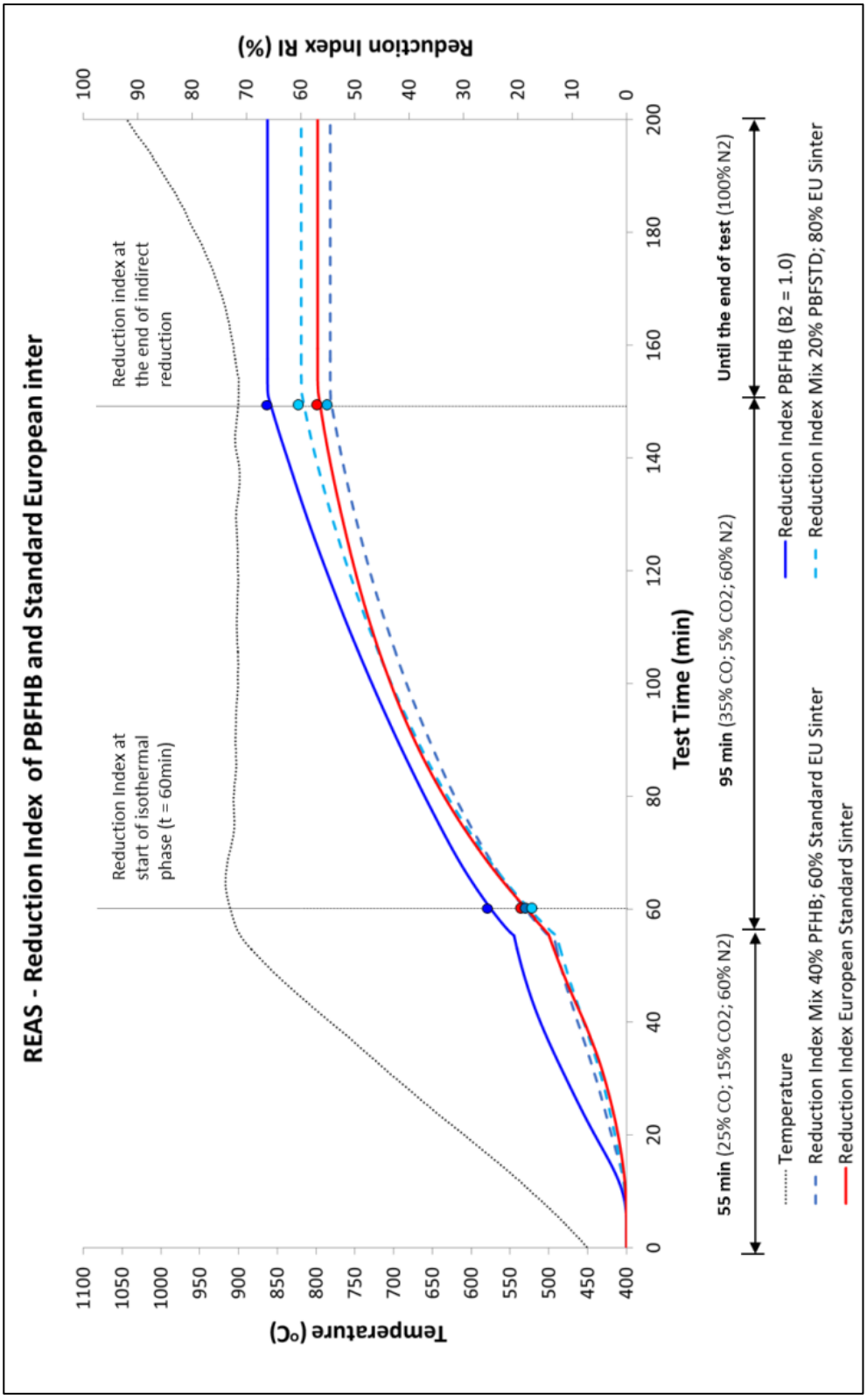

Figure 95: Reduction index of PBFHB and typical Western European Sinter separately as well as their mixtures at 20%/80% and 40%/60%.

When tested separately, all pellet samples present noticeably higher reduction index than sinter at the first stage of the test that lasts until the beginning of the isothermal phase (which afterwards will represent of the beginning of the thermal reserve zone). Reduction index at this point for PBFMB45, PBFSTD, PBFHB and Standard EU Sinter are 26.3%, 25.6%, 24.9% and 18%, respectively. Between the start of isothermal phase and the end of indirect reduction, the two most basic pellet types (PBFSTD and PBFHB) still accumulate higher reduction index whereas PBFMB45 tends to have its reducing behavior similar to the Standard EU Sinter. Reduction index of PBFMB45, PBFSTD, PBFHB and Standard EU Sinter are at this point 55%, 66%, 66% and 57% respectively. Figure 96 illustrates that during this stage of the test, the pressure differential across the bed doesn't significantly differ in the four burden types tested, which means that reducibility was a matter of intrinsic characteristics of the agglomerates rather than permeability loss of the burden. Differently from the RUL test, where PBFMB45 quickly swell and lost stability under pressure, in the REAS this product showed good potential to endure reduction and pressure under reducing conditions more equivalent to an industrial environment.

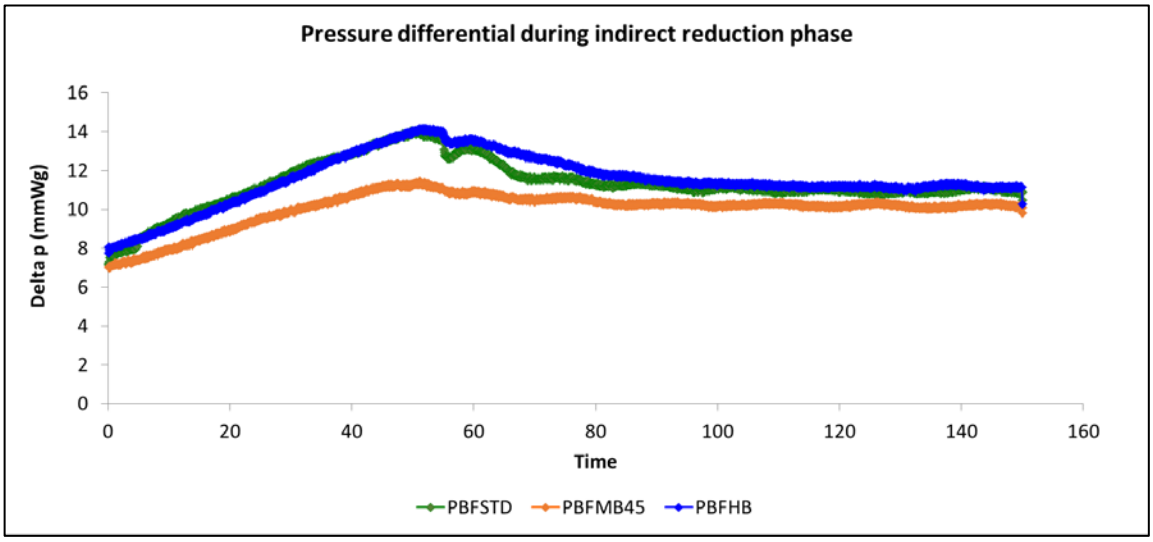

Figure 96: Pressure differential until 150 minutes of the REAS test of PBFBM45, PBFSTD and PBFHB.

In the microscopic characterization session, morphological aspects of fluxed pellets were more favorable for reducibility characteristics when compared to the most acid type and sinter, which corroborate the result found in the REAS test.

For all pellet/sinter mixtures it is reasonable to state that at both 20%/80% and 40%/60% ratios, the reduction index at the reference points followed the tendency of the highest burden component (sinter). Figure 97 describes a summary of Reduction indices at the two mentioned reference points.

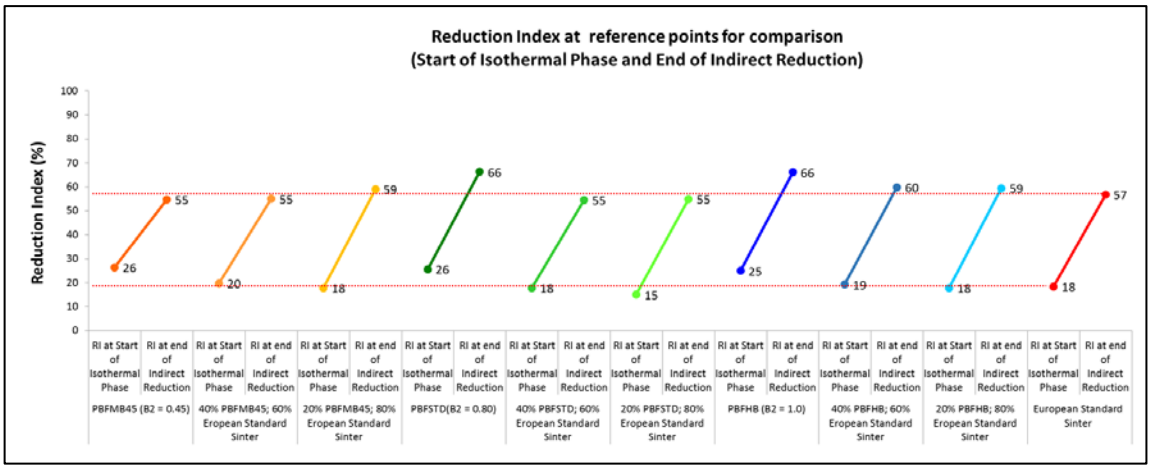

Figure 97: Reduction index at two reference points during indirect reduction of Samarco pellets, typical Western European sinter and their mixtures.

The reducibility behavior of the separate burden components is described in figure 98. In terms of reducibility Index, the most relevant observations are that compared to pellets, the sinter presents a less steep curve - therefore lower reduction kinetics - and registers only one maximum reducibility point. The single maximum reducibility peak is due to the fact that the sinter is a complex agglomerate with already the presence of a large percentage of magnetite (in this specific case FeO% = 7.55% compared to an average of 0.16% in Samarco pellets). Thus, sinter reduction takes place in a slower and more asymmetrical fashion due to the several morphologies and chemical characteristics of its components (silicates, ferrites, hematite and magnetite).

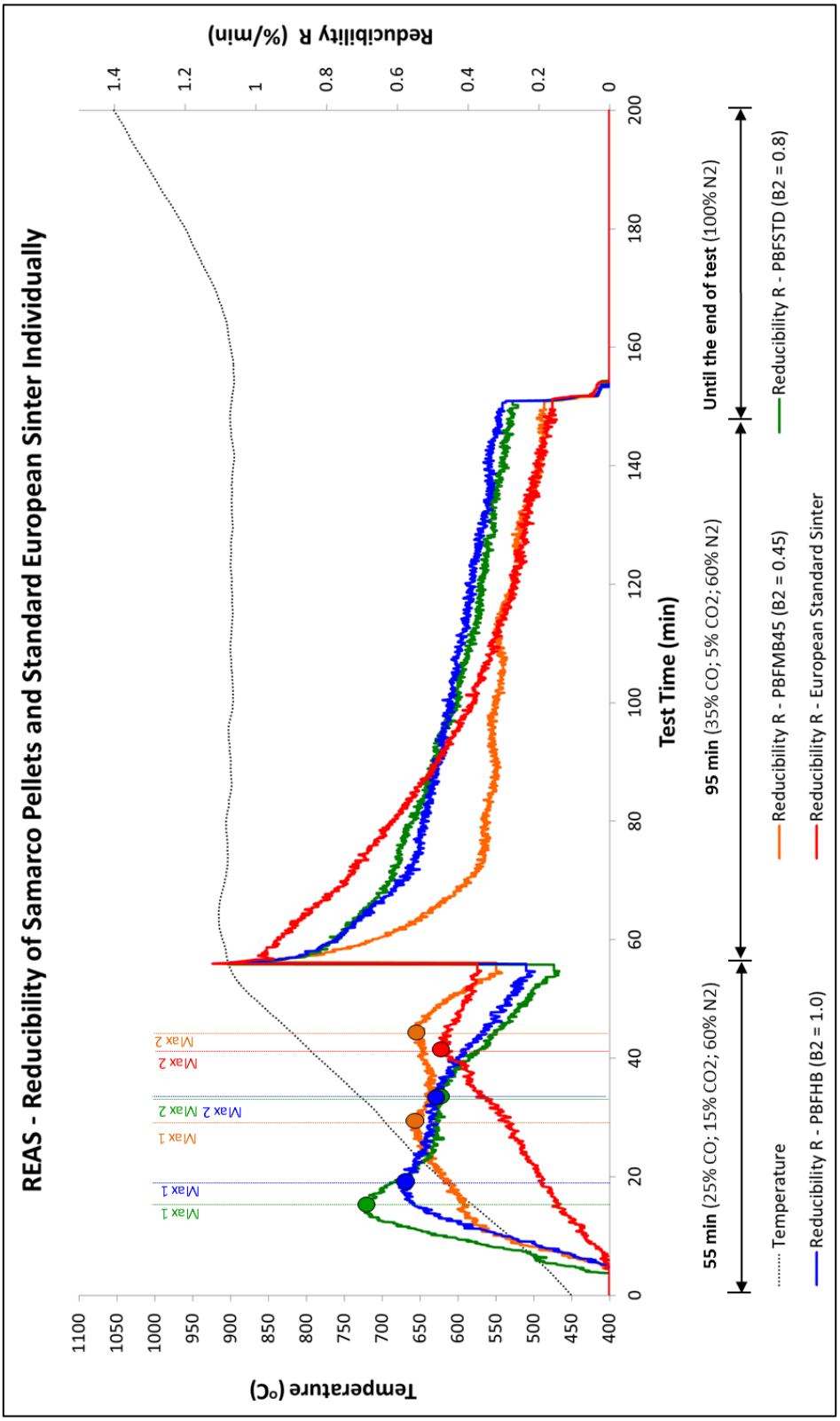

Figure 98: Reducibility R of burden Samarco pellets and typical Western European sinter tested separately.

Figures 99, 100 and 101 represent the reducibility of each pellet type mixed at the predefined proportions with sinter.

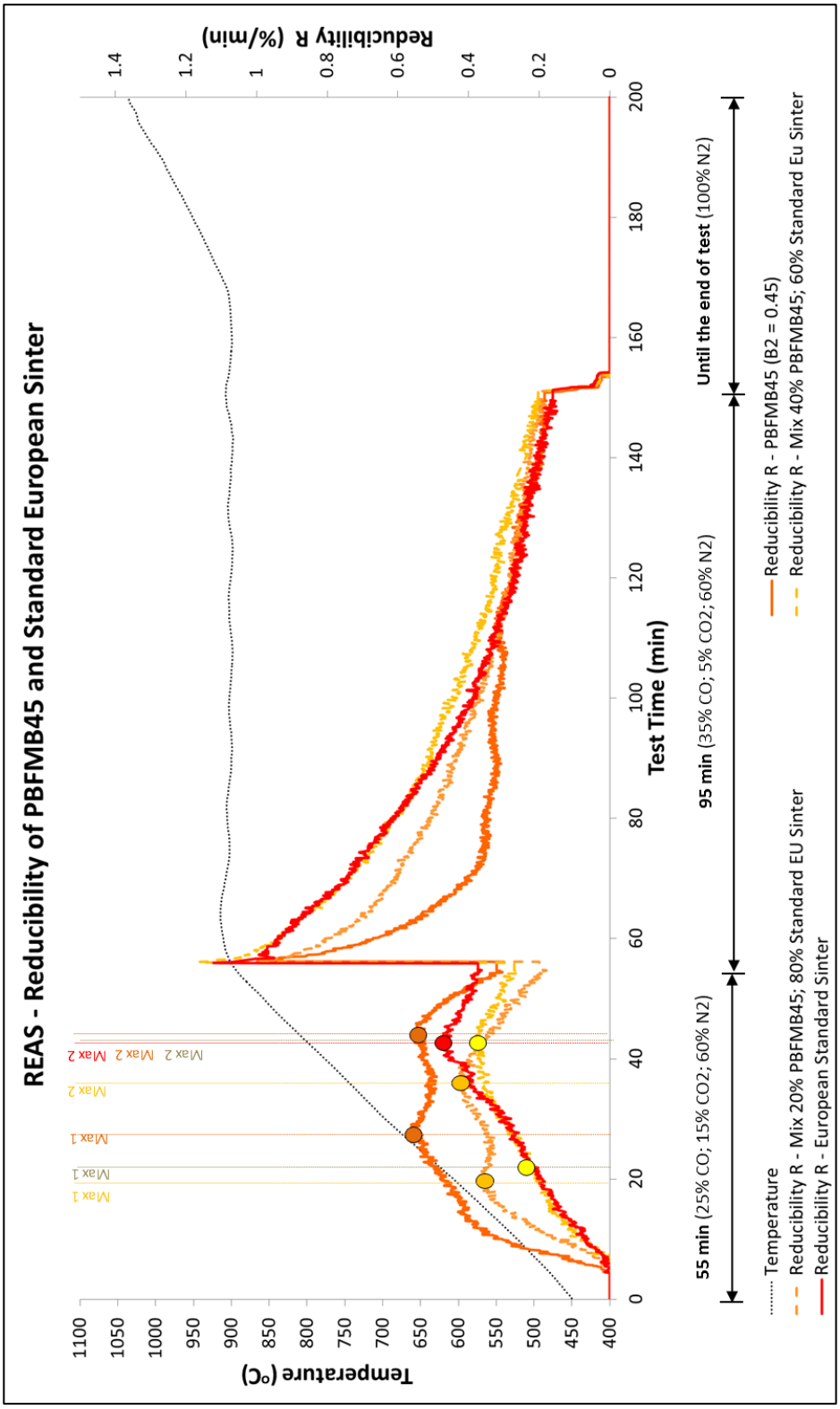

Figure 99: Reducibility R of PBFMB45 and typical Western European Sinter.

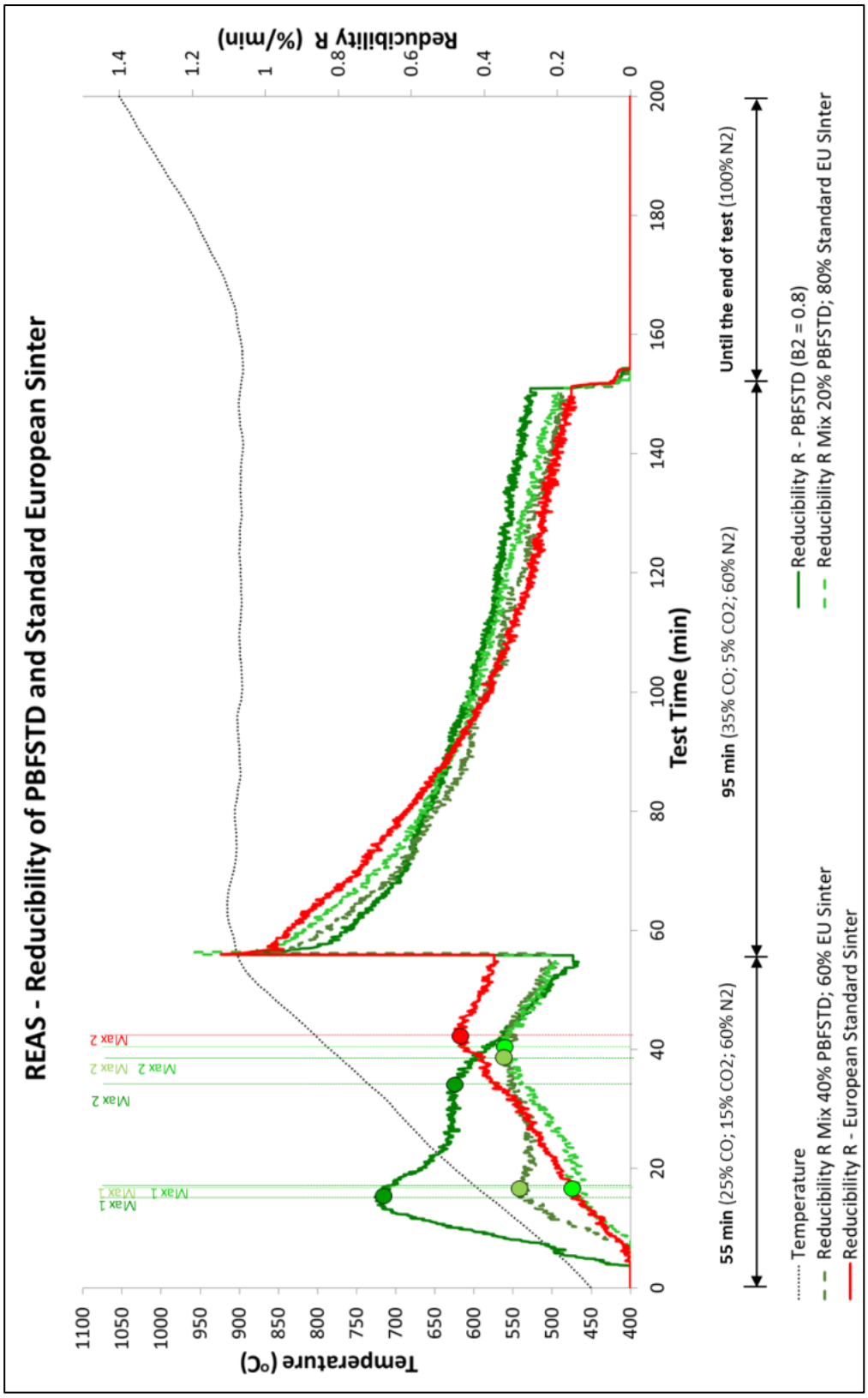

Figure 100: Reducibility R of PBFSTD and typical Western European sinter.

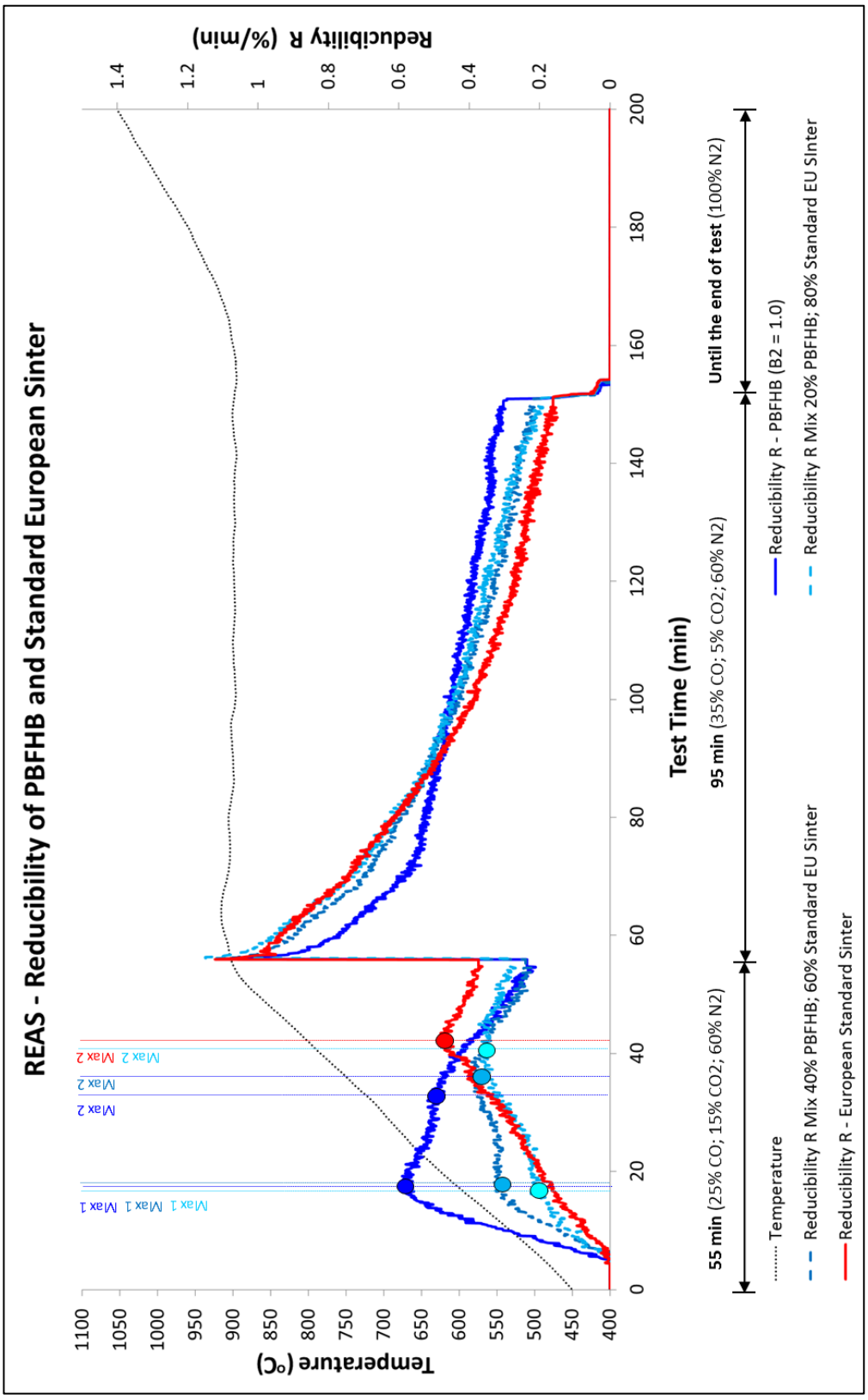

Figure 101: Reducibility R of PBFHB and typical Western European sinter.

Both reference points (maximum reducibility 1 - Max 1 - and maximum reducibility 2 - Max 2 -) are decreased in mixed burdens when compared to pellets tested separately. In other words, kinetics of indirect reduction is diminished by the utilization as sinter participation increases in the ferrous burden.

The indirect reduction phase is interrupted at 150 minutes of the test, when reducing gas is replaced by 100% N_2. The start of the direct reduction phase is indicated when CO starts being noticed in the outlet gas analysis even with only inert gas being fed to the system. In this testing standard solid-solid type reduction reaction (graphite and ferrous agglomerate) is induced to happen in great proportion whereas in a normal blast furnace operation, the direct reduction is majorly characterized also by gaseous reduction at lower regions of the reactor where the products CO_2 and H_2O are not stable and will further react with carbon.

A typical reference point for the start of direct reduction in the REAS test is the temperature at which 0.5%CO is detected in the off gas, as depicted in figure 102. It can be seen that PBFMB45 has the lowest temperature for the start of the direct reduction phase. This can be explained by its partially lower reduction index achieved in the indirect reduction phase when compared to PBFSTD and PBFHB. The sinter sample, although with same behavior of PBFMB45 in the indirect reduction phase, presented high temperature of start of direct reduction phase.

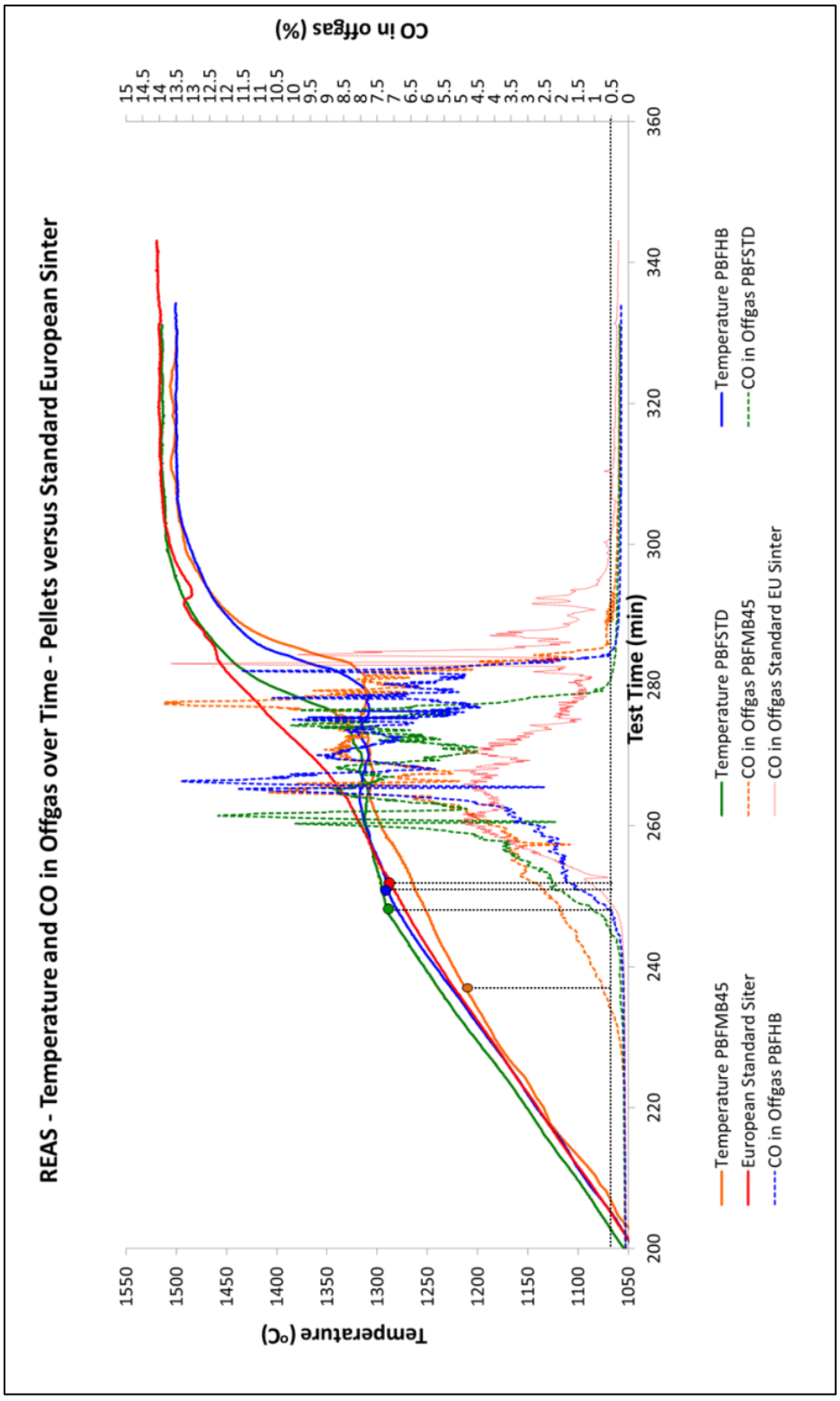

Figure 102: CO reference points for Samarco pellets and typical Western European sinter.

Figure 103 adds one more measured reduction point defined as “Reduction Index at the end of the REAS test” to the already presented figure 97. All three pellet types achieve extremely high reduction indexes and close to the theoretical 100% target after the accomplishment of the test when tested separately: PBFMB45 = 96%, PBFSTD = 97%, PBFSTD = 98%. Sinter alone presents the lowest reduction index at the end of the test: 86%. This fact can represent an increase in the consumption of reductants while processing the subject sinter in comparison to the pellets of Samarco’s portfolio. Due to its lower reducibility characteristics in both indirect and direct reduction phases, liquid compounds with higher amounts of FeO will have to be reduced by direct contact with carbon of the coke slit during its descent towards the hearth consuming more energy.

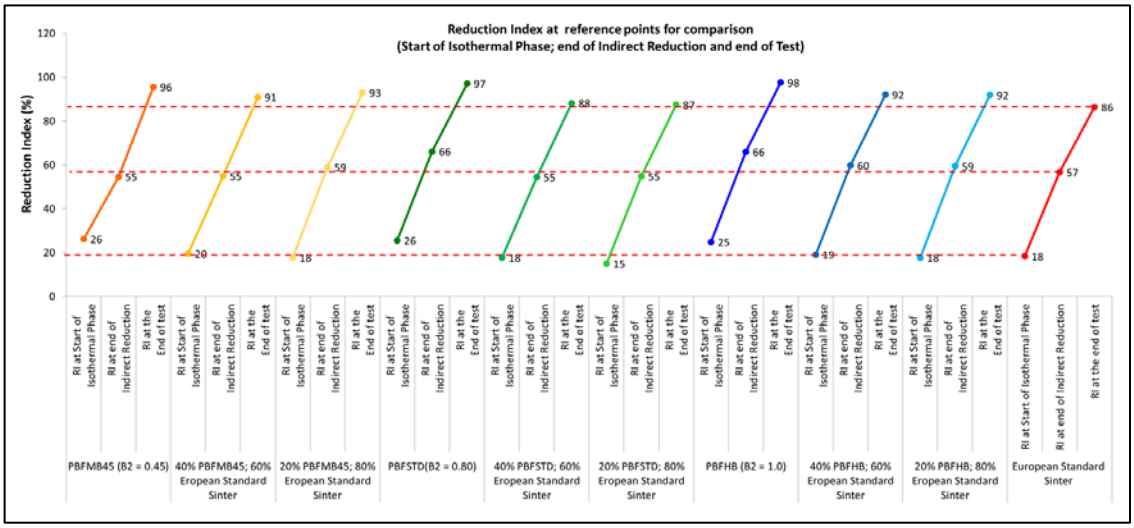

Figure 103: Reduction index at reference points (indirect reduction and end of test) of Samarco pellets, typical Western European sinter and their mixtures.

5.4.3.2 Softening and melting behavior

In an industrial operation, factors like swelling of pellets, decripitation of lump ores and degradation during reduction of all burden materials (e.g. LTD and RDI) and finally softening temperatures will play important role in the differential pressure of a Blast Furnace. The REAS is not capable of reproducing all of the factors that contribute to the increasing of resistance against process gas passage, however it provides reference data of two major indicators for softening behavior which is the most important ferrous burden property for permeability: temperature at which the sample

achieves 50% of shrinkage and temperature of maximum differential pressure of the test (200mmWG, moment when a bypass valve must be opened to prevent blow-up of molten material).

Figure 104 depicts the temperatures of 50% shrinkage of individual samples and figure 105 depicts the temperatures of 200mmWG of differential pressure.

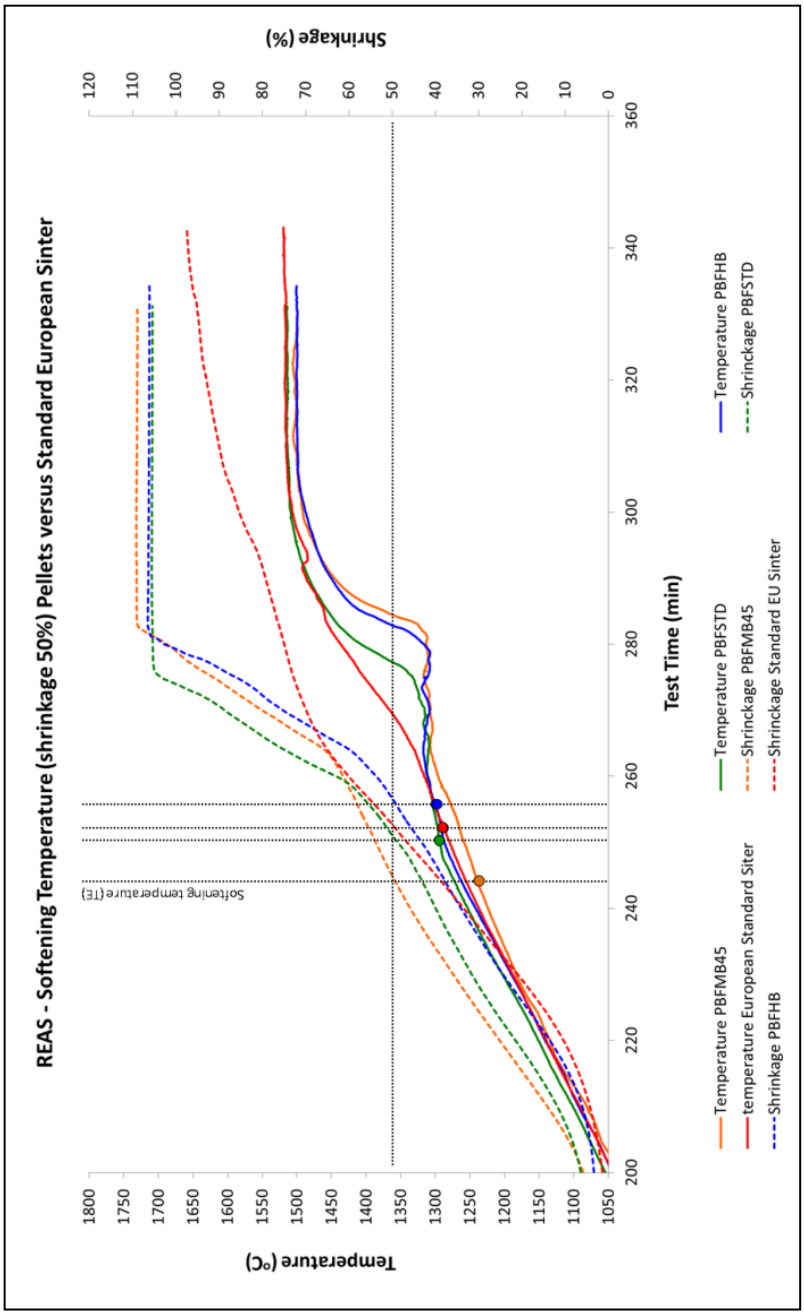

Figure 104: Softening temperature (shrinkage 50%) of Samarco pellets and typical Western European Sinter

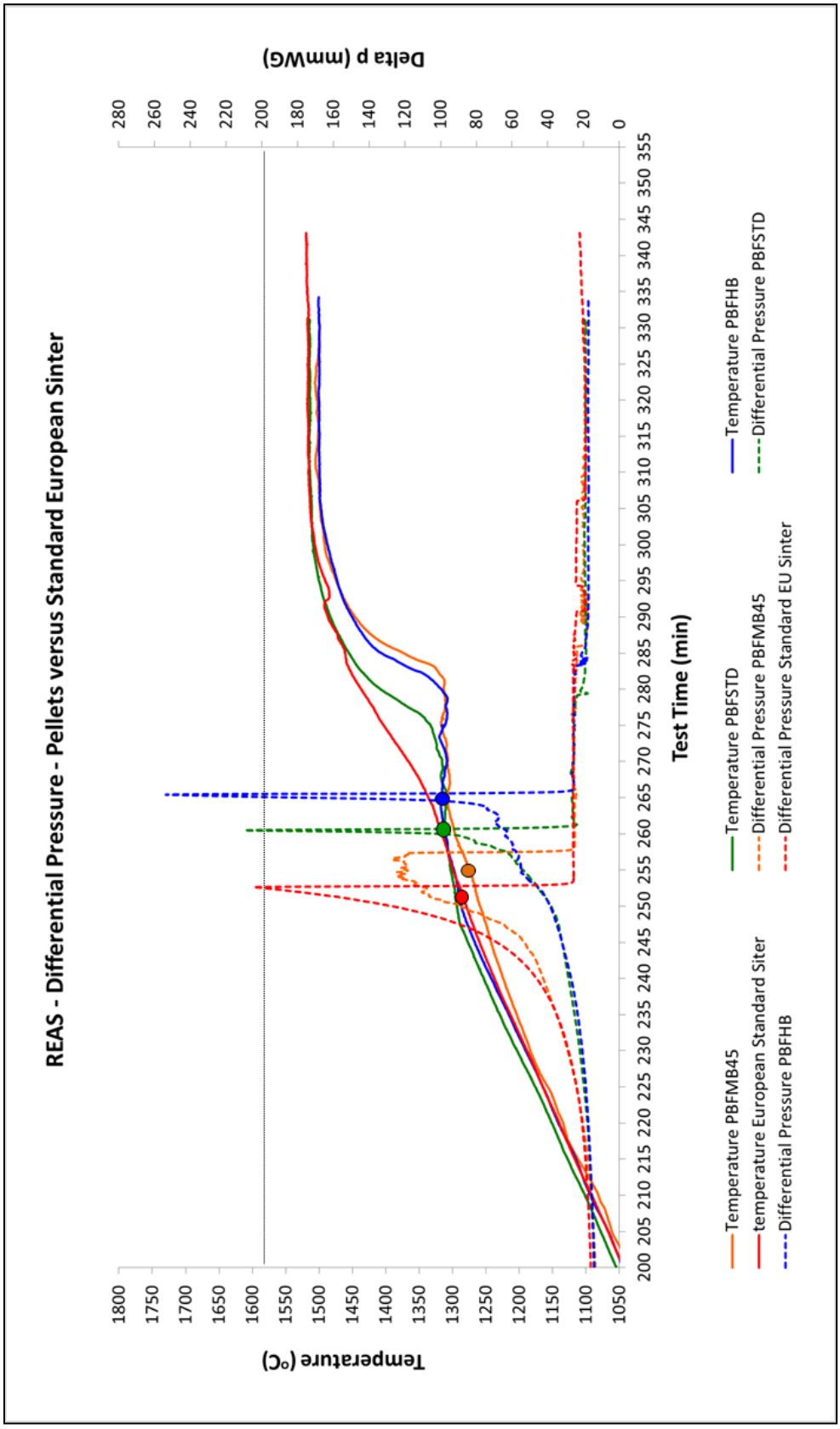

Figure 105: Softening temperature (differential pressure = 200 mmWG) of Samarco pellets and typical Western European Sinter

In both reference points there are distinctions of softening behavior of burden materials tested separately being PBFMB45 < Sinter < PBFSTD < PBFHB. When mixtures are tested, sinter behavior tends to be predominant in the case of PBFMB45 and PBFSTD; however the pellet with highest basicity PBFHB has its softening temperatures significantly increased. Figure 106 depicts the reference temperatures at both reference points.

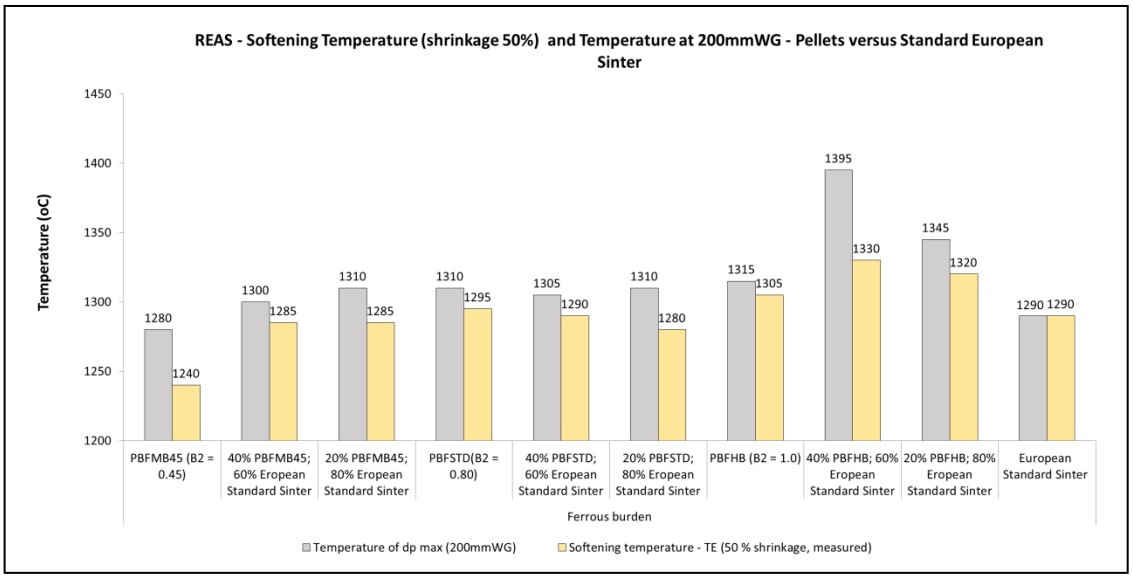

Figure 106: temperature at 50% shrinkage and temperature at dp maximum (200mmWG) of Samarco pellets, typical Western European sinter and their mixtures.

Commonly, the softening in the REAS test and also in an industrial blast furnace operation will start with the melting of oxide phases with lowest melting point in the agglomerate's core, which will act as lubricant to the remaining particles. Enclosing the remaining oxide phases there is usually a metallic shell (iron shell) which will withstand pressure and temperature before the molten material is finally exuded. The thicker the metallic shell, the better it can resist to deformation caused by the tendency of liquid phases to penetrate in its structure (interior factor) and also by the carburization effect/cementitization through direct contact with carbon (exterior factor). The attack by carbon will lead to cracks and reduction of its solidus temperatures as depicted in figure 107.

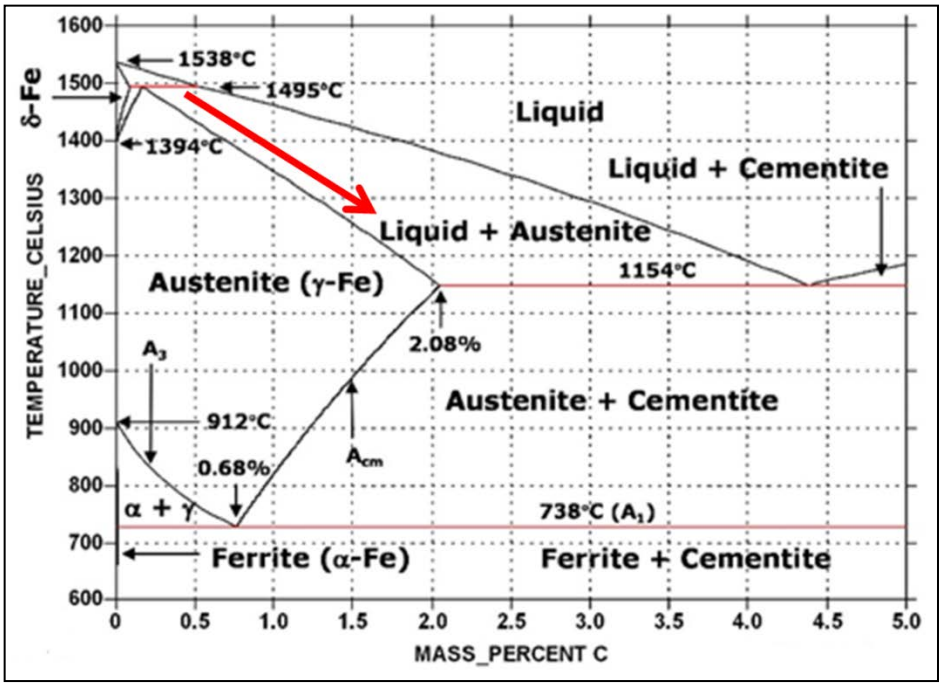

Figure 107: Fe-C binary diagram and the influence of carburization in the reduction of the solidus temperature.

The two fluxed pellets in Samarco's product portfolio (PBFSTD and PBFHB) have higher reduction rates and more regular topo-chemical reduction behavior when compared to Samarco's medium basicity pellet; therefore they will present thicker metallic shells and lower percentages of FeO, a constituting element that leads to lower liquidus temperatures. PBFMB45's larger porosity will also pose difficulties for the agglomerate's stability at high temperature and pressure. Although at this moment sinter still hasn't achieved the same reduction degree of pellets, it yet has higher basicity therefore a similar strength to withstand softening as PBFSTD and PBFHB, even with higher percentages of FeO compared these two pellet types. The ternary diagram of figure 108 depicts the liquidus temperatures according to FeO percentage in the slag. Mixtures of PBFMB45 and sinter will present higher softening temperatures when compared to this pellet type alone, as after exudation the primary slag of PBFMB45 will be exposed to a new system and immediately undergo stoichiometric adjustments which will retard the increase of its viscosity. Mixtures of PBFSTD and sinter presented similar softening characteristics of the two burden components alone. Mixtures of PBFHB and sinter presented an increase of softening temperatures.

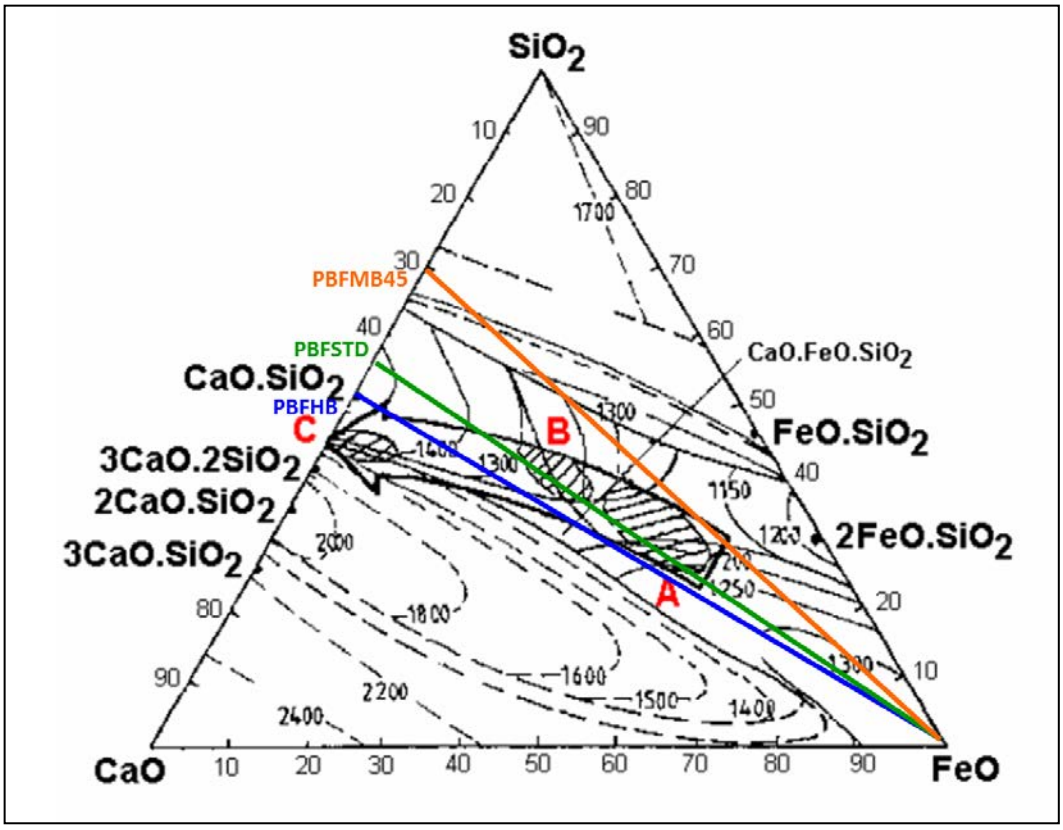

Figure 108: CaO-FeO-SiO2 ternary diagram.

The exudation of molten material from the iron shell can be also noticed by the change in slope of the temperature curve registered by the thermocouple positioned in the center of the test sample. Melting of primary slag is characterized by endothermal reactions and it is captured by the TSS measurement points in figures 109, 110, 111 and 112 for PBFMB45, PBFSTD, PBFHB and sinter, respectively. It is also associated to an increase in the CO content in the off gas, as at this moment the reduction is very much hindered by loss of permeability. The figures also present other important standard measurement points, as TA1 & TA2 and TBF1 & TBF2. TA1 represents the dripping of primary slag on the scale positioned under the perforated crucible of the REAS test and is marked by small quantity in grams, to be followed by TBF1, the dripping temperature of iron, which is marked by a significant increase of the mass quantities measured on the scale. TA2 and TBF2 are theoretical interpolated temperatures in case the curves would have followed their pre-defined slopes which are indicated by dashed lines.

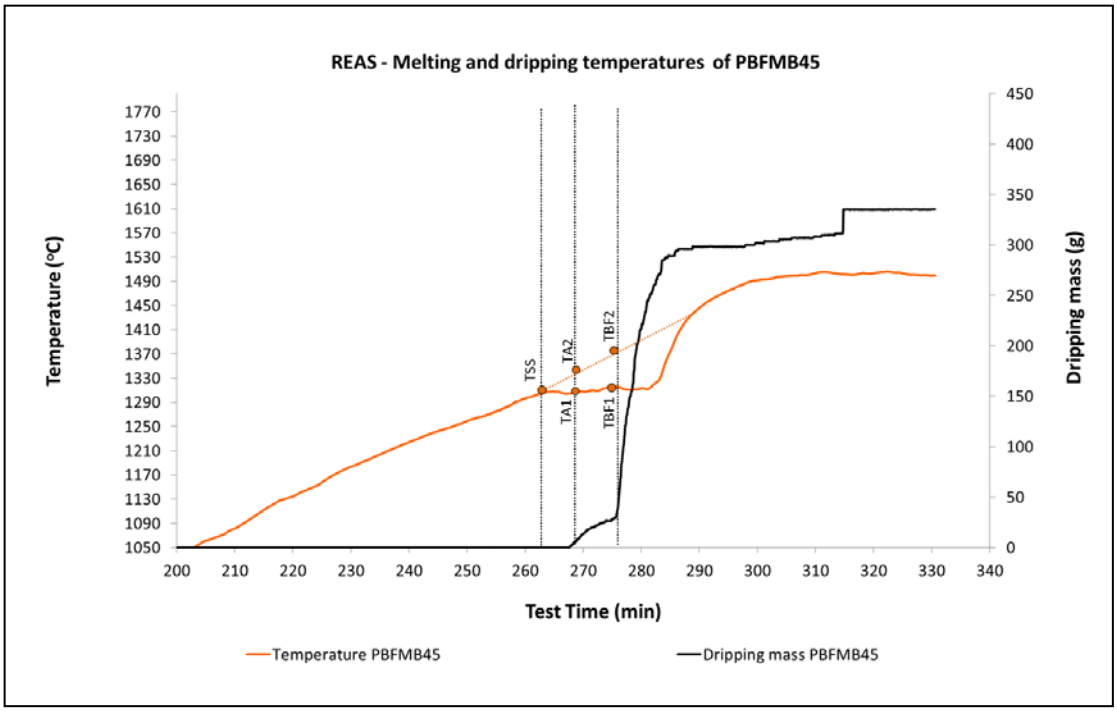

Figure 109: Melting and dripping temperatures of PBFMB45.

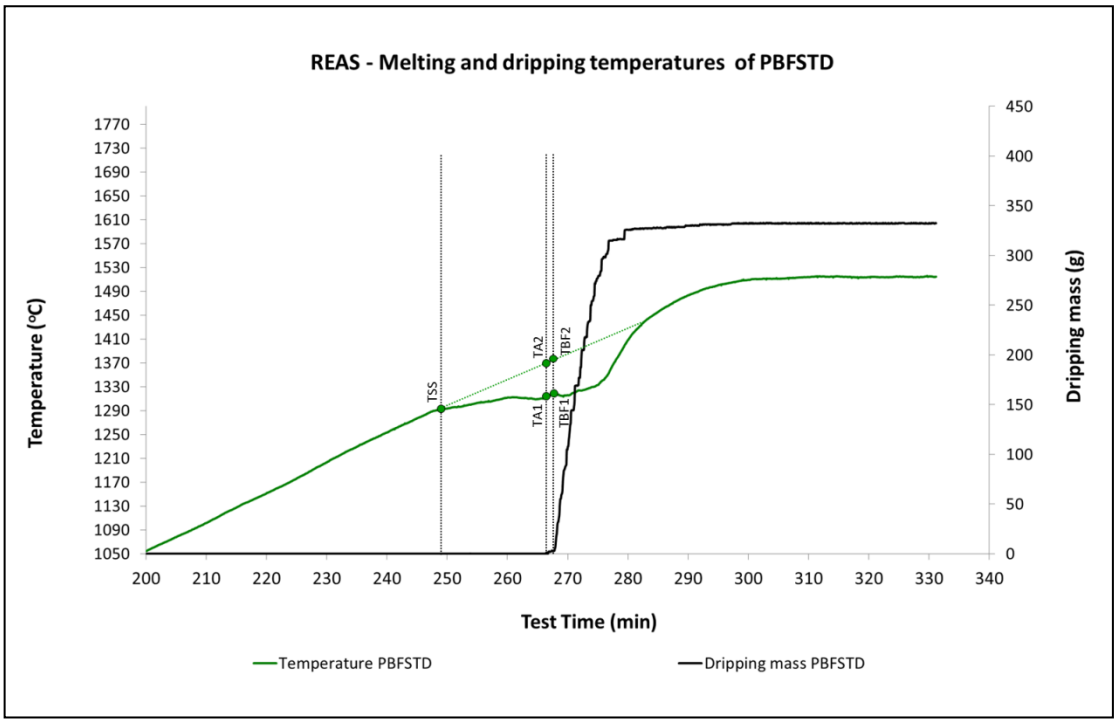

Figure 110: Melting and dripping temperatures of PBFSTD.

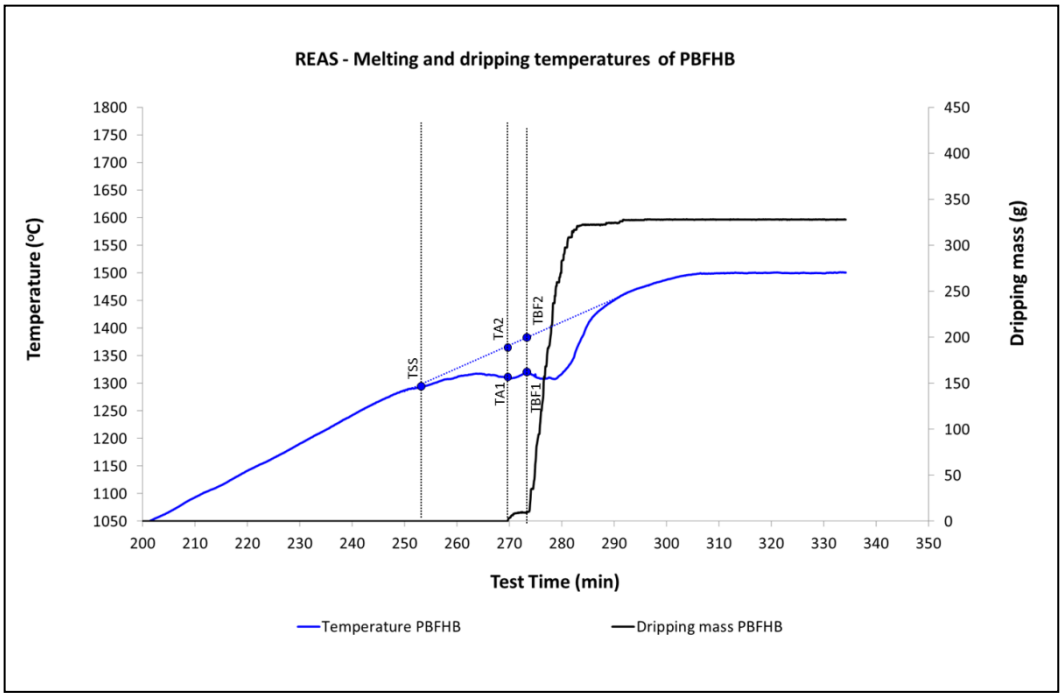

Figure 111: Melting and dripping temperatures of PBFHB.

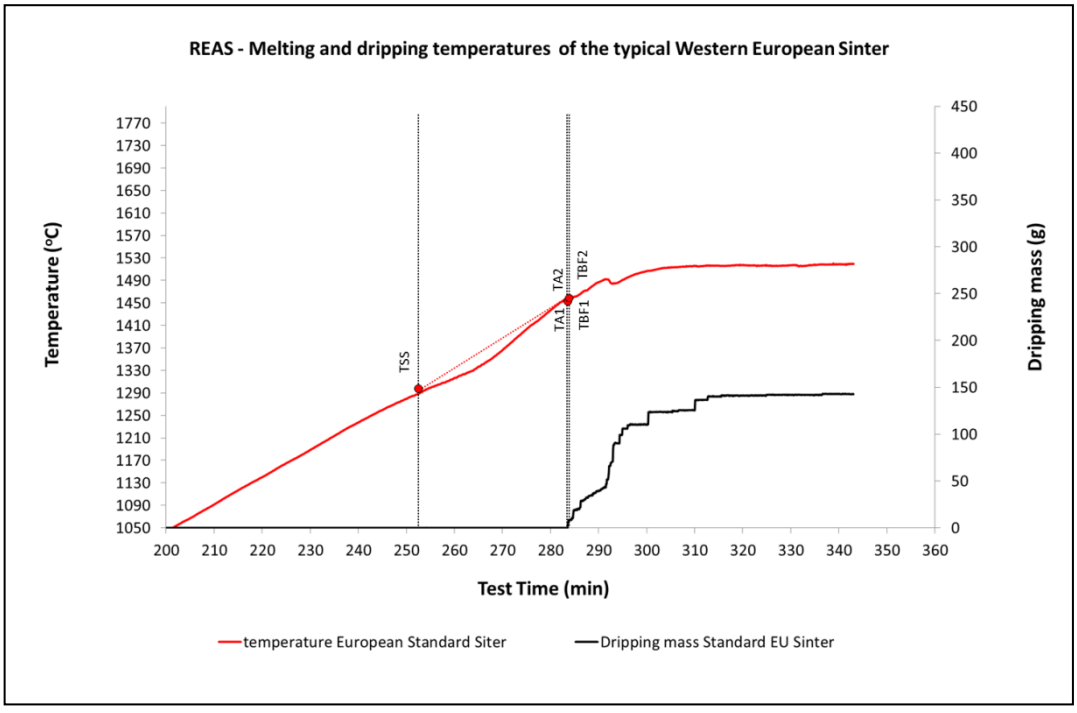

Figure 112: Melting and dripping temperatures of typical Western European sinter.

It can be noticed that all pellet types have similarly lower temperatures for the dripping of primary slag and iron when compared to the Standard European Sinter. It is also possible to state that pellets have distinguished dripping of a small portion of mass (primary slag), followed by a significant increase on the scale measurement (dripping of iron), whereas sinter doesn't present a regular distinction between both. This indicates that pellets will tend to follow the theoretical consideration of the iron shell formation followed by exudation of FeO-rich primary slag. The delayed dripping effect of the sinter has to do with its higher basicity and MgO-rich compounds with higher melting temperatures. Figure 113 depicts a summary of the dripping temperatures of all the 10 REAS tests comprised of 100% pellets and sinter separately and their mixtures at 40/60% and 20/80%. It can be noticed that for a burden with high participation of pellets (40% pellets and 60% sinter), PBFSTD and PBFHB already present very similar dripping temperatures of primary slag and iron as the one of sinter alone. At 40%/60% ratio PBFMB45 presents higher temperatures for TA1 and TBF1 but not in the same level as sinter. This behavior indicates that in high pellet participation a burden comprised of a mix PBFHB/sinter or PBFSTD/sinter tends to strongly interact and the sinter's higher melting/dripping temperatures shall prevail, whereas high participation of PBFMB45 (>=40%) may influence the cohesive zone thickness due to this pellet's lower melting/dripping temperatures. The mixtures 20% pellets 80% sinter presented high dripping temperatures for all pellet types. The result indicates that this percentage of pellets the burden will have a very homogeneous pellet/sinter interaction at high temperatures and a very stable thin and low-positioned cohesive zone is expected as result for the three products (PBFMB45, PBFSTD and PBFHB). As no tests were interrupted for microscopy assessment, the burden interaction can only be inferred according knowledge acquired through literature review. At 20% pellets strong evidences point at a burden behavior similar to sinter alone, however the major interaction steps to be considered in a burden with high pellet participation (>=40%) are:

Step one – Sintering of solid phases at the interface of different burden components: PBFHB and PBFSTD, by presenting thicker and more consolidated iron shells shall generate higher rates of sintering of solid phases with sinter when compared to PBFMB45.

Step two – incipient liquid slag formation: already explained to take place at larger proportions as pellet basicity is decreased, therefore the sequence from higher to lower presence of liquid slag formation will be PBFMB45> PBFTSTD> PBFHB.

Step three – interaction of liquid at interface: exuded liquid may react with oxide phases or the neighboring iron shell which leads to its coarsening.

Step four – interaction of core materials: liquid phases exuded from the different agglomerates will strongly interact and generate new stoichiometric compounds. The increase of all dripping temperatures of burden mixes compared to pellets alone can be attributed to this mechanism.

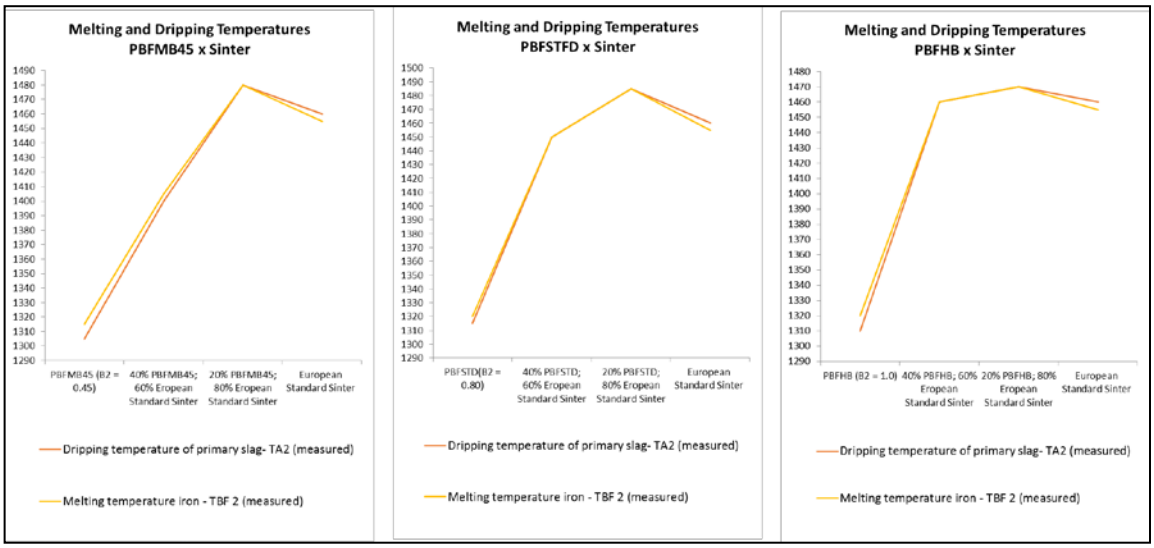

Figure 113: Comparison of melting and dripping temperatures of pellets individually and their mixtures at 40%/60% and 20%/80% with typical Western European sinter.

6. Conclusions

The lower quantity of calcium silicates allied to the inferior growth of iron oxide grains makes PBFMB45 the most porous of the pellets in Samarco's blast furnace portfolio.

PBFSTD presents larger iron oxide grain sizes and lower level of inter-granular porosity when compared to PBFMB45. The higher limestone addition of PBFSTD in comparison to PBFMB45 will lead to the formation of intergranular melting phases in larger quantities. These phases have important role as transport medium for the growth of iron oxide crystals.

PBFHB presents the highest growth of iron oxide grains of all pellet types, with also homogeneously round structure. The higher presence of silicates and ferrites made them percolate through pores, reducing their numbers. Magnetite was present in the pellet core as lower porosity causes some restriction to re-oxidation during induration.

In the case of Samarco's portfolio, all the three pellet types have superior LTD properties; however the increased percentages of silicates and ferrites from PBFMB45 to PBHB will result in slightly improved trends on this metallurgical characteristic. Silicates and ferrites will act as a supporting frame preventing exaggerated fines generation, as the tension caused by the HC – CFC transformation of Fe_2O_3 into Fe_3O_4 takes place.

All of Samarco pellets are in the acceptable range of ISO swelling and the progression to higher basicities will work in favor of the lower occurrence of whiskers.

At the Reduction under Load Test (ISO), Samarco's CaO fluxed pellets seemed to follow a reduction behavior more similar to the topo-chemical theoretical model when compared to Samarco's middle-basicity pellet. In PBFMB45 the iron formation predominated as filaments "whiskers" causing a more pronounced swelling phenomena when compared to PBFSTD and PBFHB.

It is reasonable to state that for the CaO fluxed pellet types were more able to withstand temperature and static pressure with lower bed height contraction and lower burden pressure differential. In the case of the middle basicity pellet, bed contraction was intensified as growth of whiskers took place abruptly already deeper in the agglomerate's radius, due its higher intergranular porosity.

The reducibility of Samarco pellets is usually high due to the intrinsic ore characteristics of Alegria Complex, which is the same for the three blast furnace types produced. However, the increments of basicity from the lowest level (PBFMB45) to (PBFHB) will lead to higher reduction index results under ISO 7215. The explanation for this phenomenon is in the fact that ferrites and silicates with higher molar participation of calcium oxides are, up to certain limits, more subject to fast reduction. In this specific metallurgical test it is important to mention that swelling of pellets with lower basicity will also affect the bulk permeability and hinder reducibility as a whole, as ISO 7215 is undertaken under more aggressive conditions when compared to an actual blast furnace operation.

Although in absolute numbers the quantity of pores was similar in sinter and pellet samples, their distribution and sizes are more homogeneous in the pellet sample when compared to the sinter sample. Hematite is predominant in the pellet type whereas a mixture of mostly secondary hematite and magnetite are present in the sinter sample. The presence of silicates and ferrites are much larger in the sinter sample due to its higher calcium and magnesium percentages.

In the REAS methodology, when agglomerates are tested separately, all pellet samples present noticeably higher reduction index than sinter until the start of the thermal reserve zone. Reduction index at this point for PBFMB45, PBFSTD, PBFHB and Standard EU Sinter are 26.3%, 25.6%, 24.9% and 18%, respectively.

Between the start of isothermal phase and the end of indirect reduction, the two most basic pellet types (PBFSTD and PBFHB) still accumulate higher reduction index whereas PBFMB45 tends to have its reducing behavior similar to the Standard EU Sinter. Reduction index of PBFMB45, PBFSTD, PBFHB and Standard EU Sinter are at this point 55%, 66%, 66% and 57% respectively.

During the entire indirect reduction phase in the REAS test, the pressure differential across the bed doesn’t significantly differ in the four burden types tested, which means that reducibility was a matter of intrinsic characteristics of the ores rather than permeability loss of the burden. Differently than in the RUL test, where PBFMB45 quickly swell and lost stability under pressure, in the REAS it showed good potential to endure reduction and pressure under more equivalent conditions to an industrial blast furnace.

In the microscopic characterization session, morphological aspects of fluxed pellets were more favorable for reducibility characteristics when compared to the most acid type and sinter, which corroborate the result found in the REAS test.

For all pellet/sinter mixtures it is reasonable to state that at both 20%/80% and 40%/60% ratios, the reduction index at the reference points followed the tendency of the highest burden component (sinter).

All three pellet types achieve extremely high reduction indexes and close to the theoretical 100% target after the accomplishment of the test when tested separately: PBFMB45 = 96%, PBFSTD = 97%, PBFSTD = 98%. Sinter alone presents the lowest reduction index at the end of the test: 86%. This fact can represent an increase in the consumption of reductants while processing the subject sinter in comparison to the pellets of Samarco's portfolio.

In both softening reference points of the REAS test there are distinctions in the behavior of burden materials tested separately: PBFMB45 < Sinter < PBFSTD < PBFHB. When mixtures are tested, sinter behavior tends to be predominant in the case of PBFMB45 and PBFSTD; however the pellet with highest basicity PBFHB has its softening temperatures significantly increased.

The two fluxed pellets in Samarco's product portfolio (PBFSTD and PBFHB) have higher reduction rates and apparently more regular topo-chemical reduction behavior when compared to Samarco's medium basicity pellet. They tend to therefore present thicker metallic shells and lower percentages of FeO, a constituting element that leads to lower liquidus temperatures. PBFMB45's larger porosity will also pose difficulties for the agglomerate's stability at high temperature and pressure. Although at this moment sinter still hasn't achieved the same reduction degree of pellets, it yet has higher basicity therefore a similar strength to withstand softening as PBFSTD and PBFHB, even with higher percentages of FeO compared these two pellet types.

Mixtures of PBFMB45 and sinter will present higher softening temperatures when compared to this pellet type alone, as after exudation the primary slag of PBFMB45 will be exposed to a new system and immediately undergo stoichiometric adjustments which will retard the increase of its viscosity. Mixtures of PBFSTD and sinter presented similar softening characteristics of the two burden components alone. Mixtures of PBFHB and sinter presented an increase of softening temperatures.

It can be noticed that all pellet types have similarly lower temperatures for dripping of primary slag and iron when compared to the Standard European sinter.

It is also possible to state that pellets have distinguished dripping of a small portion of mass (primary slag), followed by a significant increase on the scale measurement (dripping of iron), whereas sinter doesn't present a regular distinction between both. This indicates that pellets will tend to follow the theoretical consideration of the iron shell formation followed by exudation of FeO-rich primary slag. The delayed dripping effect of the sinter has to do with its higher basicity and MgO-rich components with higher melting temperatures.

In a burden with high participation of pellets (40% pellets and 60% sinter), PBFSTD and PBFHB already present very similar dripping temperatures of primary slag and iron as the one of sinter alone. At 40%/60% ratio PBFMB45 presents higher temperatures for TA1 and TBF1 but not in the same level as sinter.

This behavior indicates that in high pellet participation a burden comprised of a mix PBFHB/sinter or PBFSTD/sinter tends to strongly interact and the sinter's higher melting/dripping temperatures shall prevail, whereas high participation of PBFMB45 (>=40%) may influence the cohesive zone thickness due to this pellet's lower melting/dripping temperatures.

The mixtures 20% pellets 80% sinter presented high dripping temperatures for all pellet types. The result indicates that this percentage of pellets the burden will have a very homogeneous pellet/sinter interaction at high temperatures and a very stable thin and low-positioned cohesive zone is expected as result.

Suggestions for future studies

Extension of the pellet/sinter metallurgical interaction assessment to the characteristics of the other major blast furnace markets for Samarco: Asia ex-China, China, and Americas.

Throughout this work indications of lower reductant consumption of a burden with higher percentage of low-slag pellets were found through metallurgical testing. This should be further investigated with correlation with industrial operations.

Evaluation of softening and melting properties of low silica pellets with higher levels of MgO as fluxing agent and high silica acid pellets, to be compared with Samarco's current portfolio.

7. References

1. LÜNGEN, H.B., PETERS, M., SCHMÖLE, P. *Ironmaking in Western Europe – Status quo and future trends*. In: METEC & ESTAD, Dusseldorf, 2015.

2. BABICH, A., SENK, D., GUDENAU, H.W., MAVROMMATIS, K. *Ironmaking;* Textbook. Aachen: Institut fuur Eisen:uttenkunde der RWTH Aachen, 2008. 402p.

3. BARTOS, R., BROCKMANN, S., FANDRICH, R., ENDEMANN, G., HEINZEL, M.A., KEUL, C., LETZ, K., LÜNGEN, H.B., MONINGER, G., SPRECHER, M., STEELMACHER, U., WIELAND, H.J., WINKELGRUND, R., WÖCKNER, H. *Steel Manual.* Dusseldorf: Verlaag Stahleisen GmbH, 2015. 218p.

4. Samarco Mineração's business intelligence internal databank.

5. LESSA, A. *Avaliação de Valor em Uso de cargas ferríferas para Alto-Forno*. Rio de Janeiro: PUC-Rio, 2009. 123p. (Dissertação, Mestrado em Engenharia Metalúrgica).

6. Noldin. J.H. An overview of the new emergent ironmaking technologies. In: IAS, 8th Ironmaking Conference, Rosario, 2011.

7. Biswas, A. K. *Principles of Blast Furnace Ironmaking*; Theory and Practice, Cootha Publishing House, Brisbane, Australia, 1985. 253p.

8. GEERDES, M., CHAIGNEAU, R., KURUNOV, I., LINGIARDI, O., RICKETTS, J. *Modern Blast Furnace Ironmaking;* An Introduction. 3.ed. IOS Press, 2015. 219p.

9. *3rd VDEh International Ironmaking Seminar*, Cologne, Germany. Steel Academy, 2015, 300p.

10. ARAÚJO, D. R.; *Desenvolvimento de um modelo computacional de otimização e predição do Valor em Uso de pelotas de minério de ferro na rota redução direta – aciaria elétrica.* PUC-Rio, 2007. 205p, (Tese de Doutorado em Engenharia Metalúrgica).

11. Technical Archives from Samarco Mineração's metallurgical laboratory.

12. BAKKER, T. *Softening in the Blast Furnace Process*; Local Melt Formation as the Trigger for Softening of Ironbearing Burden Materials. Technische Universiteit Delft, 1999. 263p. (Dissertação de Doutorado em Engenharia)

13. Marise, B. *Influência da qualidade das matérias-primas no escoamento gasoso da zona granular do alto-forno*. Belo Horizonte: UFMG, 2014. 84p. (Dissertação de Mestrado em Engenharia Metalúrgica).

14. GEERDES, M.; VLIET, C. V. D.; TOXOPEUS, H.; MEDEIROS, F. T.; *Práticas Modernas Para Operação De Alto-Fornos*. 2007. 128 p.

15. JESCHAR, R., POTKE, W. PETERSEN, V. & POLTHIER, L. *Blast Furnace aerodynamics*. Wollongong: 1975, p. 136-147.

16. SILVEIRA, R. C.; MELO, M. A. L. *Contribuição ao Escoamento Gasoso no Alto-Forno. Metalurgia* – Vol. 30 - No. 199 - junho, 1974.

17. HASENACK, N., KISTER, H., ROLF, B., KEES, H. Low temperature Degradation of Pellets and the Effect on Blast furnace Performance. *Society of Mining Engineers*, vol. 26, p2632-2672, Set. 1976.

18. ZHU, D., CHUN, T., PAN, J., ZHANG, J. Influence of Basicity and MgO content on metallurgical performances of Brazilian specularite pellets*. International Journal of Mineral Processing,* v.125, p51s60s, Set. 2013.

19. Dwarapudi, S., Gosh, T., Shankar, A., Tathavadkar, V., Bhattacharjee, D., Venugopal, R. Influence of Pyroxenyte flux on the quality and microstructure of hematite pellets. International Journal of Mineral Processing. V.96, p45s-53s, 2010.

20. MEYER, K. Fundamentals of Pelleetizing. In *Pelletizing of Iron Ores.*Dusseldorf: Verlag Stahleisen mbH, 1980. p24s-39s.

21. DWARAPUDI, S., GOSH, T., SHANKAR, A., TATHAVADKAR, V., BHATTACHARJEE, D., VENUGOPAL, R. Effect of Pellet Basicity and MgO on the quality and microstructure of hematite pellets. International Journal of Mineral Processing. V.99, p43s-53s, 2011.

22. INTERNATIONAL STANDARDS ORGANIZATION, Switzerland. ISO13930; Dynamic test for low-temperature reduction-disintegration. Switzerland, 1998. 10p.

23. Jasienskam S., Orewczyk, J., Ledzki, A., Durak, J. Effect of reduction conditions on structure and phase composition of blast furnace charge composed of alkaline sinters and acidic pellets. *Solid State Ionics*, v.117, p129s-143s, 1999.

24. MOUSA, E.A. Effect of basicity on wustite sinter reducibility under simulated blast furnace conditions. *Institute of Materials, Minerals and Mining*. v.41, no6, p418s-428s. June, 2013

25. INTERNATIONAL STANDARDS ORGANIZATION, Switzerland. ISO7215; Determination of relative reducibility. Switzerland, 1995. 13p.

26. BAHGAT, M., ABDEL, K.S., EL-KELESH, H.A., NASR, Metallic Iron Whisker formation and growth during iron oxide reduction: K2O effect. Ironmaking and Steelmaking, v.36, no5, p379s-387s, March, 2009.

27. Xu, R., ZHANG, J., ZUE, H., JIAO, K., HU, Z., XING, X. Mechanisms of swelling of iron ore oxidized pellets in high reduction potential atmosphere. *Journal of Iron and Steel Research, International*. v.22, p1s-8s, 2015.

28. INTERNATIONAL STANDARDS ORGANIZATION, Switzerland. ISO4698; Determination of relative free-swelling index. Switzerland, 2007. 18p..

29. INTERNATIONAL STANDARDS ORGANIZATION, Switzerland. ISO7992; Determination of reduction properties under load. Switzerland, 2007. 12p.

30. NOGUEIRA, P.F., FRUEHAN, R.J., Furnace Burden Softening and Melting Phenomena: Part I. Pellet Bulk Interaction Observation. *Metallurgical and Materials Transactions B*. v.35B, p829s-838s, October 2004.

31. KAUSHIK, P., FRUEHAN, R.J., Mixed burden softening and melting phenomena in blast furnace operation Part 1 – X-ray observation of the ferrous burden. *Institute of Materials, Minerals and Mining*, v.33, no6, p507s-518s, April 2006.

32. ILJANA, M, KEMPPAINEN, A., PAANANEN, T., MATTILA, O., PISILA, E. Effect of adding limestone on the metallurgical properties of iron ore pellets. *International Journal of Mineral Processing*. V.141, p34s-43s, 2015.

33. LIU, J., CHENG, G., LIU, Z., CHU, M. Softening and melting properties of different burden structures containing high chromic vanadium titano-mavnetite. International Journal of Mineral Processing, 6p, 2015.

34. CHUANG, H., HWANG, W. LIU, S. Effects of basicity and FeO content on the softening and melting temperatures of the CaO-SiO2-MgO-Al2O3 Slag system. *Materials Transactions*, v.50, no6, p1448s-1456s, 2009.

35. KEMPPAINEN, A., ILKANA, M., HEIKKINEN, E., FABRITIUES, T. Softening behavior of iron ore pellets in the cohesive zone of a blast furnace. In METEC-ESTAD, Dusseldorf, 2015.

36. MITSUTAKA, H., NAGASAKA, T., KATSUMATA, A., HIGUCHI, K., YAMAGUCHI, K., KN-NO, N. Simulation of Primary-slag melting behavior in the cohesive zone of a blast furnaces, considering the effect of Al_2O_3, Fe_tO and Basicity in the Sinter Ore. *Metallurgical and Materials Transactions B*. v.30B, p671s-683s, August 1999.

37. Ritz, V.Reduction, softening and meelting properties of pellets, sínters lupy ore and mixed blast furnace burden; Clausthal-Zellerfeld Germany: Technical University of Clausthal, 1990. (Dissertação, Doutorado em Engenharia Metalúrgica).

38. NOGUEIRA, P.F., FRUEHAN, R.J., Furnace Burden Softening and Melting Phenomena: Part II. Evolution of the Structure of the Pellets. *Metallurgical and Materials Transactions B*. v.36B, p583s-590s, October 2005.

39. NOGUEIRA, P.F., FRUEHAN, R.J., Furnace Burden Softening and Melting Phenomena: Part III. Melt Onset and Initial Microstructural Transformations in Pellets. *Metallurgical and Materials Transactions B*. v.37B, p551s-558s, August 2006.

40. KAUSHIK, P., FRUEHAN, R.J., Mixed burden softening and melting phenomena in blast furnace operation Part 2 – Mechanism of softening and melting and impact on cohesive zone. *Institute of Materials, Minerals and Mining*, v.33, no6, p520s-528s. 2006.

41. KAUSHIK, P., FRUEHAN, R.J., Mixed burden softening and melting phenomena in blast furnace operation Part 3 – Mechanism of burden interaction and melt exudation phenomenon. *Institute of Materials, Minerals and Mining*, v.34, no1, p10s-22s. 2007.

42. Cota, M., *Influência da distribuição granulométrica do pellet feed no processo de aglomeração e na qualidade da pelota de minério de ferro para redução direta*. UFOP, 2004. 126p, (Dissertação de Mestrado em Engenharia Metalúrgica).